12-2008

Collective Behavior of Interacting Magnetic Nanoparticles

Noppi Widjaja
University of Tennessee - Knoxville

To the Graduate Council:

I am submitting herewith a dissertation written by Noppi Widjaja entitled "Collective Behavior of Interacting Magnetic Nanoparticles." I have examined the final electronic copy of this dissertation for form and content and recommend that it be accepted in partial fulfillment of the requirements for the degree of Doctor of Philosophy, with a major in Physics.

E. Ward Plummer, Major Professor

We have read this dissertation and recommend its acceptance:

Jian Shen, Pengcheng Dai, James R. Thompson, Bin Hu

Accepted for the Council:

Carolyn R. Hodges

Vice Provost and Dean of the Graduate School

(Original signatures are on file with official student records.)

To the Graduate Council:

I am submitting herewith a dissertation written by Noppi Widjaja entitled "Collective Behavior of Interacting Magnetic Nanoparticles." I have examined the final electronic copy of this dissertation for form and content and recommend that it be accepted in partial fulfillment of the requirement for the degree of Doctor of Philosophy with a major in Physics.

E. Ward Plummer
Major Professor

We have read this dissertation
and recommend its acceptance:

Jian Shen

Pengcheng Dai

James R. Thompson

Bin Hu

Accepted for the Council:

Carolyn R. Hodges,
Vice Provost and Dean of the Graduate School

(Original signatures are on file with official student record)

Collective Behavior of Interacting Magnetic Nanoparticles

A Dissertation

Presented for the

Doctor of Philosophy

Degree

The University of Tennessee, Knoxville

Noppi Widjaja

December 2008

In memory of my father (1943-2001)

I dedicate this dissertation to my mother, my sister, my brother, my husband and my son.

Acknowledgements

When I look back at my three year long journey at University of Tennessee, I feel very fortunate to have had Dr. Jian Shen and Dr. Ward Plummer as my advisors. I was always amazed by their broad knowledge in physics, their quick grasp of new research results, and their enthusiasm in the scientific research and education. They have been patiently guiding me through the unknown territories in scientific research. Their support, guidance and encouragement have allowed me to develop my experimental skills and build up my knowledge in solid state physics through conducting research on surface physics and nanomagnetism.

Next, I would like to express my special gratitude to my Ph.D committee: Dr. Pengcheng Dai, Dr. James R Thompson, Dr. Bin Hu, Dr. Adriana Moreo and Dr. Marianne Breinig for their insightful discussions, their professionalism, and their expertise during my critical time at the graduate school. Without them finding a solution to my problem, this dissertation would be significantly postponed or almost impossible.

Particular thanks also go to Dr. Lifeng Yin for his patience, his instruction and his help in taking the data, and for his continuing encouragement and inspirations. I am also grateful to work with Dr. Minghu Pan and Dr. Jiandi Zhang in the early stage of my graduate research at University of Tennessee. They taught me the basic skills in the Ultra High Vacuum (UHV) environment.

The jokes and stories of fellow graduate student and postdoc of Dr. Ward Plummer's group and Dr. Jian Shen's group made the lab a more colorful and enjoyable place to live and work. Thanks to former graduate student, Maria Asuncion Torija Juana, for passing on her

knowledge in the MOKE lab. Thanks also go to Kenji Fuchigami and Te-Yu Chien who are my office-mates. We always exchange problems and ideas that are facing us in our project and lab. I also need to thank Zac Ward for his help in writing a program to control the step motor. Gary Ownby has helped me with the technical support such as opening the chamber, etc.

Finally, I would like to thank my family: my husband and my son, my mother, my sister & her family and my brother & his family for their love, support and value of education throughout all those years of my formal education. My mother has sacrificed a year and half of her time to baby-sit my son. They always respected my choice and encourage me to pursue my dreams. When I feel down and lack of inspiration, they are always there to cheer me even with just a simple chat.

I am also remembering my late father who passed away on 2001 after battling with cancer for four years. He always had faith in me, believed that I can pursue my dreams for higher education. When he was battling the cancer, he fully revealed his unique quality: grace, courage and responsibility. Even when he was receiving chemotherapy treatment, he was still encouraging all his children to go for a better future.

Abstract

In the past, Low Dimensional Materials by Design group at ORNL in collaboration with students from the University of Tennessee, have successfully tailored and studied magnetic nanostructures in 2D, 1D and 0D spatial confinement on Cu(111) substrates. They observed a striking collective ferromagnetic long-range order in Fe-nanodots on Cu(111) surface which can be stabilized through the indirect exchange interaction mediated by the substrate. This type of magnetic interaction was expected to have little effect on promoting a global ferromagnetic order in a randomly distributed dot assembly. It is for certain that we need a better understanding of the relative roles of magnetic anisotropy and magnetic interaction in the magnetism of reduced dimensionality, in general, and nanodot assemblies, in particular. With this accomplishment in mind, I'm trying to study the collective behavior of interacting magnetic nanoparticles.

We proposed the following experiments to quantify the relative roles of magnetic anisotropy, dipolar interaction and indirect exchange interaction on the collective magnetic behavior of nanodot assemblies. They consist of two main projects:

a) study how the indirect exchange interaction is affected by modifying the surface states. The interaction is observed through the changes in the critical temperature (T_c) of Fe dots as a function of miscut angle Cu curved substrate. Depending on the buffer layer (Xe) coverage, we observed a critical terrace width above which the T_c slightly increases and below which the T_c decreases rapidly. In other words, the (T_c) depends largely on the Cu(111) miscut angle.

b) study the role of magnetic anisotropy and dipolar interaction. We used Co dots on TiO_2(110) substrate as a prototype. We observed significant perpendicular magnetic anisotropy with perpendicular easy axis for both large and small dot densities with no sign of hysteresis observed down to 2 K.

Table of Contents

List of Figures

Chapter 1 Introduction

"There is plenty of room at the bottom"

Feynman, 1959

1.1 Characteristic length effect

In his 1959 talk entitled "There is plenty of room at the bottom", Feynman speculated that striking new phenomena would arise as the size of a solid is reduced. The question is: How fine does a solid need to be structured so that its size will have an impact on its electronic and magnetic properties? The wavefunction of electrons changes when they are confined to dimensions comparable with their wavelength. This wavelength, related to the kinetic energy of the electrons, is called the de Broglie wavelength. At low temperatures the contribution to the current is mainly dominated by the electrons having energy close to the Fermi energy. Therefore, the Fermi wavelength is the relevant wavelength. The contribution from the electrons far away from the Fermi level is usually neglected. The Fermi wavelength is given by $\lambda_F = 2\pi/k_F = \sqrt{2\pi/n_s}$, where k_F is the Fermi wave vector which is proportional to the square root of the electron density n_s for a two dimensional electron gas (2DEG). Hence the wavelength is inversely proportional to the square root of the electron density and decreases with increasing carrier density. Therefore, confinement and quantization phenomena are visible in semiconductors already at dimensions greater than 200 nm [1], whereas in metals they typically are seen at 1 nm [2]. Confining electrons to small structures causes the continuous bulk bands to

split up into discrete levels, for example quantum well states in a slab. For N atomic layers in the slab there are N levels. In order to exhibit two dimensional behavior, there should be only a single level within $\pm kT$ of the Fermi level. Several levels within the Fermi cut off would already approach a three dimensional continuum. The estimation of the de Broglie wavelength at room temperature is about 8 nm [2], which is comparable with the spatial extent of the lowest quantum state. Thus, both the high electron density in magnetic metals and the requirement of room temperature operation for quantum devices point to dimensions of a few nanometers.

There are two features one encounters as one or more linear dimensions of a sample are reduced. First, when one enters the nanometer regime, a large fraction of the magnetic moment bearing species resides in the surface of interface sites. For instance, if we have an ultrathin magnetic film five atomic layers in thickness, 40 percent of the magnetic ions reside in such sites. The key aspects of magnetism are very sensitive to local site symmetry, and thus the magnetism in such a film will differ qualitatively from a bulk crystal made with the same atomic constituents. One may vary magnetic properties of the ions that reside in such sites by varying the substrate or crystal face on which the film is grown and by chemisorbing material on the outer surface. One can thus create new "designer materials" with properties and response characteristics controlled by such features. We then have spin engineering, an analog to the bandgap engineering of the semiconductor realm. In addition, an ultrathin film grown epitaxially on a substrate will have a lattice constant controlled by that of the underlying substrate and hence different from the corresponding bulk material. Also, the spacing between parallel atomic planes will differ as well, by virtue of expansion or contraction of the lattice constant parallel to the substrate surface. Hence, the site symmetries in the center of the film differ from the bulk material as well as from those on the surface or at an interface. We know very well that the

fundamental interactions that control the nature of the ordered state are highly sensitive to both local geometry and interior spacing. New crystal structures not found in bulk matter are also realized in magnetic nanostructures. One may grow stable, thick epitaxial films of fcc cobalt on suitable substrates, for example, while the bulk form of this element is hcp.

Second, when one of more sample dimensions are small or comparable to one of these fundamental lengths, we again enter a domain where the response characteristics, thermodynamic properties and other key aspects of the magnetism differ qualitatively from that found in bulk materials.

One such length is the wavelength λ_T of thermally excited spin waves. Perhaps it is more relevant to discuss their wavevector $k_T = 2\pi/\lambda_T$. If L is any linear dimension of the sample of interest, then when $k_T L \leq 1$, we are in a regime where the fundamental magnetic properties of the material differ from those in the bulk and are affected by sample size. For ferromagnetic Fe at room temperature, we have a critical crossover length $L_T = 1/k_T \approx 0.3$ nm, whereas if we cool down to liquid helium (He) temperature, $L_T \approx 3$ nm. If, then, we have an ultrathin film some two or three atomic layers in thickness, and we cool from room temperature to liquid He temperature, we cross over from a regime where the thermodynamics is three dimensional (room temperature) to a quasi-two-dimensional regime (He temperature). Similarly, if at He temperatures, we increase the thickness of the film, we can study the crossover from two to three-dimensional physics. Thus, ultrathin films (and other nanomagnetic structures) offer us the possibility of studying statistical mechanics as we make the transition from three-dimensional physics to the physics of a lower dimensional world.

Another fundamental length is the exchange length, $L_{ex} = (D/\mu_B H_A)^{1/2}$, where μ_B is the Bohr magneton, the parameter D is the exchange stiffness, and H_A is a measure of the anisotropy

field in the material. This may range from roughly 1 to 10 kG, or equivalently from 0.1 to 1 T in typical materials. The exchange length is the thickness of a domain wall of Bloch character in a bulk ferromagnet; for a Néel wall, one replaces H_A by $4\pi M_S$ where M_S is the saturation magnetization. The magnitude of $4\pi M_S$ is comparable to that of the anisotropy field. Typically, then the exchange length lies in the range of 5-10 nm. In a ferromagnet, the cost in energy to create a non-uniform state characterized by a length scale small compared to L_{ex} is very large. Thus in ferromagnetic films whose thickness is small compared to this length, the magnetization is uniform in the direction normal to the surfaces. Such a film's domain structure and hysteresis loop differ qualitatively from a bulk ferromagnet with its complex domain structure in the form of a three-dimensional network.

1.2 Introduction to nanomagnetism

Two dimensional systems, such as ultrathin epitaxial films and superlattices, display magnetic properties distinct from bulk materials. We conclude from the section above that as surface-to-volume ratio increases, material properties are increasingly dominated by surface and interface effects, for instance a 5 nm cube of bcc Fe contains ~12,000 atoms while ~2000 of which are on the surface. A challenging aim of current research in magnetism is to explore structures of still lower dimensionality.

As the dimensionality of a physical system is reduced, magnetic ordering tends to decrease as fluctuations become relatively more important. In the bulk single crystals, the crystal anisotropy solely determines the magnetization easy axis; however in the thin films, besides the crystal anisotropy, the shape anisotropy is also needed to stabilize the magnetic ordering. Surprisingly in the 1D chain, despite the spin lattice model prediction that there should be no

magnetic ordering, Gambardella *et al* [5] were able to demonstrate the existence of both short and long range ferromagnetic order for quasi-one-dimensional monoatomic chains of Co constructed on a Pt(997) surface.

Spin lattice models [3,4] predict that an infinite one dimensional linear chain with short range magnetic interactions spontaneously breaks up into segments with different orientation of the magnetization, thereby prohibiting long range ferromagnetic order at a finite temperature. These models, however, do not take into account kinetic barriers to reaching equilibrium or interactions with the substrates that support the one dimensional nanostructures. So they can only be applied to truly Heisenberg systems where the symmetry is not broken. Experimentally, the magnetic system has to be supported by a substrate, which makes the theorem no longer applicable since now the translational symmetry in the surface normal direction is broken.

In the last decade, we have witnessed the emergence of a totally new field, so called spintronics, where both electron's charge and spin are taken into account. Progress in spintronic cannot be separated from the development of nanomagetism. This rapid development in spintronic stems from the discovery of Giant Magneto Resistance (GMR). The engineering of magnetic properties at atomic level in multilayers has helped the discovery of Giant Magneto-Resistance (GMR). Progress in atomic engineering makes it possible today to build even lower dimensional magnetic materials, e.g. 1D chains [5,6,7] or 0D nanodots [8], by self assembly epitaxial techniques on suitable substrates.

Fert's group in 1988 [14] and Grunberg's group in 1989 [15] observed a sudden drop in a resistance of an order of magnitude in an antiferromagnetically coupled Fe(001)/Cr(001) superlattice system after aligning all the magnetic moment of the Fe layer with an external magnetic field. This GMR effect is attributed to the spin dependent scattering at the interface of

successive magnetic layers. In a ferromagnetic metal, the electronic current is carried by the spin ↑ (majority) and spin ↓ (minority) electrons that have different matching potentials; electrons of one spin direction can pass through the first interface and reach the second interface easily while the other spin direction will be scattered back at the first interface. In a zero field, the magnetic moments in different magnetic layers align antiparallelly leading to high resistivity. But when a sufficiently high external magnetic field is applied, the magnetic moments in different magnetic layers will all align in the same direction which reduces the resistance significantly (figure 1.1). So we can easily conclude that in order for the GMR effect to be observed, an antiferromagnetic coupling between the magnetic layers that have different spin orientation has to be satisfied. The discovery of GMR effect has led to the production of the low power, ultrahigh density nonvolatile Magnetoresistive Random Access Memory (MRAM) which is now available in market. Scientists all over the world try to discover and study new materials in the reduced dimensionality that shows interesting properties.

1.3 Motivation

Nanoscale physics is a crossover from classical physics to quantum physics where new physics will arise. We have discussed in section 1.1 that the physics in this regime is qualitatively different from that realized in bulk magnetic materials.

In the past, scientists in the Low Dimensional Materials by Design group at ORNL in collaboration with students from the University of Tennessee have successfully tailored and studied magnetic nanostructures in 2D (films), 1D (stripes) and 0D (dots) spatial confinement [5,6,7,8,9,10,11] on Cu(111) substrates. They were stunned by the fact that the collective ferromagnetic long-range order can also be stabilized in Fe-nanodots on Cu(111) surface through

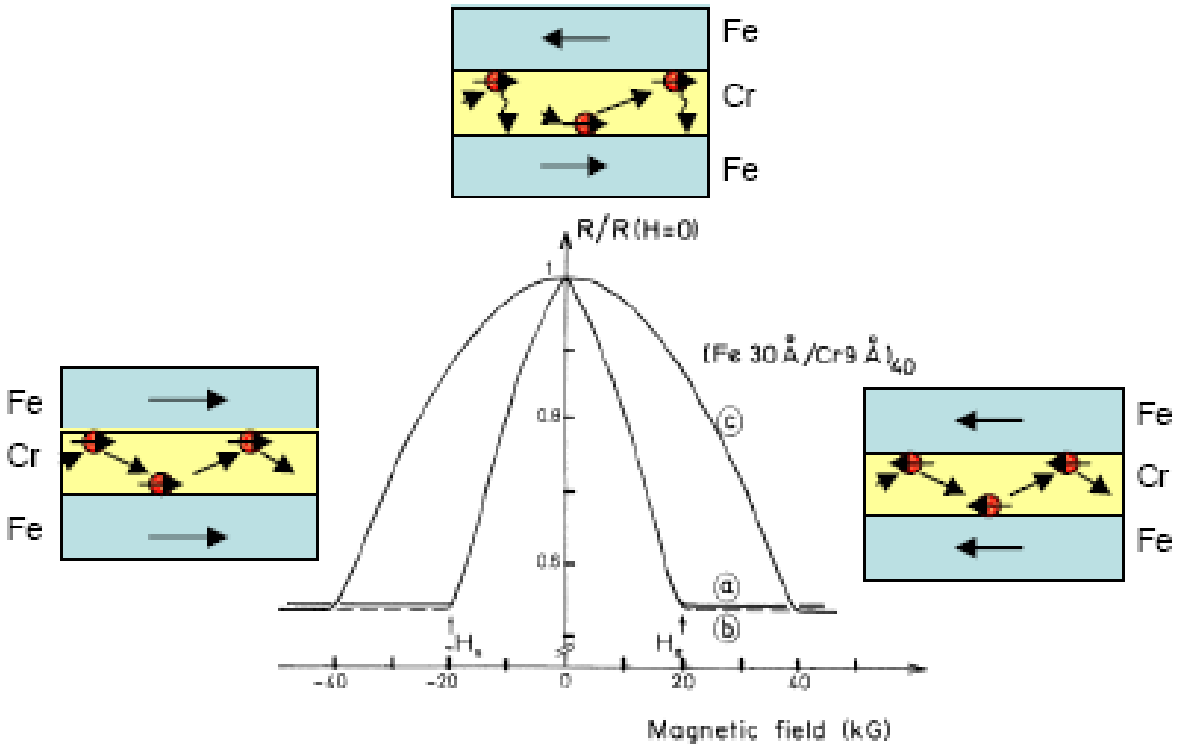

Figure 1.1: Magnetoresistance of (Fe 30 Å/Cr 9 Å)$_{40}$ at 4.2 K. Current is applied along a certain direction in the film plane with the applied field parallel to the current (curve a), applied field in the layer plane and perpendicular to the current (curve b) and applied field perpendicular to the layer plane (curve c). At low applied magnetic field, the magnetic Fe layers are not aligned, and scattering results in high resistance. At high field, magnetic layers are aligned and lower resistance occurs (after Reference 14).

the indirect exchange interaction between the nanodots mediated by the substrate [8,12,13]. This type of magnetic interaction was expected to have little effect on promoting a global ferromagnetic order in a randomly distributed dot assembly. It is our goal to have a better understanding and more complete picture of the relative roles of magnetic anisotropy and magnetic interaction (dipolar and indirect exchange interaction, tunneling induced interaction) in the magnetism of reduced dimensionality, in general, and nanodot assemblies, in particular.

1.4 Outline of the thesis

Triggered by the facts that collective ferromagnetic order can exist in the low dimensionality system, we want to have a better understanding about the relative role of magnetic anisotropy and magnetic interaction (dipolar and indirect exchange interaction, tunneling induced interaction) to stabilize the magnetic ordering in reduced dimensionality system. In this dissertation, I will focus mainly on how the interaction between the magnetic nanodots, the magnetic anisotropy and the surface state electrons influence the overall magnetic behavior of the system.

Chapter 2 provides the necessary foundation in nanomagnetism so that readers are better equipped with some of the terms and concepts used in this dissertation. Some results obtained by the previous group members are also presented as a background of this dissertation's work.

Chapter 3 gives the insight about the experimental tools that are used in this thesis research, as well as the details on how we prepare the sample and do the measurement.

In chapter 4, we modify the surface states by introducing miscut angle and study the impact of modifying vicinal surface states on the ferromagnetic behavior of Fe dots. We introduce a novel way, curved Cu(111) substrate, to smoothly changed the surface states. We

grow Fe-dots on a Cu(111)-curved substrate where the miscut angle changes from 0° (very large terrace width) to 8° (15 Å terrace width). With this curved substrate, the same growth parameter can be ensured in the whole miscut angle studied. We observe competition between the terrace width and the Fe-nanodots diameter. We also show that the importance of surface state on ferromagnetism in this low dimensional system is very robust. The vicinal surface strongly affects the coupling between Fe-nanodots.

Chapter 5 studies the interplay between the magnetic anisotropy, dipolar interaction and tunneling induced coupling in nanodot assemblies. For this purpose, cobalt magnetic dot assemblies grown on rutile TiO_2(110), which is a semiconducting templates, are used to rule out indirect exchange interaction. Meanwhile, the rather short-ranged tunneling induced coupling can be conveniently ruled in or out by changing the dot-dot spacing. Our results show significant *perpendicular magnetic anisotropy* (PMA) with perpendicular easy axis for both large and small dot's density with no sign of hysteresis observed down to 2 K.

In chapter 6, I will summarize the results of this dissertation.

Chapter 2 Theory

2.1 Magnetism in magnetic materials

Magnetism reflects the underlying band structure of the magnetic materials [1]. The electronic structure of materials consists of two electronic states which correspond to the two different spin states of the electrons, i.e. spin up and spin down electrons. In non magnetic materials, they have equal density of states (DOS) meaning that they have the same number of spin up and spin down electrons. On the other hand, the origin of the magnetization of the material is the imbalance density of states of spin up and spin down states in magnetic materials. Figure 2.1 gives a better insight of the DOS in the magnetic and non-magnetic materials.

There is much more to magnetism than the spin split band structure [1]. Magnetic domains provide a large scale texture that adds enormous complexity. As a consequence, there are many more magnetic properties than band structure parameters, and a large number of techniques to measure them. The variability of an $H(M)$ hysteresis loop reflects a complex domain structure. Interestingly, the situation becomes simpler in nanostructures, which are smaller than the typical extension of a domain wall (0.1 – 1 μm). They often exhibit a square hysteresis loop. Magnetic anisotropy and magnetostriction in thin films demonstrate that magnetic ordering is sensitive to small energy changes induced by the presence of an interface and by strain.

Magnetic coupling and magnetic moment are sensitive to the interatomic spacing and the atomic volume respectively. Both are dominated by the coulomb and/ or exchange interactions at small distances. In a somewhat oversimplified atomic orbital picture, the moment is created by

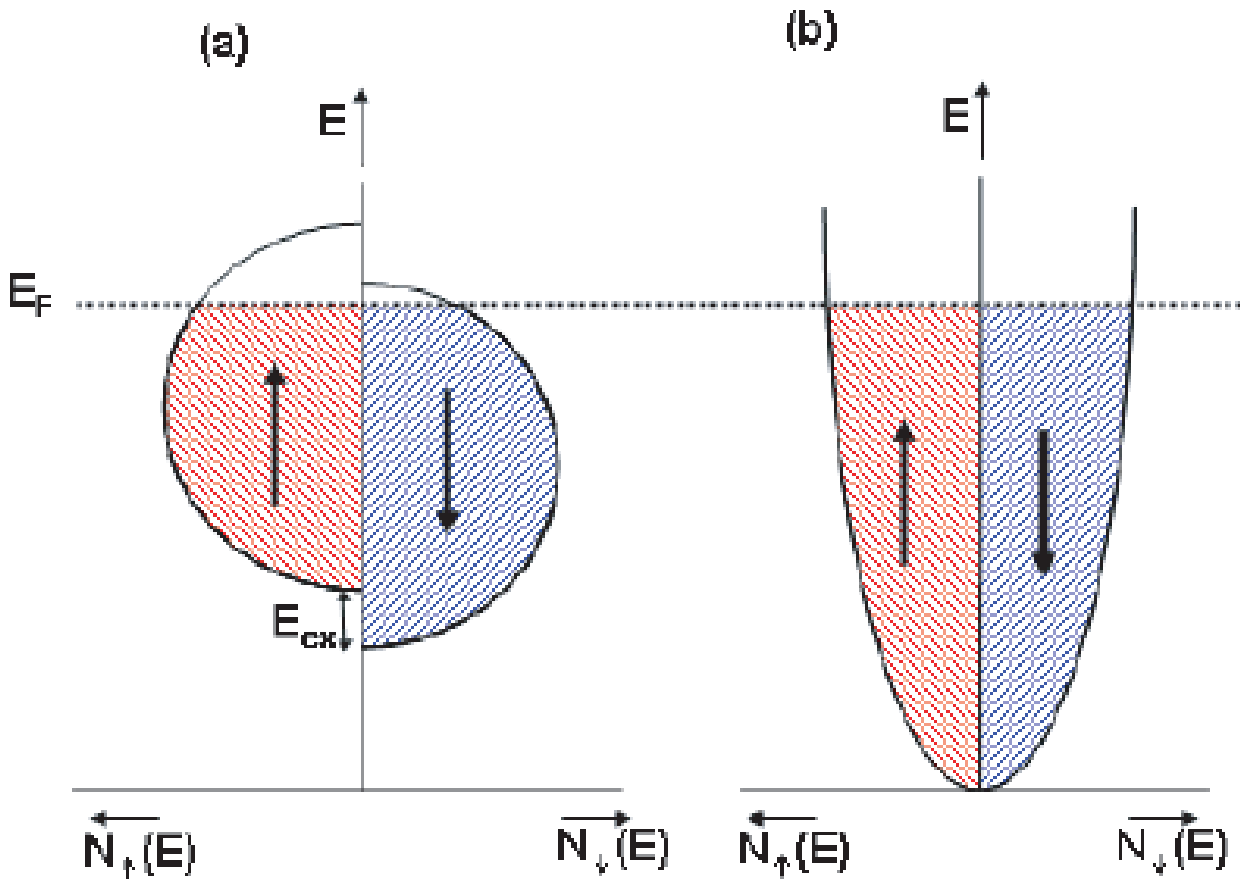

Figure 2.1: (a) Schematic representation of the spin- dependent DOS of the *d*-bands in a ferromagnetic transition metal (itinerant ferromagnetism). (b) Free electron like DOS for the nonmagnetic metal.

interaction between electrons on the same atom and the coupling between electrons on different atoms. Spins are aligned antiparallel at the smallest distances or volumes, since Pauli's exclusion principle prevents parallel spins from occupying the same spot. This reduces the moment of an individual atom and produces antiferromagnetic coupling between atoms. The interaction changes its sign as soon as the wavefunctions cease to overlap strongly. The moment increases and the coupling become ferromagnetic. At even larger distances the magnetic coupling becomes indirect, using conduction electrons as mediators. It oscillates with a period determined by Fermi wave vectors, thereby bringing orientation dependent Fermi surface parameters into the picture.

2.1.1 Rare earth magnets

Lanthanides or rare earths (La-Lu) are 4*f* elements with partially filled 4*f*-shells, which can lead to a variety of magnetic effects. The typical rare earth atomic configuration is $[Xe]4f^n5d^{(1\text{ or }0)}6s^2$. Electrons in such orbitals are strongly localized and therefore easily retain their magnetic moments and function as paramagnetic centers. The rare earths have large magnetic moments. The *f*-shell can contain up to 7 unpaired electrons, therefore enhancing the size of the magnetic moment. Rare earths also have strong ferromagnetic coupling between the magnetic moments.

The 4*f*-shells, responsible for paramagnetism in the rare earth ions, lie deep inside the ions, within the 5*s* and 5*p* shells; thus will not experience the intense inhomogeneous electric field called the crystal field. The crystal field is an electric field derived from neighboring atoms in the crystal. Due to strong spin-orbit interaction and negligible crystal field in rare earths, Hund's third rule is obeyed and the orbital moment is not quenched.

2.1.2 Itinerant ferromagnetism

Contrary to the 4*f* rare earths, the partially filled 3*d*-shells of transition metal (Sc-Zn) ions are the outermost shells, therefore they will experience much stronger crystal field interaction than the spin-orbit interaction. Hence, Hund's third rule, which is based upon the fact that the spin-orbit interaction is the next most significant energy term after Coulomb interaction, is violated in 3*d* ions. The 3*d* systems choose a ground state such that $L = 0$ and the orbital moment is said to be quenched. This effect is known as orbital quenching.

The magnetic moment per atom in 3*d* transition metals, i.e. Fe, Co, and Ni, is about 2.2 μ_B, 1.7 μ_B, and 0.6 μ_B respectively at 0 K (see table 2.1). This non-integral value is not possible to understand on the basis of localized moments on atoms. It is therefore a strong evidence for itinerant ferromagnetism in which the magnetization is due to spontaneously split spin bands. The conduction electrons in itinerant ferromagnetism are delocalized and can wander freely through the sample. The magnetism of itinerant electrons follows the free electron model where the periodic potential due to the lattice is ignored. However if it is included as a perturbation (the nearly free electron model), energy gaps will open up at the Brillouin zone boundary.

The Stoner model can be used to understand how bands in some materials can become spontaneously spin split. The basic assumption in this model is that spin sub-bands are shifted with respect to each other due to the presence of the exchange interaction. It can be best described by figure 2.2 where in the absence of an external magnetic field, energy bands for spin up and spin down electrons at the Fermi energy are separated by $2\delta E$. Specifically we take spin down electrons with energies from $E_F - \delta E$ up to E_F and flip their spins, placing them in the spin up band with energies from E_F up to $E_F + \delta E$. The number of electrons moved is $g(E_F)\ \delta E/2$ and they increase in energy by δE, where $g(E_F)$ is the density of states at the Fermi energy and δE is

Material	$T_C(K)$	magnetic moment (in μ_B/atom)
Fe	1043	2.22
Co	1394	1.715
Ni	631	0.605
Gd	289	7.5

Table 2.1: Properties of some common ferromagnetic. T_c is the Curie temperature of the material below which non-zero magnetization occurs hence the material is ferromagnetic at T < T_c. μ_B is the Bohr magneton.

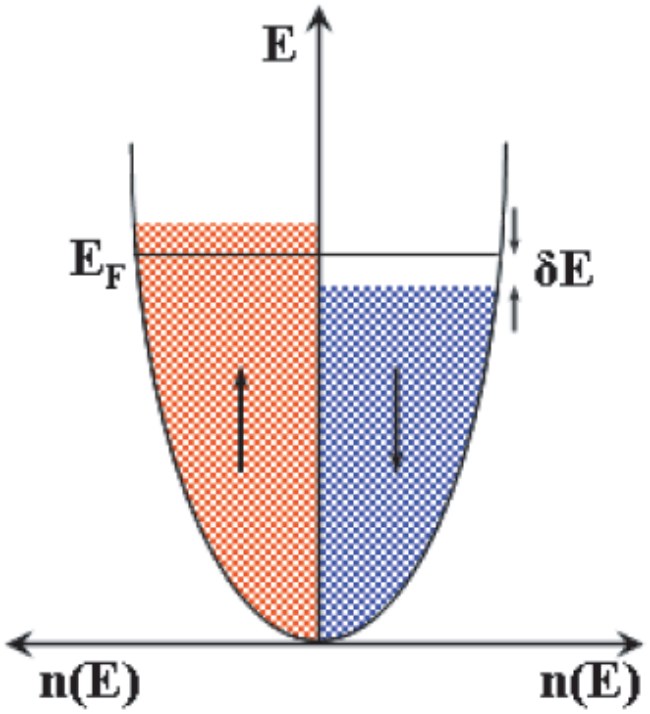

Figure 2.2: Density of states showing spontaneous splitting of energy bands without an applied magnetic field. [after reference 1].

the increase in energy. The total energy change is $g(E_F)\delta E/2\times\delta E$. The total kinetic energy change $\Delta E_{\mathrm{K.E}}$ is therefore,

$$\Delta E_{K.E}=\frac{1}{2}g(E_F)(\delta E)^2 \tag{2.1}$$

This is an energy cost so this process looks unfavorable. However, the interaction of the magnetization with the Weiss molecular field (mean field) gives an energy reduction which can outweigh this cost. In mean field theory we say that all spins feel an identical average exchange field λM produced by all their neighbors, where λ is a constant that parametrizes the strength of the mean field as a function of the magnetization. In ferromagnets due to large Coulomb energy involved in the exchange interaction, the mean field is often found to be extremely large. In a metal, the mean field can magnetize the electron gas M which in turn be responsible for the mean field (chicken-egg scenario).

The number density of spin up is $n_\uparrow=\frac{1}{2}\left(n+g(E_F)\delta E\right)$ and the number density of spin down is $n_\downarrow=\frac{1}{2}\left(n-g(E_F)\delta E\right)$. Hence the magnetization is $M=\mu_B(n_\uparrow-n_\downarrow)$, assuming each electron has a magnetic moment of 1 μ_{B}. The mean field energy is

$$\Delta E_{\mathrm{P.E}}=-\int_0^M\mu_0(\lambda M')\mathrm{d}M'=-\frac{1}{2}\mu_0\lambda M^2=-\frac{1}{2}\mu_0\mu_B^2\lambda(n_\uparrow-n_\downarrow)^2 \tag{2.2}$$

Writing $U=\mu_0\mu_B^2\lambda$, where U is a measure of the coulomb energy, we have

$$\Delta E_{\mathrm{P.E}}=-\frac{1}{2}U(g(E_F)\delta E)^2 \tag{2.3}$$

Hence the total change of energy ΔE is

$$\Delta E = \Delta E_{K.E} + \Delta E_{P.E} = \frac{1}{2} g(E_F)(\delta E)^2 (1 - U g(E_F)) \tag{2.4}$$

Thus spontaneous ferromagnetism is possible if $\Delta E < 0$ which implies that

$$U g(E_F) \geq 1 \tag{2.5}$$

which is known as the Stoner criterion. This condition for the ferromagnetic instability requires that the coulomb effects are strong and the density of states at the Fermi energy is large. If there is spontaneous ferromagnetism, the spin up and spin down bands will be split by an energy Δ. If the Stoner criterion is not satisfied, then spontaneous ferromagnetism will not occur [1].

It is important to keep the characteristic energy scales for band structure and magnetism in mind; the width of the *s*, *p* bands is given by the kinetic energy at the Fermi level, which is on the order of 10 eV. The magnetic band splitting δE_{ex} of about 1 eV derives from the coulomb and/ or exchange interactions. The spin orbit coupling, which gives rise to crystalline anisotropy, is on the order of 0.1 eV for the 3*d* electrons in ferromagnets. The magnetic exchange coupling *J* is of the order of 0.01 eV/ atom. The crystalline magnetic anisotropy is only about 10^{-5} eV/ atom in the bulk but can increase to 10^{-4} eV/ atom in the lower symmetry of a surface. Then it matches the shape anisotropy, which reflects the magnetic dipole-dipole interaction [1].

2.2 The Mermin-Wagner-Berezinskii theorem

A solid is ordered at $T = 0$ but at non-zero temperature, the order is disrupted by thermally excited lattice vibrations, which are quantized as phonons. In a similar manner, a ferromagnet is perfectly ordered at $T = 0$ but at non-zero temperature the order is disrupted by spin waves which are quantized as magnons.

Magnons have a spin of one. As we learned from Statistical Mechanics, all spin one particles are bosons which have the number of modes excited at temperature T, n_{magnon} given by

$$n_{magnon} = \int_0^\infty \frac{g(\omega)\mathrm{d}\omega}{\exp(\hbar\omega / k_B T) - 1} \tag{2.6}$$

The integral converges in three dimensions; however it diverges in one and two dimensions. As a result, spontaneous ferromagnetism is not possible in the isotropic 1D and 2D Heisenberg models for all $T > 0$ because $M \rightarrow 0$. The absence of long range order in two-dimensional systems (with a continuous symmetry) is often referred to as the Mermin-Wagner-Berezinskii theorem [1].

This result only applies to an isotropic Heisenberg ferromagnet which possesses rotational symmetry so that all of the spin directions can be globally rotated without any additional energy cost. However, if there is a significant anisotropy, there will be an energy cost associated with rotating the spins from their ground state value that suppresses the growth of fluctuations. It turns out that it is the presence of such anisotropy that can stabilize long range order in 2D systems.

2.3 Magnetic Domain

Weiss first proposed that a ferromagnet contains a number of small regions called domains which are separated from each other by domain walls. It costs energy to make a domain wall but if it outweighs the dipolar energy (demagnetization energy or magnetostatic energy), then the formation of a domain wall is favorable. So the formation of domains is a balance between the cost of dipolar energy and the cost of a domain wall formation, while the size of a domain wall is determined by a balance between the exchange and anisotropy energies.

In many ferromagnetic samples, the lowest energy state at zero applied field is the demagnetized state, so that the overall magnetic moment is zero. If the sample size is reduced, the energy cost for the domain wall formation become progressively more costly in comparison with the demagnetizing energy. Thus a critical dimension may be reached below which it is energetically favorable to remove the domain walls so that the sample consists of a single domain.

2.3.1 Superparamagnetism

If ferromagnetic particles are small enough, they will be single domain because the energy cost of domain wall formation does not outweigh any saving in demagnetizing energy. The magnetization of a small, single domain ferromagnetic particle is often constrained to lie parallel or antiparallel to a particular direction. This can be due to magnetocrystalline anisotropy or shape anisotropy (associated with the demagnetizing energy and the shape of the particle). A particle of volume V needs activation energy of $\Delta E \approx KV$ to flip its moments 180°. For very small particles, such that KV is small compared to $k_B T$, the magnetization can be easily flipped by thermal fluctuations.

Consider a distribution of these small ferromagnetic particles in a non-magnetic matrix and assume that the particles are separated far enough apart so that interparticle interactions can be neglected. For $k_B T >> KV$ the system will therefore behave like a paramagnet and is called a superparamagnetic system. At high temperatures the moments on the particles are able to fluctuate rapidly. The fluctuations will slow down as the sample is cooled. We can define a temperature, so called blocking temperature T_B, above which the thermal energy, which causes fluctuations in the magnetic moment of the dots, becomes significant enough to overcome the

anisotropy energy barrier and randomize the orientation of the ferromagnetic moment. If we consider only the existence of the thermal energy without any interactions, there are at least two consequences:

(1) The magnetization should decay exponentially with time according to the exponential law $M(t) = M_0 \exp(-t/\tau)$, with time constant τ: $1/\tau = f_0 \exp(-\alpha)$, and $\alpha = \Delta E / k_B T$.

(2) The enhanced anisotropy energy will only increase the blocking temperature but the system will remain in the superparamagnetic state.

However, if we increase the density of the dots so that the spacing between the magnetic particles is not too large, the influence of the dipolar magnetic interaction on the superparamagnetic behavior usually can not be neglected, because not only will it modify the superparamagnetic relaxation but also change the ground state of the system. Magnetic anisotropies are covered in depth in section 2.4, while magnetic interactions are covered in depth in section 2.5.

Blocking temperature (T_B) can be measured by a zero field cooling-field cooling (ZFC-FC) process [see figure 2.3]. To measure signals via ZFC-FC, the sample containing single domain particles is first brought to liquid helium temperature in zero applied magnetic field. During this cooling, the particles tend to magnetize along energetically preferred directions in the lattice; since the orientations of the particles vary, the net moment of the system will be zero when approaching the lowest temperature. Even when a small external field is applied, the moments will remain locked into the preferred orientations. A ZFC magnetization vs. temperature curve is measured while heating the sample at a constant rate in the presence of small applied magnetic field. As the temperature increases, more thermal energy is available to

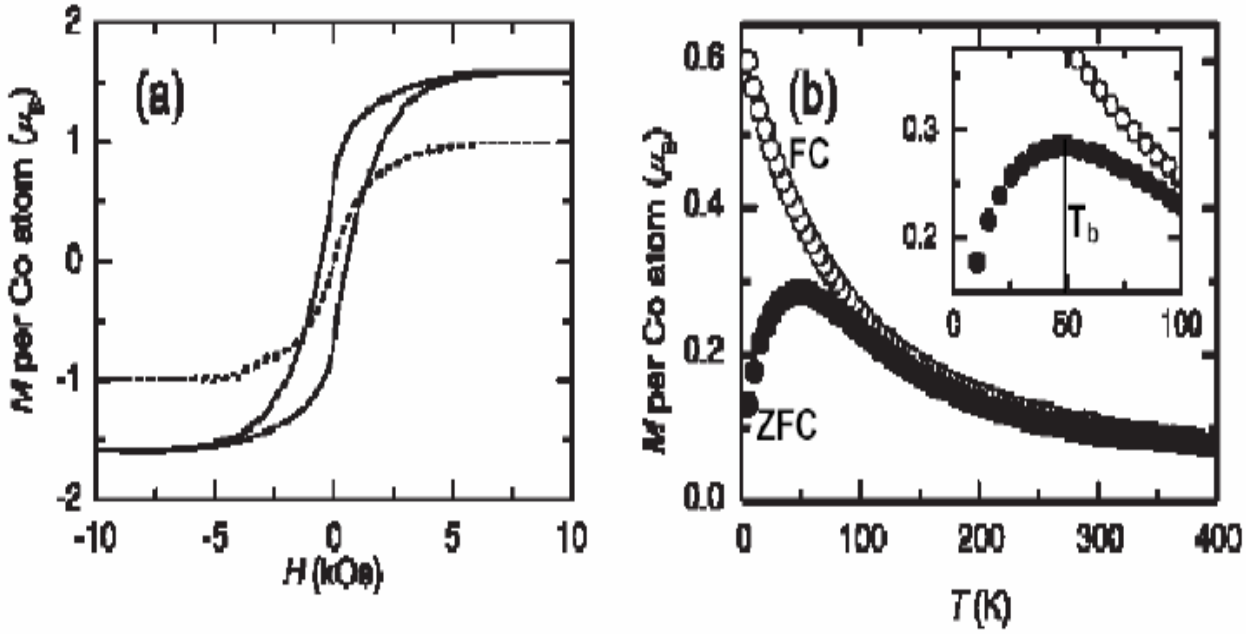

Figure 2.3: Example of the ZFC-FC curves with nanometer scale Co clustering in Co ion implanted epitaxial TiO_2 films. (a) Hysteresis loops at 5 K and 300 K show drastically decreasing H_C to almost zero as temperature is increased [single curve without hysteresis loop at 300 K, clear hysteresis loop at 5 K]. (b) The ZFC-FC curves show features of superparamagnetic behavior with the observation of $T_B \sim 80$ K. ZFC-FC curves show substantial divergence at low temperatures. [after reference 2]

disturb the system, and more moments will align with the external field direction. This peak temperature is T_B. As temperature rises above T_B, thermal energy is strong enough to overcome the Zeeman energy, and thus randomize the moments, resulting in a decrease of total moment. A FC magnetization vs. temperature curve is obtained and measured with the same small applied magnetic field while temperature decreases or the sample is cooled. The FC curve will diverge from the ZFC curve at temperatures lower than the blocking temperature. This divergence occurs because during field cooling the spins from each particle will tend to align with the easy crystalline axis that is closest to the applied field direction and remain frozen in that direction at low temperature. Thus the divergence of the ZFC-FC curves indicates that single domain particles dominate the magnetic signal.

2.4 Magnetic Anisotropy

Ferromagnetic single crystals exhibit ‘easy’ and ‘hard’ directions of the magnetization; i.e. the energy required to magnetize a crystal depends on the direction of the applied field relative to the crystal axes. The role of this magnetic anisotropy is crucial in the magnetism study to explain the existence of magnetic curve, hysteresis loop, and magnetic easy and hard axis; it requires a smaller field to saturate the electron spins along the easy axis than the hard axis. Several magnetic phenomena that occur in the surface study can also be understood by grasping the idea of magnetic anisotropy, such as 2D spin reorientation transition, 2D magnetic long range ordering, step induced magnetic behavior. One has to keep in mind that the anisotropy energy is larger in low symmetry lattices than in high symmetry lattices [3].

The simplest form of magnetic anisotropy is the uniaxial anisotropy that exists if there is a broken translational symmetry. This type of anisotropy can also exist in the bulk materials with

a non-cubic symmetry. To the lowest order, the anisotropy energy of a ferromagnetic layer can be written as

$$E_{an} = K \sin^2 \theta \tag{2.7}$$

where θ is the angle between the magnetization and the surface normal and K (J/m^3) is the effective anisotropy energy density, which could be separated in a volume contribution K_v (J/m^3) and a contribution from the interfaces K_s (J/m^2) and approximately obeyed the relation:

$$K = K_{eff} = K_v + 2K_s / t \tag{2.8}$$

This relation represents a weighted average of the magnetic anisotropy energy (MAE) of the interface atoms and the inner atoms of a magnetic layer of thickness t. The relation is presented under the convention that K_s / d (with d the thickness of a monolayer) represents the difference between the anisotropy of the interface atoms with respect to the inner or bulk atoms. Also the layer is assumed to be bounded by two identical interfaces accounting for the prefactor 2. A positive K_{eff} means the system favors magnetization perpendicular to the layer plane. The negative K_{eff} means the system favors in-plane magnetization. The interface anisotropy, initially proposed by Neél, is generated because of the broken translational symmetry along the surface normal direction and able to overcome the shape anisotropy and induce a stable perpendicular magnetization in ultrathin films and multilayers. The strength of the magnetic surface anisotropy is inversely proportional to the layer thickness t. Below a certain thickness $t_c = -2K_s / K_v$ the interface anisotropy contribution outweighs the volume contribution, resulting in a perpendicularly magnetized system. Above this critical limit, the magnetization will become in-plane. This directional switching of the magnetization is called a spin reorientation transition

(SRT). As will be shown later on, the volume energy corresponding to these demagnetizing fields form the major contribution to K_v in most cases.

Basically, the two main sources of the magnetic anisotropy are the magnetic dipolar interaction and the spin-orbit interaction. In the absence of spin-orbit and dipolar interaction, the total energy of the electron-spin system does not depend on the direction of the magnetization.

2.4.1 Magnetic dipolar anisotropy (shape anisotropy)

Among the most important sources of the magnetic anisotropy in thin films is the long range magnetic dipolar interaction, which senses the outer boundaries of the sample. Due to its long range character, the dipolar interaction generally results in a contribution to the anisotropy, which depends on the shape of the specimen and is largely responsible for the in-plane magnetization usually observed. Neglecting the discrete nature of matter, the shape effect of the dipolar interaction in ellipsoidal ferromagnetic samples can be described, via an anisotropic demagnetizing field, H_d given by $H_d = -NM$. Here M is the magnetization vector and N is the shape dependent demagnetizing tensor. For a thin film, all tensor elements are zero except for the direction perpendicular to the layer: $N^{\perp} = 1$. The magnetostatic energy can be expressed as

$$E_d = -\frac{\mu_0}{2V}\int M \bullet H_d \, dv \tag{2.9}$$

where μ_0 is the permeability of vacuum. The results of an anisotropy energy contribution per unit volume V of a film is:

$$E_d = \frac{1}{2}\mu_0 M_s^2 \cos^2\theta \tag{2.10}$$

Here the magnetization is assumed to be uniform with a magnitude equal to the saturation magnetization M_s and subtends an angle with the film normal. According to this expression, the contribution favors an in plane preferential orientation for the magnetization. Because the thickness of the film does not enter into the continuum approach employed above, it contributes only to K_v.

However when the thickness of the ferromagnetic layer is reduced to only a few monolayers (ML), the film should not, in principle, be considered as a magnetic continuum, but has to be treated as a collection of discrete magnetic dipoles on a regular lattice. Depending on the symmetry of the interface, the outer layers experience a dipolar anisotropy which can be appreciably lower than the inner layers. For the inner layers, the dipolar anisotropy is rather close to the value based on the continuum approach. Consequently, the average dipolar anisotropy can be phenomenologically expressed by a volume and an interface contribution. The magnitude of the dipolar interface contribution, however, is of minor importance, and other sources of interface anisotropy, such as spin orbit coupling, appear to be dominant.

2.4.2 Magnetocrystalline anisotropy

In a localized picture, the spins are coupled via the spin-orbit interaction to the orbits which, in turn, are influenced by the crystal lattice. For itinerant materials, the spin-orbit interaction induces a small orbital momentum, which then couples the total (spin plus orbital) magnetic moment to the crystal axes. This result is a total energy which depends on the orientation of the magnetization relative to the crystalline axes, and which reflects the symmetry of the crystal. This is known as the magnetocrystalline contribution to the anisotropy. As a conclusion, the magnetocrystalline anisotropy originates from the spin-orbit interaction, which

transfer the lattice symmetry from the electron wave functions to the electron spins to break the spin isotropy. Thus, magnetocrystalline anisotropy gives special directions for the electron spins.

2.4.3 Magneto-elastic anisotropy

Strain in a ferromagnet changes the magnetocrystalline anisotropy and may thereby alter the direction of the magnetization. This effect is the inverse of magnetostriction, the phenomenon that the sample dimensions change if the direction of the magnetization is altered. The energy per unit volume associated with this effect can, for an elastically isotropic medium with isotropic magnetostriction, be written as

$$E_{me} = -K_{me} \cos^2 \theta \tag{2.11}$$

with $K_{me} = -\frac{3}{2}\lambda\sigma = -\frac{3}{2}\lambda E\varepsilon$.

Here σ is the stress which is related to the strain, ε, via the elastic modulus E by $\sigma = E\varepsilon$. The magnetostriction constant λ depends on the orientation and can be positive or negative. The angle θ measures the direction of the magnetization relative to the direction of uniform stress. If the strain in the film is non zero, the magneto-elastic coupling contributes in principle to the effective anisotropy. When the parameters are constant (not depending on the magnetic layer thickness, t) this contribution can be identified with a volume contribution K_v.

Strain in films can be induced by various sources. Among them are thermal strain associated with differences in thermal expansion coefficients, intrinsic strain brought about by the nature of the deposition process and strain due to non matching lattice parameters of adjacent layers.

Of particular interest in the present context, is the strain due to lattice mismatch η of a material A deposited on material B:

$$\eta = (a_A - a_B)/a_A \tag{2.12}$$

where a is the lattice parameter of material A or B. If the lattice mismatch between the lattice parameters is not too large, minimizing the total energy leads to a situation whereby, below a critical thickness t_c, the misfit can be accommodated by introducing a tensile strain in one layer and a compressive strain in the other such that ultimately the two materials A and B adopt the same in plane lattice parameter. This regime is called the coherent regime, the lateral planes are in full lattice registry.

The elastic energy associated with the coherent situation is proportional to the strained volume. Increasing the thickness of layer A will therefore increase the elastic energy. This energy increase will not persist. At a certain critical thickness t_c, it becomes energetically more favorable to introduce misfit dislocations which partially accommodate the lattice misfit, allowing the uniform strain to be reduced. The lattice registry is then partially lost and the layers become partially coherent or incoherent.

A separate interpretation of the magnetic anisotropy must be made in the regions above and below t_c. In the coherent region below t_c, the volume anisotropy K_v incoporates shape anisotropy, magnetocrystalline anisotropy (K_{mc}) and strain anisotropy ($K_{me,v}$) with interface anisotropy being solely Néel type.

$$K_s = K_N \tag{2.13}$$

$$K_v = -\frac{1}{2}\mu_0 M_s^2 + K_{mc} + K_{me,v}^{coh} \tag{2.14}$$

with $K_{me,v}^{coh} = \frac{3}{2}\lambda E_A \eta$ [3]. In this region, the influence of misfit strain thus appears as a volume contribution to the anisotropy. In the incoherent region above t_c, the magneto-elastic interface anisotropy has been shown to lead to an apparent interface contribution:

$$K_s = K_N + K_{me,s}^{inc} \tag{2.15}$$

$$K_v = -\frac{1}{2}\mu_0 M_s^2 + K_{mc} \tag{2.16}$$

with $K_{me,s}^{inc} = -\frac{3}{8}\lambda G b$, G is the shear modulus and b is the Burgers vector of the dislocation [3].

2.4.4 Step anisotropy

In this section the subject of magnetic anisotropies arising from steps will be addressed briefly. It is clear that in practice magnetic films are never perfectly flat but exhibit steps in the layer thickness resulting from the particular growth mode or from the surface topology of the substrate on which the film has been deposited. Atoms located at such steps are obviously in a different environment than those located at the flat portions of the surface or within the interior of the film. They are therefore expected to give rise to an additional contribution to the magnetic anisotropy. A quantitative determination of the latter therefore requires control and knowledge of the number of step atoms in the film. One convenient way to manipulate the number of step atoms is to deliberately polish the substrate at a non-zero angle with respect to a crystal axis. Such a procedure yields a terraced surface with known terrace widths and consequently a known number of steps per unit length. This procedure is employed to make a curved substrate. This terraced surface is covered in depth in chapter 4 of this dissertation.

2.4.5 Surface versus interface anisotropy

The distinction between surface and interface is based on the presence, at the boundary of a material, of either vacuum or another material. If the boundary of a material is with another material, then we call it interface anisotropy. And if the boundary of a material is with vacuum, for example a free standing Co monolayer, then we call it surface anisotropy. Such a free standing monolayer cannot be realized experimentally as some means of support is required. One surface can be made but one needs to be equipped for in situ characterization of the magnetic anisotropy to avoid contamination.

The surface anisotropy is usually obtained in a study of the dependence of the magnetic anisotropy on the thickness of a non-magnetic overlayer. After subtracting the contribution of the interface with the supporting substrate found in the same study or obtained from the literature, the contribution of the surface remains. This interface anisotropy is covered in depth in chapter 5 of this dissertation.

2.5 Magnetic Interaction

In general, three types of magnetic interactions exist: (1) dipole-dipole magnetostatic interaction, (2) direct exchange interaction, and (3) electron mediated indirect exchange interaction. The importance of the dipolar interaction is most evident in high density recording media because not only it affects the barrier height for flipping the spin of each individual dot, but also gives a significant contribution to the collective behavior of the dot assemblies. However, it is not clear yet at this moment, whether the dipolar interaction results in faster or slower spin flipping in dot assemblies. But Morup [4] pointed out that in the strong interaction

limit, a transition from a superparamagnetic state to an ordered state might occur. Several years later, Morup's prediction was confirmed both experimentally [5] and theoretically [6] in a coalescence of Co islands on Cu(001) where a long range ferromagnetic order with a Curie temperature of about 200 K was observed.

The other type of magnetic interaction is direct exchange where the electrons on neighboring magnetic atoms interact via an exchange interaction. This is because the exchange interaction proceeds directly without the need for an intermediary. Though this seems the most obvious route for the exchange interaction to take, the reality in physical situations is rarely that simple.

Very often direct exchange cannot be an important mechanism in controlling the magnetic properties because there is insufficient direct overlap between neighboring magnetic orbitals. For example, in rare earth the 4*f* electrons are strongly localized and lie very close to the nucleus, with little probability density extending significantly further than about a tenth of the interatomic spacing. This means that the direct exchange interaction is unlikely to be very effective in rare earths. Even in transition metals, such as Fe, Co, and Ni, where the 3*d* orbitals extend further from the nucleus, direct exchange does not necessarily lead to the observed magnetic properties. These materials are metals which mean that the role of the conduction electrons should not be neglected, and a correct description needs to take account of both the localized and band character of the electrons.

In metals, the exchange interaction between magnetic ions can be mediated by the conduction electrons. A localized magnetic moment spin polarized the conduction electrons and this polarization in turn couples to a neighboring localized magnetic moment a distance *r* away. The exchange interaction is thus indirect because it does not involve direct coupling between

magnetic moments. It is known as the RKKY (Ruderman, Kittel, Kasuya, and Yosida) interaction (it does not present in insulators). The coupling takes the form of $1/r^n$, where r is the distance between the magnetic moments and n is the dimensionality of a system. The interaction is long range and has an oscillatory dependence on the distance between the magnetic moments. Hence depending on the separation it may be either ferromagnetic of antiferromagnetic. The coupling is oscillatory with a period of π / k_F, k_F is a wave vector of a Fermi surface and thus depends on the orientation of the Fermi surface.

The indirect exchange interaction, which explains very well the occurrence of the oscillatory behavior in the coupling between two ferromagnetic layers separated by a nonmagnetic layer, has been considered to have little effect on promoting a global ferromagnetic order in a randomly distributed dot assembly because the origin of the oscillatory behavior is a spin dependent quantum size effect. This belief needs to be modified because, as we will discuss soon, Pierce *et al* [7] observed ferromagnetic stability in Fe nanodot assemblies on Cu(111) induced by indirect coupling through the substrate. The ferromagnetic ordering temperature appears to be strongly dependent on the average spacing between the dots. As will be shown later in the section 2.6, for relatively dense nanodot assemblies, the exchange interaction is strong enough to allow the ferromagnetic order persists above room temperature.

Besides the dipolar interaction and indirect exchange interaction, other non-classical ferromagnetic interactions between nanodots include (1) the weak magnetic Casimir force [8] that arises from zero-point quantum fluctuation when the magnetic order changes, and (2) magnetic coupling by tunneling electrons [9] which exists only if the insulating substrate is used where the tunneling barrier is small. In a specific case, the tunneling induced coupling was

reported to be the origin for the room temperature ferromagnetism in Fe dots on insulating CaF_2/Si(111) substrate [10].

Competing with thermal fluctuations, the dipolar magnetic interaction, indirect exchange interaction, Casimir force, tunneling induced coupling, along with the size dependent magnetic anisotropy should have strong influences on the overall magnetic behavior of a magnetic dot assembly. Therefore, to understand the magnetism of a nanodot assembly, it is essential to distinguish the relative roles of magnetic anisotropy and the magnetic interactions (dipolar interaction, indirect exchange interaction, and tunneling induced interaction). To tackle these challenging issues, we consider the following points:

- Magnetic anisotropy is generally related to the properties such as crystallographic structure, size and shape of each individual particle; while the dot-dot interactions are strongly dependent on both the size and the spacing between the dots.
- Dipolar interaction is much less affected by the electronic structure of the host matrix as compared to the indirect exchange interaction; while the tunneling induced interaction occurs only when the hosting template is an insulator.

Each interaction has its own characteristic dependence on the dot-dot spacing, D. Dipolar interaction decays as $1/D^3$, indirect exchange interaction decays as $1/D^2$ if it is mediated by surface states, and tunneling induced interaction decays exponentially as e^{-D}.

2.6 Results from prior studies: Tailored magnetic nanostructures on surfaces

If the surface free energy of the materials being grown is higher than that of the substrate, then the dots can grow directly on the substrate; otherwise a growth technique, so called BLAG

(Buffer Layer Assisted Growth), needs to be employed to assist the indirect growth of the dots. In the BLAG method, an inert gas buffer layer (Xe, for example) is adsorbed on a substrate with very low adsorption temperature (~30 K), for example 240 L [1 L = 10^{-6} Torr-sec], to allow a solid phase of Xe to form on top of the substrate; then the magnetic nanodots are formed on top of that frozen buffer layer. The low surface free energy and the high mobility of adatoms on Xe should allow nanodots to form easily on the buffer layer. After that, the buffer layer is evaporated away by gently warming the system up to room temperature to allow the dots to land on the substrate.

Surprisingly, even though the surface free energy of Fe is higher than Cu, direct deposition of Fe on Cu(111) does not result in the growth of Fe nanodot; and buffer layer assisted growth method was employed to grow Fe dot on Cu(111). Unlike Fe/Cu(111) films which exhibit perpendicular magnetization at low thickness, the easy magnetization axis of the Fe/Cu(111) dots lies in the plane of the Cu(111) surface.

In situ MOKE measurements reveal collective ferromagnetic stability behavior in these two-dimensional Fe dot assemblies supported by single crystal Cu(111) surface. Due to the superparamagnetic nature of the nanodot assembly [see section 2.3.1], the occurrence of ferromagnetism in this low dimensional system is very remarkable. Even more intriguing is the unusually high blocking temperature ~120 K, contrary to the theoretical calculation ~2 K. The Monte Carlo simulation, performed on this system, rules out the dipolar interaction as the major driving force for the observance of such ferromagnetic behavior. Without dipolar interaction, the critical temperature would be 100 K, which is still significantly higher than 2 K [see figure 2.4].

In order to find the major driving force behind the collective ferromagnetic ordering in this Fe/Cu(111) low dimensional assemblies, Pierce *et al* [7] systematically study the roles of

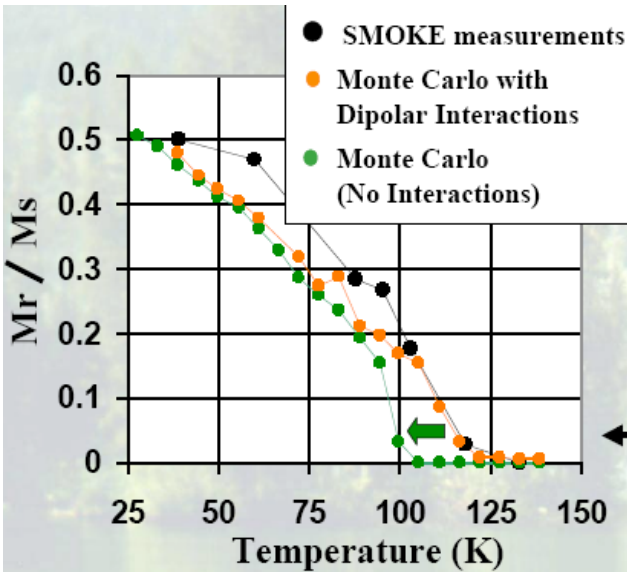

Figure 2.4: Result of the Monte Carlo simulation, performed on the Fe-dot assemblies on Cu(111) substrate. Without dipolar interaction, the critical temperature would be ~100 K which is still significantly higher than ~2 K. Dipolar interaction is not the major driving force for the ferromagnetism in Fe-dots/Cu(111). [after reference 15]

interactions and magnetic anisotropies in stabilizing the ferromagnetic behavior. They control the density and the size of the dots by changing the Xe exposure as well as the Fe dosage. Figure 2.5 (a) shows the size and density of Fe dots for a 200 L exposure of Xe as a function of the Fe dosage; while figure 2.5(b) the size and density dependence on the Xe exposure for 1 ML Fe. The results are quite surprising: the Xe exposure has more dramatic effect in changing the size of the dots than the Fe dosage. Figure 2.6 shows that by fixing the dot's size and changing the dot's density by a factor of 5 ($0.3 \times 10^4/\mu m^2$ to $1.5 \times 10^4/\mu m^2$), the remanent magnetization as a function of temperature changes dramatically. The repeated experiment on different pair of dot assemblies shows the same result. Since the dots' sizes are equal, the contribution of the magnetic anisotropy to the thermal stability of M_r in each case should be identical. The discrepancy of T_c allows us to rule out the enhanced magnetic anisotropy as the root of the high T_c ferromagnetism and infer the existence of strong dot-dot interactions for stabilizing the ferromagnetic order in this system, although the anisotropy energy and the dipolar contributions can not be neglected.

To further investigate the origin of the dot-dot interactions, Torija *et al* [7] performed a series of experiments to manipulate the density of states of the substrate in several ways:

(1) Growing Fe dots on different substrates. They prepared 1 ML of Fe nominal thickness on Cu(111), Cu(100), and Ge(111); the plot of critical temperature of Fe dot assemblies as a function of Xe exposure exhibit that Fe dots grown on Cu(111) has the highest T_c while the dots grown on the semiconducting Ge(111) has the lowest T_c [see figure 2.7]. Cu(111) has the most pronounced surface states.

(2) Capping the Fe dots with the substrate material (copper) to change the coupling between Fe dots from the surface states to bulk states. It is shown in figure 2.8(a) that capped Fe-dots have lower T_c compare to uncapped Fe-dots;

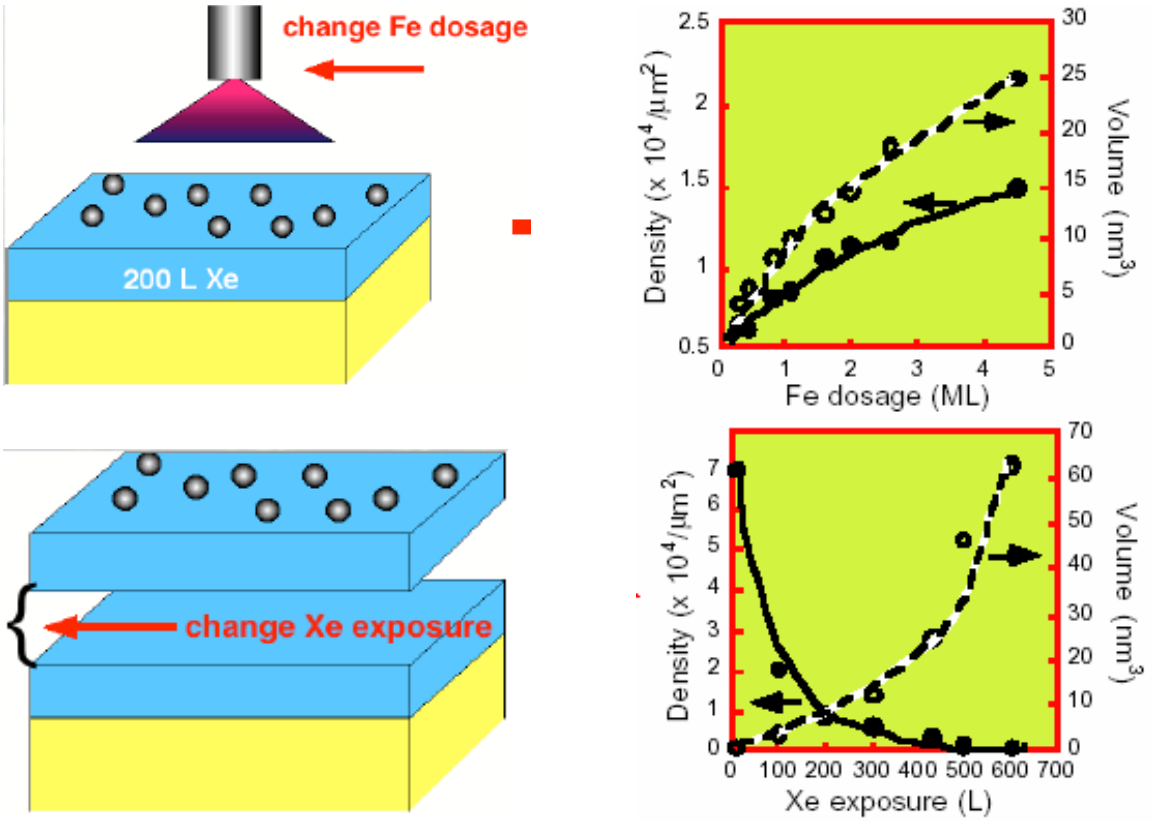

Figure 2.5: Average size and density of Fe/Cu(111) dots assemblies as a function of (a) Fe dosage , and (b) Xe exposure. The solid and dashed lines are the guides for the eyes. [after reference 7]

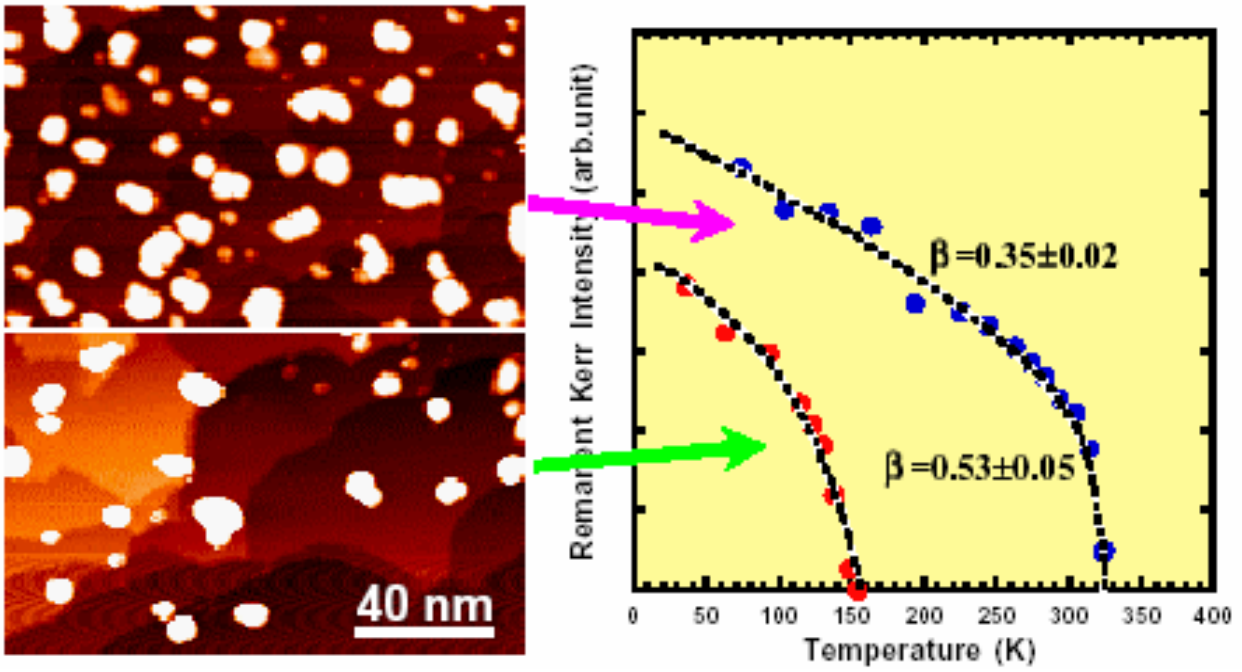

Figure 2.6: Morphology of two Fe/Cu(111) nanodot assemblies with the same average size but different density. The denser dot assembly exhibits a considerably higher Curie temperature [after reference 7]. Magnetic anisotropies unimportant but the dot-dot interactions are the major driving force in stabilizing ferromagnetic ordering on Fe/Cu(111) nanodot assemblies.

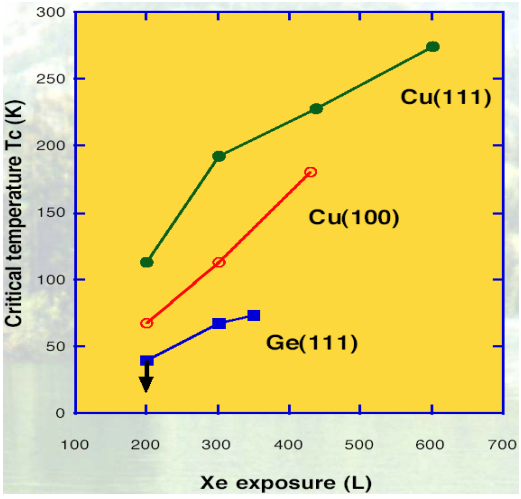

Figure 2.7: T_c of 1 ML Fe-dot assemblies on various substrates: Cu(111), Cu(100), Ge(111) as a function of Xe exposure. The arrow for the Fe/Ge(111) dots (200 L Xe) indicates that the T_c is below 40 K. [after reference 7]

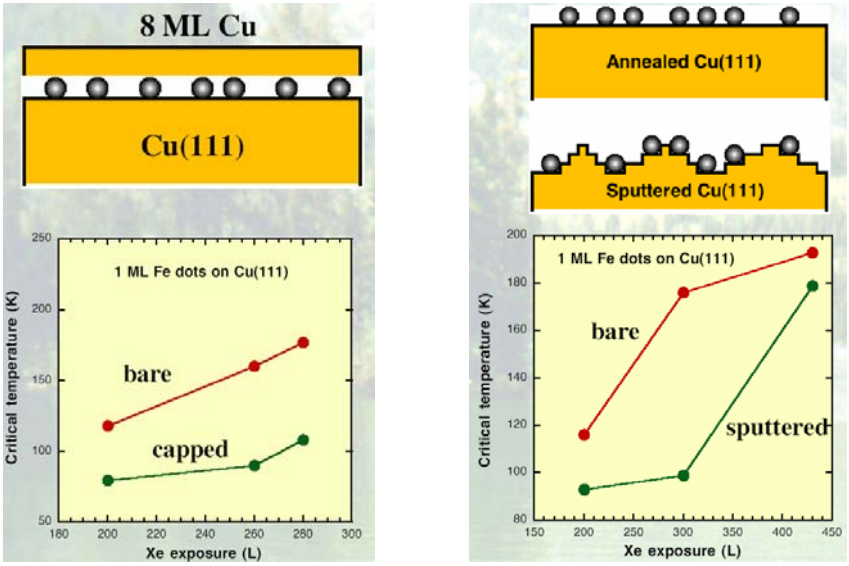

Figure 2.8: Fe-dots grown on (a) Cu(111) {bare: red line} has considerable higher T_c than when the Fe-dots are capped with Cu {capped: green line}. (b) annealed/ smooth Cu(111) {bare: red line} has higher T_c than when the dots are grown on rough Cu(111) surface {sputtered: green line}. [after reference12]

(3) Growing the Fe dots on annealed and non-annealed substrates. Figure 2.8(b) shows that the Fe dots grown on the smooth/ annealed Cu(111) substrate have higher T_c than when they are grown on the rough/ non-annealed substrate.

These results show that the substrate-mediated indirect exchange interaction stabilizes the ferromagnetism in Fe/Cu(111) dot assemblies.

Torija *et al* [11] also designed a new experiment to study the crossover from 2D to 3D surface states by stacking the 2D Fe nanodot assemblies with Cu spacer layers to allow the formation of multilayer Fe nanodots. They observed a striking ferromagnetic to spin glass transition where the topmost layer of the Fe dots remains to be ferromagnetic throughout the phase transition creating a live surface ferromagnetism, while all the layers underneath behave like a spin-glass system. This interesting scenario is likely caused by the fact that the surface state-mediated coupling is stronger than the coupling in bulk layers. Figure 2.9 shows the schematic view of multilayer dot assembly. Figure 2.10 (a) shows the N (number of multilayer Fe-dot) dependence of saturation magnetization, M_S, and (b) the relative critical temperatures, T_c.

All results from the previous studies show the importance of the surface state electrons in stabilizing the collective ferromagnetic behavior on Fe/Cu(111) nanodot assemblies.

2.7 One-dimensional quantum wells in metal-on-metal systems

2.7.1 Bound states in finite potential wells

Let's recall the undergraduate physics problem of a particle in a one-dimensional box which is a representative problem of a one-dimensional well with infinite barriers. Although this is a very crude model, it serves to illustrate the basic ideas and provides a good starting point.

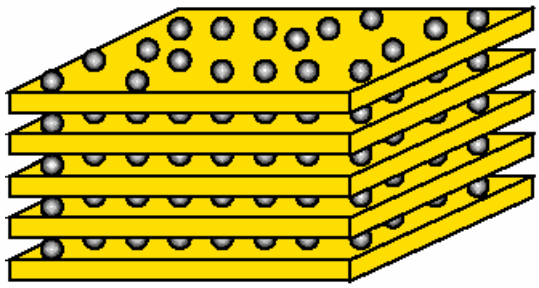

Figure 2.9: Schematic view of mutlilayer dot assembly for magnetic critical behavior study.

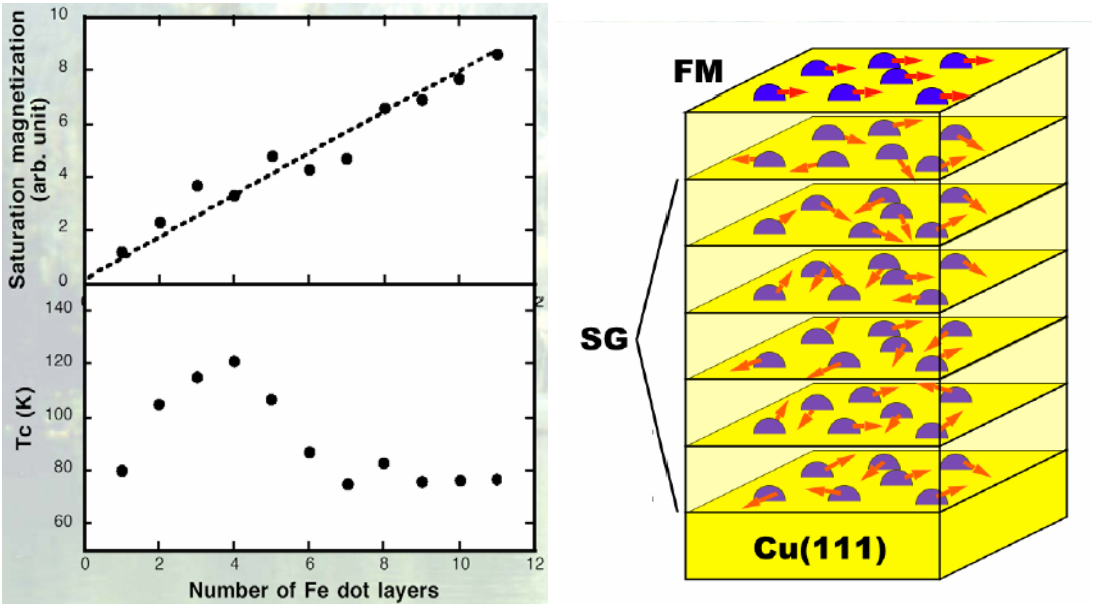

Figure 2.10: (a) (top) The N (number of multilayer Fe-dot) dependence of saturation magnetization, M_S, and (bottom) the relative critical temperatures, T_c. Saturation magnetization increases linearly with increasing N, which is expected since all the Fe-dot layers contribute to the measured of M_S under the saturation field. In contrast, T_c vs. N shows dramatically different behavior, which strongly suggests that the surface and bulk Fe-dot layers have distinctly different magnetic behavior. (b) Schematic picture of the speculated spin structures of the Fe dots multilayer in regions I, II, and III. [after reference 11]

The key result is that the particle or an electron must be represented by a standing wave having nodes at the walls of the well. The allowed wave vectors k for stationary states, or quantum well states, are determined by the requirement that standing wave patterns fit into the geometry:

$$k = \frac{n\pi}{L} \tag{2.17}$$

where n is an integer quantum number and L is the film thickness or box dimension. The energy levels are given by

$$E_n = \frac{\hbar^2 k^2}{2m} = n^2 \frac{h^2}{8mL^2} \tag{2.18}$$

where m is the free electron mass and h is Planck's constant. The wave functions are given by

$$\psi(z) \propto \sin\left(\frac{n\pi z}{L}\right) \tag{2.19}$$

Figure 2.11(a) shows the associated wavefunctions for the lowest lying states. Notice that in this rectangular well, the quantized energy levels have energy proportional to n^2, and thus become more widely spaces as the energy increases. By contrast, the quantized energy level in the hydrogen atom is proportional to $1/n^2$, thus becoming more and more closely spaced with increasing n.

A somewhat more realistic model of the particle-in-a-box problem is to take a rectangular well with finite potential walls. In this case the solutions are very similar to those of the infinite barrier walls, but the wavefunctions at the well walls inside the well walls inside the well now match the exponential tails outside the well (see figure 2.11(b)). The proper solution is already more complicated but it is clear that the presence of the exponential tails on the wavefunctions

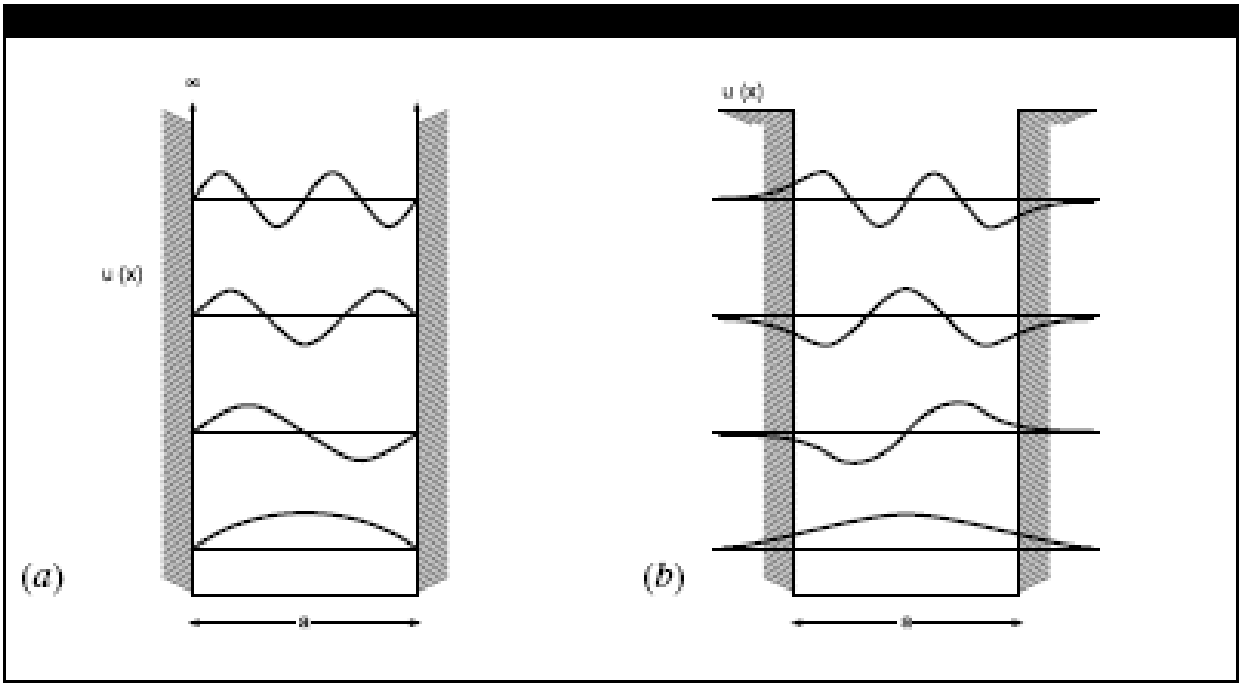

Figure 2.11: Schematic representations (not normalized) of the wavefunctions of the first few solutions for electron states in a one-dimensional square potential well, $U(x)$, of width a with (a) infinite walls, and (b) finite walls. [after reference 13].

leads to a slight increase in the wavelength relative to the infinite barrier case and thus a slight lowering of the energies. A rather direct practical illustration of this problem, which has been observed using STM, is the case of electron states localized at metal surfaces which may also be constrained in their motion parallel to the surface by being trapped between two (single-atom height) atomic steps. Figure 2.12 shows an example of results from such an experiment. The surface under study is Ag(111), which is known to show a surface-localized (Shockley) state which is free-electron-like in its movement parallel to the surface. The state is localized at the surface because it has a binding energy which lies in a gap in the projection of the bulk band structure onto this surface. Two parallel surface steps then provide scattering barriers which effectively form a one-dimensional well. In STM one measures the electron current which tunnels through the vacuum gap between the surface and a fine conducting tip brought to within atomic dimensions of the surface. By varying the bias voltage between these, one detects changes in the current as the bias makes new bound states accessible for tunneling, and the spatial variation of this change, as one scans the tip along the line between the two steps, provides a rather direct way of observing the spatial variation of the charge-density standing wave. At different bias voltages, corresponding to the bound state energies of these quantized energy states, one can map out the different charge densities. Figure 2.12 shows rather graphically that these variations are very similar to those predicted for the simple finite rectangular well of figure 2.11(b).

2.7.2 Particle in a flat box

Quantum well states are usually associated with discrete quantized electronic states in small artificial structures with adjustable physical dimensions. The interesting questions are:

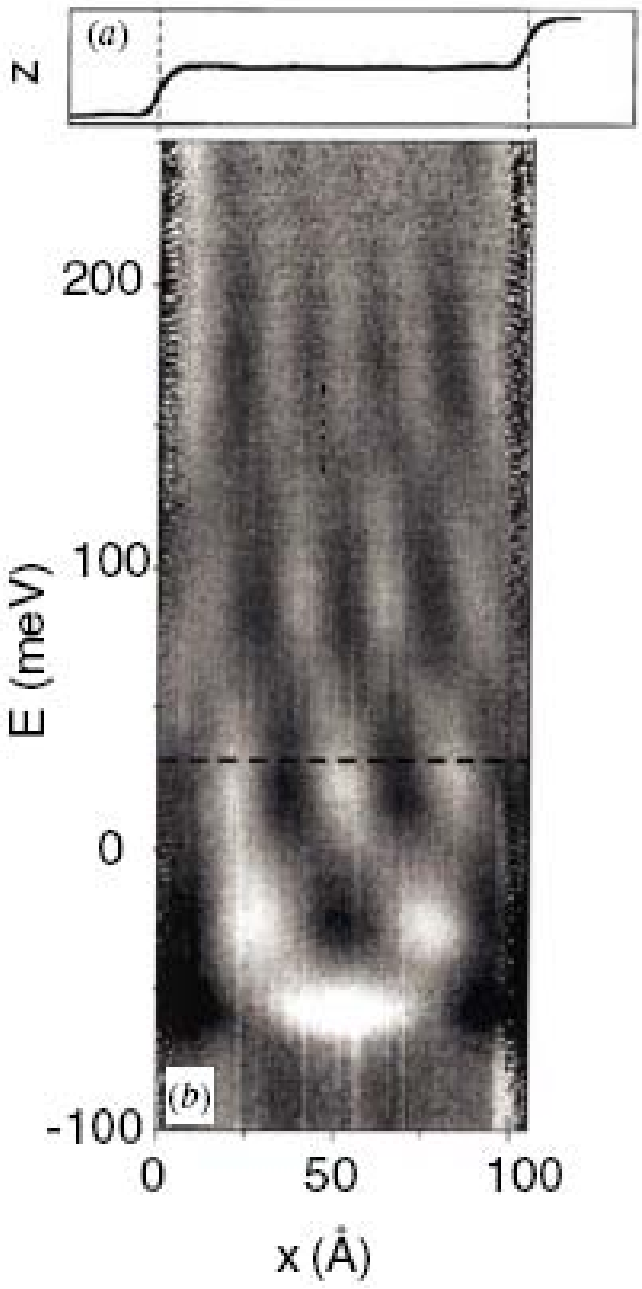

Figure 2.12: (a) STM constant-current line scan of the relative tip height above the surface over a 104 Å wide Ag(111) terrace confined by two single-atom-height steps that act as electron mirrors (broken lines). (b) Grey scale representation of the corresponding differential conductance as a function of sample-tip voltage showing the spatial variations in the electron density at different energies due to the confinement of the *s*-*p* surface state electrons [after reference 14].

(1) Do the quantum well states exist in magnetic nanostructures? (2) How do the quantum well states behave in metallic systems? There are no absolute gaps at the Fermi level in metals, and electrical conduction through a metal-to-metal junction is an everyday experience. There are no such things as threshold voltages or rectifying junctions as in semiconductors. For these reasons, one might have the impression that confinement in a metallic system would be impossible/ rare. It is not. For epitaxial films, all that is required is a 'relative gap' in the substrate. Namely, if there is a gap for a particular direction (usually perpendicular to the film), electrons propagating along that particular direction can be confined. Relative gaps are actually fairly common in metals. Electrical conduction through a metal-to-metal junction is not a direction-specific probe of the junction properties. It involves a wide range in **k** space, and therefore the gap effect is generally not apparent.

In the case of metallic films deposited on metal surfaces, the natures of the two barriers which create the QW at the substrate/film interface and at the film/vacuum interface are quite different. At the surface/vacuum interface, the barrier arises because we are concerned with bound states which lie between the bottom of the conduction band of the film and the vacuum level. At the film/substrate interface, on the other hand, an electron can only be confined in the film if its energy lies in a band gap of the substrate. Of course, a metal does not have a total gap in the occupied part of the conduction band; however, the electronic bands of a real metal depend on the direction, and the Fermi surface is far from spherical for many metals, so gaps do appear around the Fermi level in specific directions. Moreover, even in directions in which the metal does have band states around the Fermi level, the fact that these states have a well-defined symmetry may mean that there is a 'symmetry gap' relative to states in the film of a different symmetry which cannot then couple to the bulk states. In practice, there are many metal surfaces

for which, relative to propagation perpendicular to the surface, the solid has a band gap (or a symmetry gap) which may have a width of a few eV and is centered within a few eV of the Fermi level. Under these circumstances an electron in the overlayer film moving perpendicular to the surface with an energy lying within the projected bulk gap cannot couple to any bulk states and will therefore be reflected at the film/substrate interface.

In order to gain a quantitative understanding of this situation, quantum well state positions in the energy-thickness plane are calculated by using phase accumulation model (also referred to as the Bohr-Sommerfeld quantization rule) where one treats the problem as one of a travelling electron wave bouncing back and forth between the substrate/film and film/vacuum interface. If the round-trip phase accumulation associated with the propagation between the barriers and the phase shifts associated with reflections is an integral multiple of 2π, then a standing wave solution corresponding to a bound state occurs. The simplification achieved by treating the problem in this way arises because one can describe the influence of the underlying substrate by a phase shift, ϕ_C, experienced at the substrate/film boundary which can be calculated from a simple two-band model of the substrate. The condition for a standing wave, and thus a quantized state of the well of width L, is

$$\phi_B + \phi_C + 2kL = 2\pi n \tag{2.20}$$

where k is the electron wave vector in the film perpendicular to the surface, $2kL$ is the phase accumulated in traveling back and forth in the film and ϕ_B is the phase shift on reflection at the film/vacuum interface [13]. Notice, incidentally, that L is measured between the two interfaces, usually taken to be located at one half of an atomic layer spacing beyond the termination of the crystal substrate and the outermost atom layer of the film. The fact that the image potential

barrier extends beyond this terminating plane is accounted for in the associated phase shift. A useful approximation for this phase shift is

$$\frac{\phi_B}{\pi} = \sqrt{\frac{3.4(eV)}{E_V - E}} - 1 \tag{2.21}$$

in which the energies of the vacuum level, E_V, and of the bound state of the electron, E, are expressed in eV. For the substrate/film phase, the phase shift at the interface varies from $-\pi$ at the bottom of the band gap to 0 at the top, and in a simple two-band nearly-free electron picture of the substrate one can write as an approximate and purely empirical formula

$$\phi_C = 2\sin^{-1}\sqrt{\frac{E - E_L}{E_U - E_L} - \pi} \tag{2.22}$$

where E_L and E_U are the energies of the lower and upper energies of the band gap [13].

Chapter 3 Experimental Details and Apparatus

3.1 Synthesis of Fe dots on Cu(111)

It is known that when the surface free energy of the materials being grown is higher than that of the substrate, then the dots can grow directly on the substrate, e.g. Cobalt nanodots can grow directly on TiO_2 substrate. On the other hand, due to the lower surface free energy of the Fe than Cu, direct deposition of Fe on Cu(111) does not result in the growth of Fe nanodot; thus buffer layer assisted growth (BLAG) is employed to assist the indirect growth of Fe nanodots on Cu(111) substrate. The BLAG method involves two crucial steps:

(1) An inert gas buffer layer (Xe, for example) is adsorbed on a substrate with very low adsorption temperature (~30 K) for different Langmuir (L) Xe coverage [1 L = 10^{-6} Torr-sec] to allow a solid phase of Xe to form on top of the substrate then the magnetic Fe nanodots are formed on top of that frozen buffer layer. The low surface free energy and the high mobility of adatoms on Xe should allow nanodots to form easily on the buffer layer because the dots tend to form clusters, rather than wet the surface.

(2) After that, the buffer layer is evaporated away by gently warming the system up to room temperature to allow the dots to land on the substrate. It is confirmed that the epitaxial crystalline order is restored by this post-deposition annealing. One has to put in mind is that when the Xe layer is evaporated, it carry some Fe-dots, leaving the substrate with less Fe-dots coverage than one initially thought and can drastically affect the spatial and size distributions of the dots. The size and spatial distribution of the Fe dots can be modified by varying either the thickness of the Xe buffer layer or the dosage of Fe atoms.

Figure 3.1 gives a schematic view of the two crucial steps involved in the BLAG method. STM studies indicate that the BLAG process results in the formation of Fe dots on the Cu substrate that are shaped like flattened hemispheres.

After the sample is made, the in-situ study of magnetic properties is performed by using SMOKE both in the polar (magnetic field is applied perpendicular to the plane) and longitudinal (magnetic field is applied parallel to the plane) geometry. Occasionally, SQUID (Superconducting Quantum Interference Device) will be used for the ex-situ magnetization measurement after the sample is capped with a nonmagnetic material to prevent the oxidation of the dots.

The experiment itself is conducted at ORNL and University of Tennessee by using the state of art MBE (Molecular Beam Epitaxy) equipped with the analysis tools for the in-situ study, e.g. AES (Auger Electron Spectroscopy), LEED (Low Energy Electron Diffraction), SMOKE (Surface Magnetic Optical Kerr Effect) and VT STM (Variable Temperature Scanning Tunneling Microscopy). Details will be provided in the characterization technique. All of the tools mentioned above are operated under the ultra high vacuum environment with the pressure around $1x10^{-10}$ Torr so that the surface contamination and oxidation can be significantly reduced.

In chapter 4, we find a new way to smoothly modify the surface state by introducing curved Cu(111) substrate. The curved Cu(111) substrate changes from 0° to 8° miscut angle continuously [see figure 3.2]. By using this method, we can ensure the same growth parameter for the whole miscut angle studied and systematically study the effect of quasi 2D and 2D surface states on the dot-dot interactions. We study how T_C changes as function of miscut angle for different Xe coverage (L). In chapter 5, semiconducting TiO_2 substrate is used to study the role of magnetic anisotropy and dipolar interaction in the reduced dimensional system.

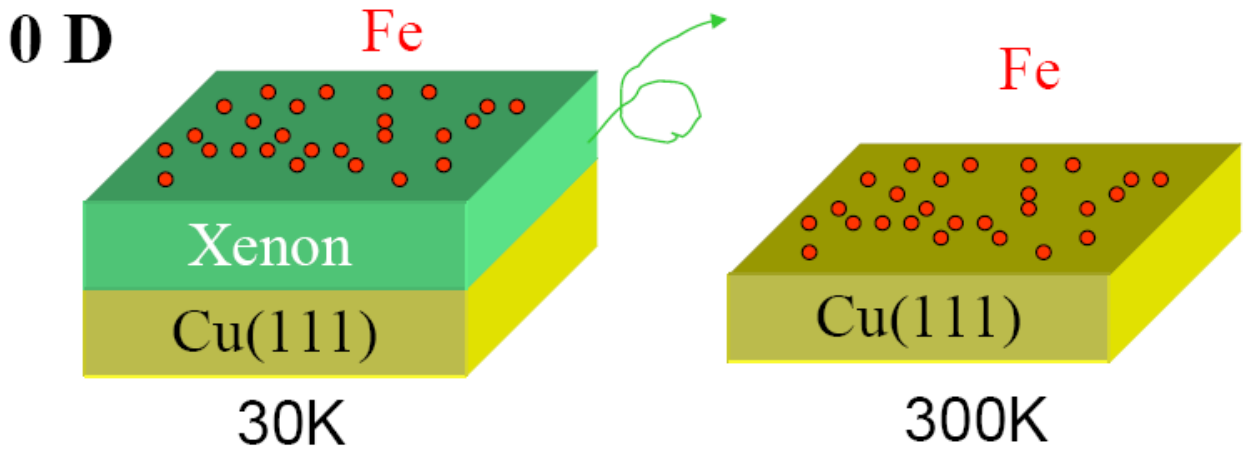

Figure 3.1: Two crucial steps in Buffer Layer Assisted Growth (BLAG). (Left) Xe is adsorbed on a substrate with very low adsorption temperature (~30 K). (Right) Xe is evaporated away by gently warming the system up to room temperature to allow the dots to land on the substrate.

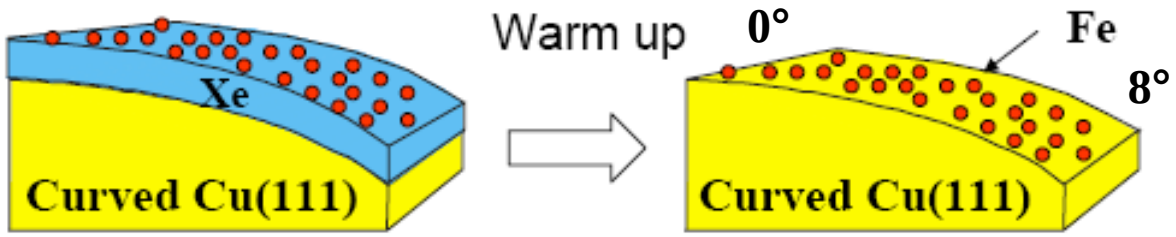

Figure 3.2: Schematic drawing of curved Cu(111) substrate. The miscut angle of curved substrate changes from 0° to 8° continuously. The Fe dots are grown with the BLAG method.

The substrate needs to be polished both mechanically and chemically, then it will be ultrasonically cleaned before we introduce it into the UHV (Ultra High Vacuum) chamber for further intrinsic study. Prior to the thermal deposition, the substrate will be cleaned with subsequent cycles of 1 keV Ne ion sputtering until the sharp AES and LEED signals are obtained.

3.2 Experimental Apparatus

3.2.1 Ultrahigh Vacuum (UHV) chamber

The surface of a material is very prone to contamination or oxidation; therefore a UHV chamber with an excellent base pressure is very crucial to prevent or delay the contamination/ oxidation and keep the sample as clean as possible.

In order to get the excellent base pressure ($1x10^{-10}$ Torr), three types of pump are used. To get a mid-vacuum pressure (10^{-3} Torr), a mechanical/ rough pump has to run for about 15 minutes. After the pressure reach 100 mTorr, a turbo pump backed by a mechanical pump can be turned on to reach high vacuum pressure (10^{-7} Torr or 10^{-8} Torr). The turbo pump rotates its blades as fast as tens of thousand rpm to pump the air out. It usually takes several hours to reach high vacuum stages. The final type of pump is ion pump, which can bring the pressure to $1x10^{-10}$ Torr. The ion pump can not be used to pump away the inert gas, e.g. argon, xenon, neon. These gases will be permanently trapped inside the ion pump which makes the ion pump cannot reach ultrahigh vacuum stages. Turbo pump is the best candidate to pump those gases away. Besides mechanical, turbo and ion pump, Titanium Sublimation Pump (TSP) can be run occasionally to

improve the base pressure quickly. We pass a current, approximately 45 A, through the titanium wire until it sublimates and binds reactive gases, e.g. hydrogen and oxygen.

When we open the chamber, it is important to introduce positive pressure to the chamber by flowing dry gas (e.g. N_2 or He gas) so that air cannot get into the chamber. After the chamber is closed, it will be baked for 48 hours to remove the contaminants, such as H_2O, O_2, CO_2 and CO. Several cycles of degassing the filaments are needed after the baking procedure is done, to insure the amount of contaminants as low as possible.

There are many kinds of gauges to measure the pressure of vacuum chamber. Two kinds of gauges are most often used. One is the Pirani gauge (thermo gauge) which relies on the fact that the ability of a gas to conduct heat decreases with pressure and can measures down to 10^{-3} Torr. Since the gauge only covers low vacuum range, it is often used to check the vacuum between a mechanical pump and a turbo pump. The Pirani gauge head is based around a heated wire placed in a vacuum system, the electrical resistance of the wire being proportional to its temperature. At atmospheric pressure, gas molecules collide with the wire and remove heat energy from it (effectively cooling the wire). As gas molecules are removed, i.e. the system has better pressure or pumped down; there are fewer molecules and therefore fewer collisions. Fewer collisions mean that less heat is removed from the wire and so it heats up. As it heats up, its electrical resistance increases. A simple circuit utilizing the wire detects the change in resistance and once calibrated can directly correlate the relationship between pressure and resistance.

The pressure of ultra high vacuum chamber can be measured by the hot cathode ionization gauge. An ion gauge is mainly composed of three electrodes: a filament, a grid, and a collector; all acting as a triode, where the cathode is the filament. The filament is used for the production of electrons by thermo-ionic emission. The grid has positive voltage which pulls the

electrons from the filament. Electrons circulate around the grid passing through the fine structure many times until eventually they collide with the grid. Gas molecules inside the grid may collide with circulating electrons. The collision can take an electron from the gas molecule and make it positively ionized. The collector inside the grid has negative voltage and attracts these positively charged ions. The number of ions collected by the collector is directly proportional to the number of molecules inside the vacuum system. By this method, measuring the collected ion current gives a direct reading of the pressure.

3.2.2 Thermal Deposition

In thermal deposition, the deposited material is created by thermal evaporation of material from a crucible coiled by tungsten wire. The vacuum allows vapor particles to travel directly to the substrate. This evaporated material then condenses on the substrate. To reduce the degassing of the chamber due to the evaporators or from the evaporators themselves, the crucibles are enclosed by tantalum shell and the whole evaporator is surrounded by a cooling water jacket. The source and the crucible have to be well degassed before growing the samples to avoid the contamination during the deposition. During the evaporation, the pressure should be kept under $1x10^{-9}$ Torr. Almost all metals can be evaporated, although the deposition rate for high melting point metals may be rather low.

The evaporation rate is monitored by using a quartz crystal microbalance and Auger Spectroscopy. The quartz oscillator measures the surface phonon frequency, which decreases with the deposition of materials on quartz due to the change of mass. The rate of reduction of surface phonon frequency is converted to the growth rate using inputs such as density of material, *Z* factors and the tooling factor. *Z* factor is a parameter that corrects the frequency-

change-to-thickness transfer function for the effects of acoustic-impedance mismatch between the crystal and the deposited material. The tooling factor is a ratio of evaporation between the position of QCM and substrate where the sample will grow. The surface phonon frequency also depends on the temperature, thus the QCM is often cooled by water. The density and *Z* ratio of Fe is 7.86 g/cc and 0.349, respectively.

After applying current on an evaporator, the growth rate needs to be watched for tens of minute until the rate become stable. The shutter of the evaporator is then closed so that the substrate can be moved to the growth position. We start growing the sample after the shutter is re-opened. The thickness is calculated from the growth rate and growth time.

Substrate temperature, use of buffer or seed layers and the deposition rate are parameters of the evaporation process that can be manipulated. Typical thermal energies of the condensing atoms are 0.1 eV plus any binding energy liberated at the substrate surface. This implies that the surface mobility can be largely controlled with the substrate temperature. Buffer or seed layers can promote a specific structure or orientation.

3.2.3 Scanning Tunneling Microscopy (STM)

The STM is based on the concept of quantum tunneling. When a conducting tip is brought very near to a metallic or semiconducting surface, a bias between the two can allow electrons to tunnel through the vacuum between them. For low voltages, this tunneling current is a function of the local density of states (LDOS) at the Fermi level, E_F, of the sample. Variations in current as the probe passes over the surface are translated into an image. STM can be a challenging technique, as it requires extremely clean surfaces and sharp tips.

The instrument consists of a sharp conducting tip which is scanned with respect to a flat conducting sample. When a voltage V is applied between tip and sample, a current will flow, and this current can be measured as a function of (x,y) position and as a function of V. If the sample is biased by a positive voltage $+V$ with respect to the tip, this effectively lowers the Fermi level of the sample electrons with respect to the tip electrons. Electrons will tend to flow out of the filled states of the tip into the empty states of the sample. Likewise, if the sample is biased by a negative voltage $-V$ with respect to the tip, this effectively raises the Fermi level of the sample electrons with respect to the tip electrons. Electrons will then flow out of the filled states of the sample into the empty states of the tip.

For most of the time, we only need a topography mode for the STM measurement. In this mode, we raster the tip across the surface at a fixed sample bias voltage V_{set} and employ a feedback loop which controls the voltage on the z piezo to keep the tunneling current constant at I_{set}. By recording the voltage to the z piezo, we can effectively map the contour of the surface.

3.2.4 Auger Electron Spectroscopy (AES)

AES is used to determine the surface appearance, its cleanliness, the elemental composition of the top few layers of the substrate and to analyze the amount of the materials that has been deposited (in term of monolayer/ML). AES is sensitive up to 1% of constituent of the top most layer. This technique probes the material's surface by 3 keV electron beam bombardment to measure the energy of the knock out electrons (Auger electrons) which represent the characteristic of the material's elements. The high energy electron ionizes the atom in the substrate by removing an electron in a core level (call it A; 2s/2p or L level for Cu). One electron from a higher core level falls down to the empty level and fills it (call it B; 3s/3p or M

level for Cu). And another electron is emitted from the substrate (call it C; from *M* level for Cu) with kinetic energy E_{KE} to satisfy energy conservation: $E_{KE} = E_A - E_B - E_C$. The spectral peak positions of the kinetic energy of the emitted electron are determined by core energy levels which are unique to an element. For example, positions of *LMM* peaks of Cu are around 776, 850, and 920 eV; higher than Fe (598, 651, and 703 eV). Oxygen and carbon have *KLL* peaks around 500 and 300 eV, respectively. From the spectrum, the constituents of substrate can be checked by comparing the intensity of the peaks that belong to different materials. The surface sensitivity of AES comes from escape depth of the emitted electron so it is only sensitive to the first few atomic layers. Since the electrons in the heavy elements are more tightly bound to the nucleus, the emission of Auger electrons is more probable for lighter elements than heavy elements and therefore AES technique is more sensitive to the lighter elements.

3.2.5 Low Energy Electron Diffraction (LEED)

LEED is used to determine the structural properties of the surface, such as surface symmetry, surface reconstruction, or the smoothness. An electron beam, of which the de Broglie wavelength is around the inter-atomic distance of the surface, are directed to the surface and then the elastically back-scattered electrons form diffraction patterns in the surface reciprocal lattice on the phosphor screen which can be interpreted to yield the surface real-space lattice vector. Since the lattice constants are in the order of 1 Å, the energy of electron is chosen between 30-300 eV. Relation between energy and de Broglie wavelength are: $E = \frac{p^2}{2m} = \frac{h^2}{2m\lambda^2} = \frac{150.8eV}{\lambda^2}$

where E is energy, p is momentum, m is mass, λ is de Broglie wavelength and h is Planck constant.

Surface sensitivity of LEED is also determined by the scattering cross section of electron. Since LEED uses elastically diffracted electrons, both its incoming and outgoing electrons have a large back scattering cross section, thereby contributing to the surface sensitivity. Quality of substrate can be known from the sharpness of diffraction spots or existence of reconstruction pattern.

3.2.6 Surface Magneto Optic Kerr Effect (SMOKE)

SMOKE is a powerful and inexpensive method to study the surface magnetism. The time reversal symmetry is broken the magnetic system, thus giving rise to different optical response of right and left polarized light. Magneto-optic effects can be explained through macroscopic dielectric theory or microscopic quantum theory. Macroscopically, magneto-optic effects originate from the antisymmetric, off-diagonal elements of the dielectric tensor [2,3]. Microscopically, the spin-orbit interaction that couples the electron spin and the orbital motion is responsible for the magneto-optic effects [2,3].

Light consists of left- and right-circularly polarized modes. As it propagates in a medium, the electrical field of the light generates the motions of the electron in the medium. In a non-magnetized medium, there will be no Faraday rotation. The two circularly polarized modes will propagate with the same velocities; therefore the electron orbit of the left- and right-circularly polarized light has the same radius. When light propagates in a magnetized medium, there are two processes that will take place. First, the two circularly polarized components will gain different phase shifts due to their different propagating velocities, resulting in a rotation of the polarization plane. Second, the different absorption rates of the medium for the two circularly polarized modes affect the ellipticity.

3.2.6.1 Macroscopic origin of the magneto-optic effect

The 3x3 dielectric tensor of a medium, ε_{ij} with i, j = 1, 2, 3, can be decomposed into symmetric and antisymmetric parts. A medium that has the symmetric part diagonalized and the dielectric tensor is reduced to a dielectric constant, ε_0 is called isotropic medium and does not give rise to the Faraday Effect. To understand the effect of the antisymmetric part of the dielectric tensor, let's analyze the following dielectric tensor:

$$\tilde{\varepsilon} = \varepsilon \begin{pmatrix} 1 & iQ_z & -iQ_y \\ -iQ_z & 1 & iQ_x \\ iQ_y & -iQ_x & 1 \end{pmatrix} \tag{3.1}$$

The two normal modes are left circularly polarized with $\varepsilon_L = \varepsilon\left(1 - \mathbf{Q} \bullet \hat{\mathbf{k}}\right)$, and right circularly polarized with $\varepsilon_R = \varepsilon\left(1 + \mathbf{Q} \bullet \hat{\mathbf{k}}\right)$, where $\mathbf{Q} = \left(Q_x, Q_y, Q_z\right)$ is known as the Voigt vector which is proportional to the magnetization vector, and $\hat{\mathbf{k}}$ is the unit vector along the light propagation direction. Thus, it is the off-diagonal antisymmetric parts of the dielectric tensor $\mathbf{Q} = \left(Q_x, Q_y, Q_z\right)$ that produce the difference in the refractive indexes between the two circularly polarized modes and give rise to the Faraday Effect. The real part of the complex rotation is responsible for the Faraday rotation, and the imaginary part yields the Faraday ellipticity.

3.2.6.2 Microscopic origin of the magneto-optic effect

Hulme [4] pointed out that the magneto-optic effect microscopically originated from the spin-orbit interaction that couples the electron spin to its orbital motion. The spin-orbit interaction, $\sim \left(\nabla \mathbf{V} \times \mathbf{p}\right) \bullet s$, is a consequence of the interaction between the electron spin ***s*** with the magnetic field it experiences when it moves with momentum ***p*** through the electric field

$-\nabla \mathbf{V}$ inside a medium. As a result of this spin-orbit interaction, the optical response, i.e. speed and absorption coefficient of light in the media, between left and right polarized light will be different. When the linear polarized light shines on the magnetic sample, difference of the phase shifts of the left polarized part and the right polarized part make polarization direction rotates. This effect gives Kerr rotation. The difference in absorption changes polarization from linear to elliptic. This effect gives Kerr ellipticity. In magnetic material, both Kerr rotation and Kerr ellipticity exist. However, in metals, Kerr ellipticity usually dominates over Kerr rotation.

Hulme also calculated the two refraction indices for right and left polarized light by using the Heisenberg model of a ferromagnet and got the conclusion that the different in the two refraction indices is a result of the energy splitting due to the spin-orbit interaction. This theory is somewhat unsatisfying because the quenching of the orbital angular momentum in ferromagnets gives no energy splitting. He did not take into account the change of the wave function due to the spin-orbit interaction. Kittel [5] later showed that it is the change of the wave function due to the spin-orbit interaction that gives rise to the correct order of magnitude of the difference in the two refraction indices.

It was mentioned above that the polarization plane of a linearly polarized light can be rotated upon the reflection from the magnetized surface. By passing the reflected light through a polarizer and catching it with a detector, we can record the Kerr intensity (the intensity of the reflected light) which is proportional to the magnetization of the entire films thickness that is probed by the laser. The thickness of magnetic films that can be probed depends on the probing depth (the penetration depth) of light used. Although the application of the Kerr effect to study surface magnetism was just introduced in 1985 by Moog and Bader [6], it has been widely accepted due to its ability to show the hysteresis loop. Both magnetization in the polar (magnetic

field is applied perpendicular to the sample) and longitudinal (magnetic field is applied parallel to the sample) geometry can be obtained.

To provide a quantitative analysis, the Kerr intensity, measured by the photodetector after the light has passed through an analyzing polarizer that is set at an angle δ from extinction, is defined as

$$I = \left| E_p \sin\delta + E_s \cos\delta \right|^2 \approx \left| E_p \delta + E_s \right|^2 \tag{3.2}$$

Provided that $E_s / E_p = \phi' + i\phi''$ gives the Kerr rotation ϕ' and Kerr elipticity ϕ'', equation (3.2) can be rewritten to

$$\begin{aligned} I &= \left| E_p \right|^2 \left| \delta + \phi' + i\phi'' \right|^2 \approx \left| E_p \right|^2 \left(\delta^2 + 2\delta\phi' \right) \\ &= I_0 \left(1 + \frac{2\phi'}{\delta} \right) \end{aligned} \tag{3.3}$$

with $I_0 = \left| E_p \right|^2 \delta^2$ as the intensity at zero Kerr rotation. The measured intensity as a function of applied field yields a magnetic hysteresis loop. Upon reversing the saturation magnetization, the maximum Kerr rotation ϕ_m' can be determined by the relative change of the Kerr intensity, $\Delta I / I_0$ through this relation: $\phi_m' = \frac{\delta}{4} \frac{\Delta I}{I_0}$.

In reality, the ultrahigh vacuum (UHV) viewport window (*w*) usually produces a birefringence, $\phi_w' + i\phi_w''$, that makes the extinction condition impossible to be realized. In this situation, the extinction can be achieved with the use of a quarter waveplate (lambda quarter plate) which is usually placed in front of the analyzing polarizer to cancel the birefringence of the UHV window. In other words, the quarter waveplate produces a *π/2* phase difference

between the *s* and *p* components so that the analyzing polarizer will see $i\left(\phi' + i\phi''\right) = -\phi'' + i\phi'$, i.e. the rotation and ellipticity are interchanged. The measured Kerr intensity now becomes

$$I = \left|E_p\right|^2 \left(\delta^2 + 2\delta\phi''\right) = I_0\left(1 + \frac{2\phi''}{\delta}\right) \tag{3.4}$$

In this case, the relative Kerr intensity determines the Kerr ellipticity instead of the Kerr rotation. To measure the Kerr rotation, a half wave plate can be used to replace the quarter wave plate.

3.3 Experimental setup

Our SMOKE setup consists of He-Ne laser, simple optics, lambda quarter plate, polarizer and photodetector; they are mounted outside the UHV chamber. A magnet made of two separate coils is mounted inside the UHV chamber.

Although the idea behind SMOKE is quite simple and it does not require complicated setup, it takes practices and experiences to adjust the setup in order to get good signal-to-noise ratio. Not only has it had to be adjusted in the beginning of the experiment, but also from time to time during the experiment.

After the discussion about the advantage of the SMOKE mentioned above, I will list two major drawbacks of the SMOKE as a technique to measure surface magnetism. First, if we have another magnetic layer beneath the magnetic layer's surface, SMOKE will pick up magnetism signal from both magnetic layers given that the surface's layer is thin. Even though SMOKE is very surface sensitive to a limited thickness from the surface, it cannot distinguish surface or interface magnetism from that coming from the magnetic layer beneath. Another drawback is it can not distinguish an antiferromagnetic and nonmagnetic phase.

Chapter 4 Artificial Nanomagnet with Lateral Confinement

Abstract

We introduce a novel way, curved Cu(111) substrate, to smoothly modify the surface states by introducing miscut angle and study the impact of modifying vicinal surface states on the ferromagnetic behavior of Fe dots. Fe-dots are grown on a Cu(111)-curved substrate where the miscut angle changes from 0° (very large terrace width) to 8° (15 Å terrace width). With this curved substrate, the same growth parameter can be ensured in the whole miscut angle studied. When the Fe dot assemblies have in-plane easy axis, two distinct regimes and a critical terrace width, separating these two regimes, can be identified. However, when the Fe dot assemblies have perpendicular easy axis, we only observe one regime which is marked by a slight decrease in the critical temperature (T_c). There are contributions from three factors: the vicinal surface state, the competition between the Fe-dots diameter and the terrace width, and the in-plane uniaxial magnetic anisotropy. The couplings between these three factors lead to the interesting behavior observed in the Fe/vicinal Cu(111) nanodot assemblies. The vicinal surface strongly affects the coupling between Fe-nanodots.

4.1 Vicinal surface

The vicinal surfaces show a rich variety of novel behavior which is a result from the broken translational symmetry by the surface atomic steps. The presence of a free electron like Shockley surface state on the correspondingly flat (111) surface will be interrupted on vicinal

surface. Vicinal surfaces of noble metals have been the object of intense research for the past decade. This particular interest is determined by several reasons. On one hand, vicinal surfaces are very suitable objects for studying low dimensional nanostructures: they can be used as templates to grow 1D wires [1]. On the other hand, noble metal surfaces support Shockley surface states. These electronic states arise in the inverted L gap of a metal band; they are well localized in the direction perpendicular to the surface by the surface potential step and the crystal band gap; they also exhibit dispersive quasi-two dimensional free electron-like behavior [2]. Surface states scatter strongly at point defects, steps, etc., thus modulating the local density of states (DOS) at the Fermi level [3].

Vicinal surfaces can also be used to study the archetypal 'particle in a box' behavior. Burgi *et al* [4] built a Fabry-Perot quantum resonator from two perfectly straight and parallel steps on Ag(111) surface and demonstrated that quasi 2D surface states can be confined within parallel steps. They also demonstrated that the resonator could be decoupled from its surrounding through the absorption of surface state electrons at steps. The coupling of surface state electrons to the bulk states can be rationalized by the strength of confining potentials at the step edges. In this manner, vicinal surfaces can be treated as an array of confining potentials. Due to the surface-bulk coupling, the strength of confining potentials depends on the exact structure of a vicinal surface. There is no such coupling on the flat (111) substrate, and the coupling is small for vicinal surfaces with a rather large terrace width. In this case, potential barriers are large, all the terraces are decoupled, surface state electrons are confined to the terraces, and each step can be treated as a quantum well (QW). The coupling of surface states with bulk states increases when the terraces get narrower. This will result in the reduction of confining potentials, and surface state electrons can propagate above the vicinal surface.

4.2 Importance of vicinal surface state

All the results obtained by the two previous graduate student at the University of Tennessee, i.e. J. P. Pierce and M. A. Torija, show that surface state is very important in stabilizing the collective ferromagnetic behavior in Fe dots/ flat Cu(111) [see section 2.6]. In this chapter, we modify the surface states by introducing miscut angle and study the impact of modifying vicinal surface states on the ferromagnetic behavior of Fe dots. We introduce a novel way, curved Cu(111) substrate, to smoothly changed the surface states. Our curved substrate changes from 0° (very large terrace width) to 8° (15 Å terrace width). With this curved substrate, the same growth parameter can be ensured in the whole miscut angle studied. Experimental and theoretical studies have shown that the surface states change with miscut angle [3, 5, 6].

The surface state propagation can be probed using the Scanning Tunneling Microscope (STM), providing the direct observation of wave functions in the local density of states. The wave function of a step lattice is modulated by two periodicities, that of the superlattice [figure 4.1 a] and that of the atomic corrugation of the terraces [figure 4.1 b]. These two models were supported by strong evident which are inconsistent with each other. The scanning tunneling microscope (STM) pictures, taken by Crommie *et al* [3], produce well defined standing waves/ quantum well states which lie in the Cu(111) plane of the terraces, thus giving rise to a model wave function similar to that in figure 4.1 b. On the other hand, Sanchez *et al* [5] observed lateral partial confinement of the surface electrons within the terraces bounded by a regular array of step barriers. The angle resolved photoemission data produce $E(k)$ band dispersions that lead to the picture in figure 4.1 a. In order to find out whether or not these two models are compatible with each other, Ortega *et al* [6] have mapped the vicinal Cu(111) surface state by angle resolved photoemission. They found a switch, at a miscut of 7° (17 Å terrace width), from the step

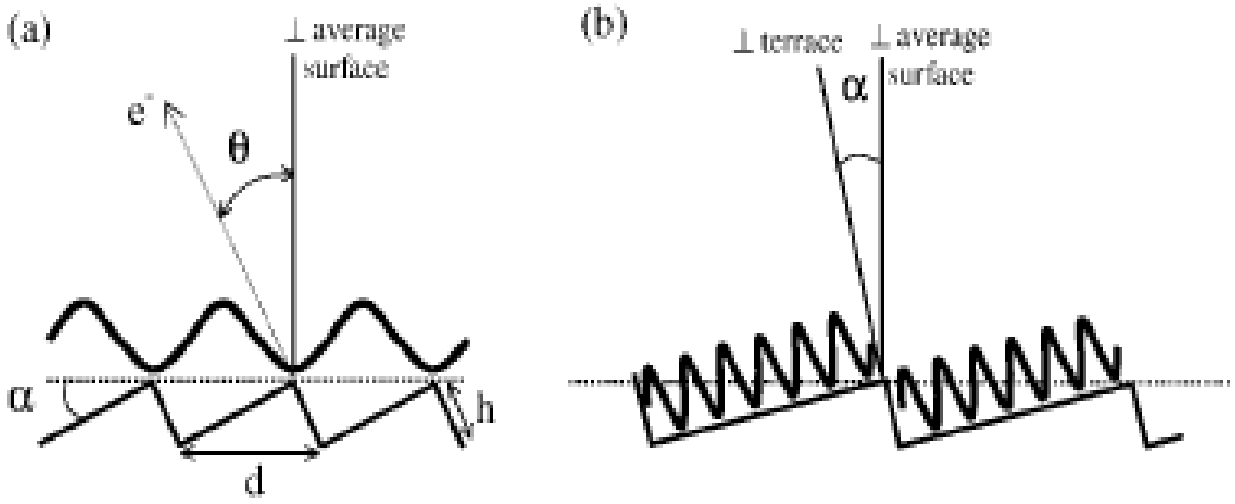

Figure 4.1: Schematic description and the measurement geometry of two different models for the wave function on vicinal surfaces. (a) Superlattice propagating model: the wave function propagates above the vicinal surface and decays perpendicular to the average surface. (b) Quantum well states model: the wave function is confined within the terrace and decays perpendicular to the terraces. [after reference 6]

modulation of the wave function (for small terrace width) to the terrace modulation (for large terrace width). The nature of the wave function is also known. For small terrace width, the wave function decays perpendicular to the average surface; while the wave function for large terrace width decays perpendicular to the terraces. Later, Baumberger *et al* [7] showed that this qualitative change at terrace width around 17 Å must be described as a change from propagating states at small terrace width to one dimensional quantum well states at large terrace width; such transition runs continuously. Both of these states have the band bottom shifted toward higher energies. While partially confined propagating states have dispersive bands, quantum well states exhibit a quantized band structure with a number of discrete energy levels.

Hansmann *et al* [8] studied surface states on Cu(111) vicinals particularly in the transition region by means of STS and/or STM. They performed measurements on surfaces with the terrace width ranging from 16 up to 70 Å and observed that the dimensionality of the (111) derived surface state changes from 2D to 1D when the electron energy and wave vector comply with the lateral confinement conditions of the individual terrace. The analysis of their results yields two common features in all measured spectra: the first feature is a surface state-like onset of the spectra and the second is a broad but very distinct peak. The surface state-like onset indicates that Cu(111) extended 2D surface states still exist on the considered vicinal surfaces, only partially affected by the finite transparency of the step superlattice. The second feature, i.e, the peak, originates from local confinement of surface electrons to the terraces.

Zhang *et al* [13] used vicinal surfaces, i.e. Pt(997), to study the magnetism of Fe clusters with Buffer Layer Assisted Growth (BLAG) method. The cluster size was controlled by the thickness of the Xe layer. They found that when the cluster diameter is smaller than the Pt terrace width, then the Fe clusters will be ferromagnetic and align along the step edges of the Pt(997),

thus forming ordered array linear cluster chains. However when the cluster diameter is larger than the terrace width, then the Fe clusters will show superparamagnetic behavior and there will be no alignment along the step edges; instead, large disordered agglomerates are found.

4.3 Result and Discussion

The Fe dot assemblies are grown on curved Cu(111) substrate with the BLAG method. See section 3.1 for details on the BLAG method.

Figure 4.2(a, b) show the schematic description of two different models for the wave function on vicinal surfaces and the measurement geometry. Knowing that 1 ML Cu(111) is equal to 2.083 Å, we can calculate the vicinal Cu(111) terrace width (d) with this formula: $Sin\ \alpha = h/d$, where α is the miscut angle and h = 2.083 Å. For example, the terrace width (d) for 8° miscut angle is about 15 Å and the terrace width (d) for 1° miscut angle is about 119 Å. From the calculation, it is clear that when the miscut angle becomes smaller, the terrace width becomes larger; and when the miscut angle becomes larger, the terrace width becomes smaller. Figure 4.2(c) shows the ratio between remanent magnetization (M_r) and saturation magnetization (M_s) as a function of temperatures. The critical temperature (T_c), defined as the temperature at which M_r / M_s becomes zero, is about 193 K for the 0.9 ML Fe nanodots grown with the assistance of 300 L Xe and measured at 1.0° vicinal surface Cu(111). The inset in figure 4.2(c) shows typical MOKE hysteresis loops measured from 0.9 ML Fe nanodots at 1.0° vicinal surface Cu(111) at various temperatures.

We plot together two different curves in the same figure 4.3. Black squares curve is the diameter of 1 ML Fe-dots grown on flat Cu(111) as a function of Xe adsoption. It was obtained from several experiments done by the two previous graduate students [17,18]. The red circles

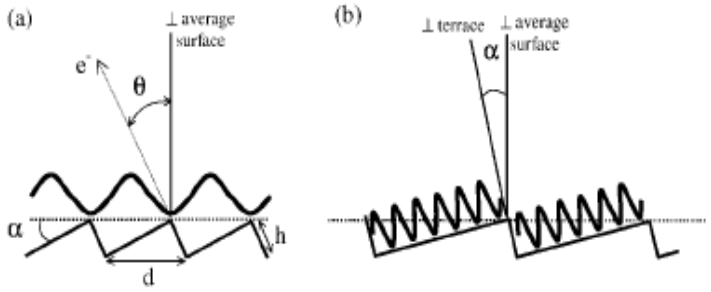

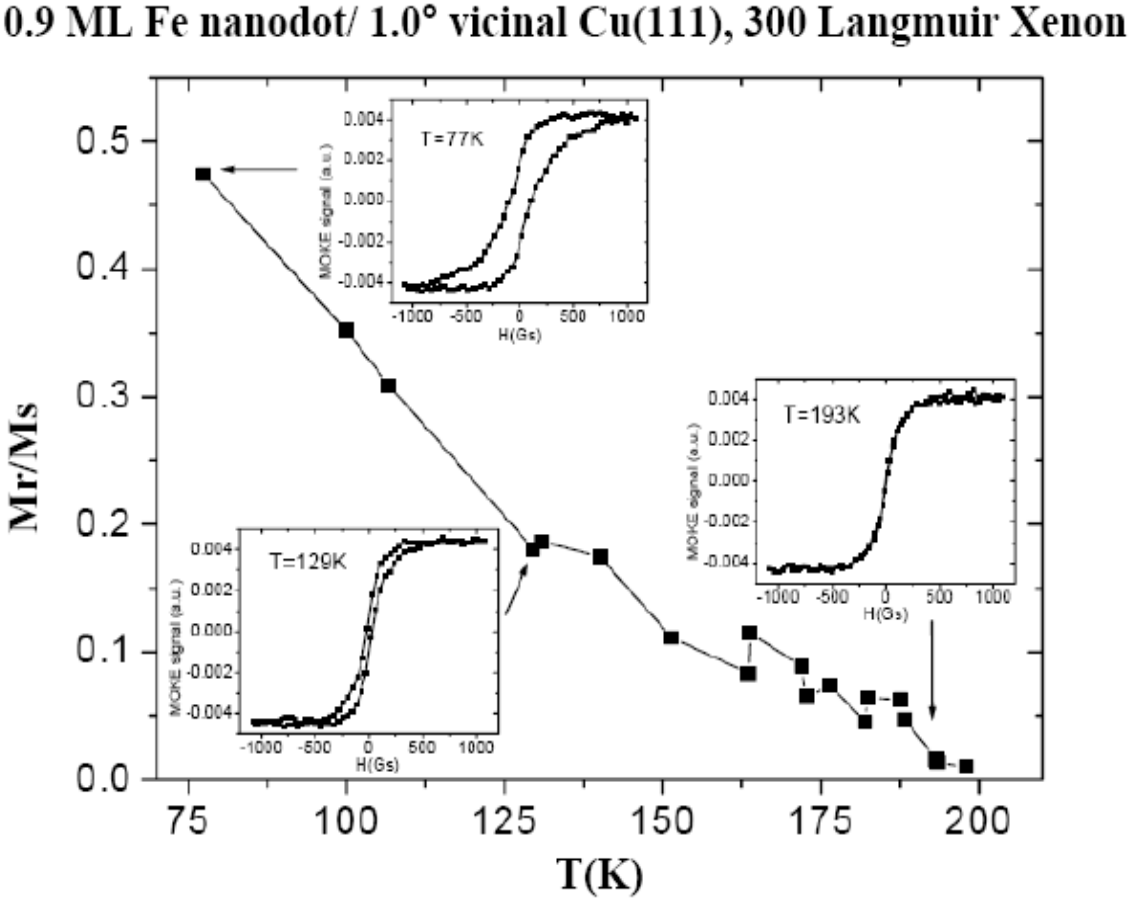

Figure 4.2: (a, b) Schematic description and the measurement geometry of two different models for the wave function on vicinal surfaces. (bottom) Ratio of the remanent magnetization (M_r) and the saturation magnetization (M_s) as a function of temperatures.

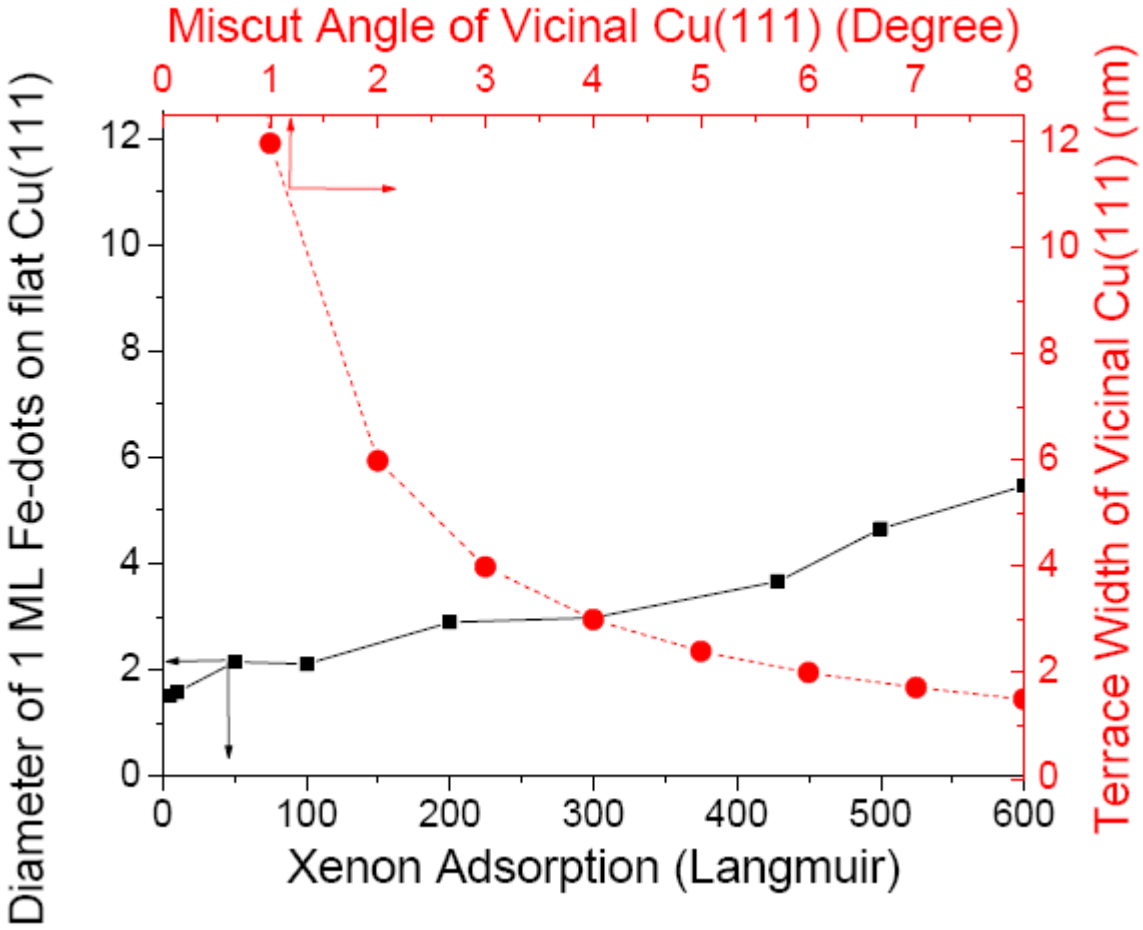

Figure 4.3: Two curves in one figure: Diameter of Nanodot/ Flat Cu(111) as a function of Xe adsorption (black squares), and Terrace Width of Vicinal Cu(111) as a function of Miscut Angle of Vicinal Cu(111) (red circles).

curve is the terrace width of vicinal Cu(111) as a function of the vicinal Cu(111) miscut angle. By examining figure 4.3, we can meet our research goals by carefully choosing the right parameter for the Fe-dots growth condition. For example, if we grow 1 ML Fe-dots with the assistance of 300 L Xe adsoption on the flat Cu(111) surface, the corresponding diameter of the Fe-dots is about 3 nm (black curve). If we use the same growth parameter (1 ML Fe dots with 300 L Xe) to grow Fe dots on curved Cu(111) substrate, the red curve shows that for miscut angle smaller than 4°, the terrace width of vicinal Cu(111) is larger than 3 nm and while the miscut angle is larger than 4°, the terrace width of vicinal Cu(111) is smaller than 3 nm.

The Fe dots' magnetization easy axis undergoes reorientation from perpendicular to in-plane magnetization easy axis when we increase the xenon adsorption beyond 10 L [see figure 4.4]. For large portion of Xe adsorption, the Fe-nanodots have an in-plane easy axis. Interestingly, we observe that at very tiny Xe adsorption (approximately less than 20 L Xe), the Fe-dots have perpendicular easy axis.

We observe two distinct regimes when the Fe dots have in-plane easy axis [see figure 4.5]. The first regime is marked by a slight increase in the critical temperature, followed by a sudden decrease in the critical temperature. A critical miscut angle can be identified to separate these two regimes. The nanodot diameter of 1 ML Fe dots with 250 L Xe is about 3.1 nm. The critical miscut angle for this growth parameter is 3.9°, the terrace width at 3.9° is about 3.1 nm. When the miscut angle is smaller than the critical angle, we find a slight increase in T_c (from about 137 K to about 145 K). However, when the miscut angle is larger than the critical angle, the T_c suddenly decreases, reaching 95 K at 7° miscut angle. It is hardly a coincidence that the terrace width where this switch takes place is almost the same with the nanodot diameter. We also measure more samples with different langmuir Xe adsorption while maintaining the same Fe

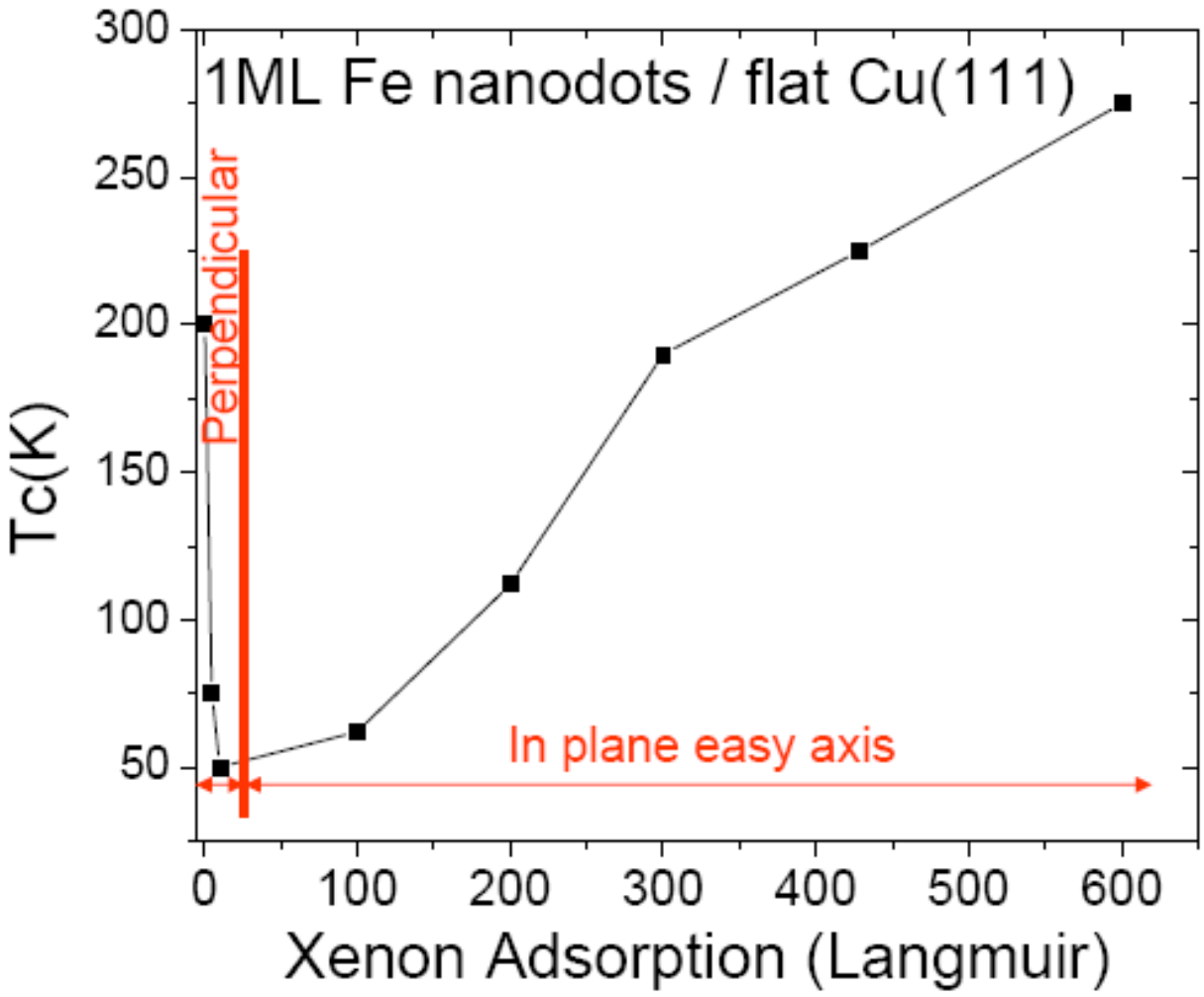

Figure 4.4: Summary of the T_c of 1 ML Fe nanodots/ flat Cu(111) as a function of Xe adsorption including the nanodots' easy axis.

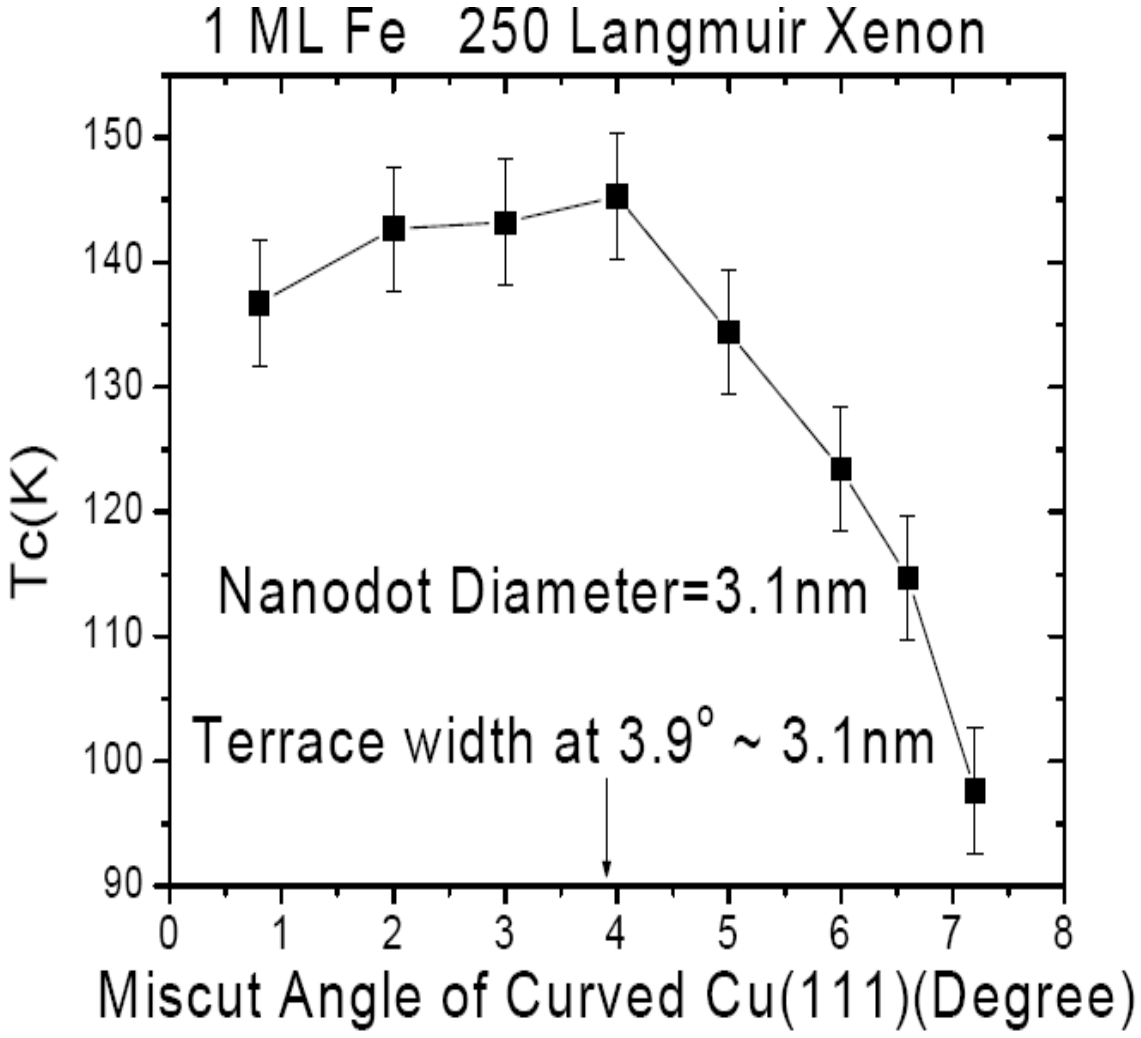

Figure 4.5: Critical temperature (T_c) of 1 ML Fe with the assistance of 250 L Xe as a function of Cu(111) miscut angle. The nanodot diameter is about 3.1 nm. The terrace width at 3.9° miscut is about 3.1 nm. When the miscut angle is less than 3.9°, the dot diameter is smaller than the terrace width; however, when the miscut angle is larger than 3.9°, the dot diameter is larger than the terrace width. The switch of T_c occurs at about 4°.

nominal thickness (approximately 1 ML), all of them show the similar behavior. See figure 4.6, 4.7, 4.8, and 4.9 for clarity. All the data shows that when the nanodot diameter is smaller than the terrace width, the critical temperature (T_c) is only slightly increased. However, the T_c decreases rapidly when the nanodot diameter becomes larger than the terrace width. The turning point occurs when the nanodot diameter is equal to the terrace width.

We explain this behavior due to very strong dot-dot interaction mediated through Cu(111) surface states. At small miscut angle, when the dot diameter is smaller than the terrace width, the coupling originates mainly from Cu(111) surface states. As a result, the Fe dots will experience strong coupling through the Cu(111) surface states. However, when the dot diameter is larger than the terrace width, and with increasing miscut angle, the coupling starts to become more and more (110)-like. This is because the step edge surface that is perpendicular to (111) surface is [-110] oriented with a (100) microfacet. Surface state exists in Cu(110), however this step edge plane only has 1 ML, so we should not call it surface state. Rather, bulk state is more appropriate than surface state. Therefore, with the increasing miscut angle, the coupling of Fe dots through Cu(111) surface states decreases and T_c drops dramatically.

However, when the Fe dots have perpendicular easy axis, we do not observe two distinct regimes. Instead, only a slight decrease in the critical temperature (T_c) is observed as a function of miscut angle. The T_c at 0.8° and 7.2° miscut angle is 36 K and 28.5 K, respectively [see figure 4.10]. This slight decrease in T_c is explained due to the stronger intra-layer (within one terrace) Fe-dots interaction than the inter-layer (between terraces) Fe-dots interaction. At high miscut angle (small terrace width), there will be less Fe-dots that can be accomodated within one terrace. As a result, the intra-layer Fe-dots interaction at high miscut angle is smaller than the intra-layer Fe-dots interaction at small miscut angle.

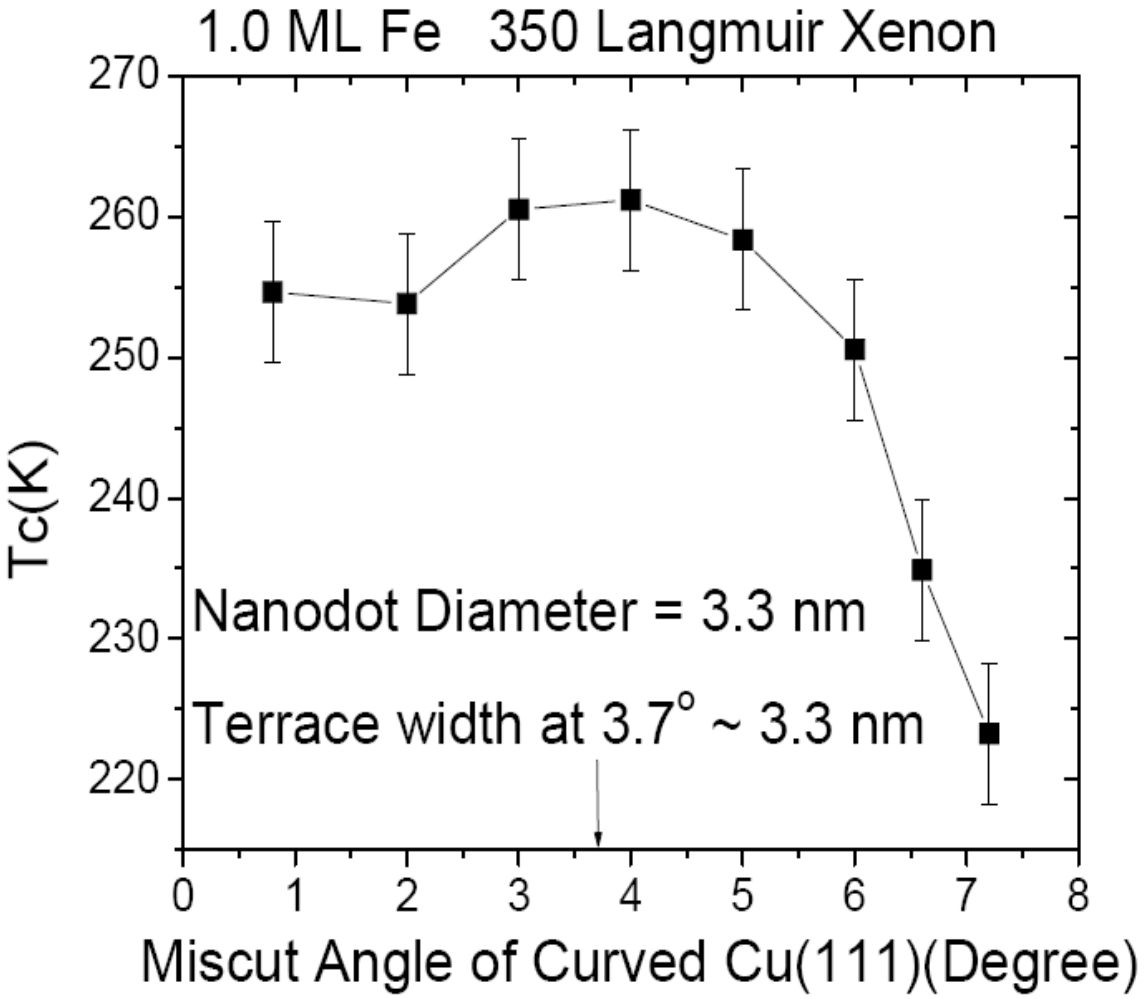

Figure 4.6: Critical temperature (T_c) of 1.0 ML Fe with 350 L Xe as a function of Cu(111) miscut angle. The nanodot diameter is about 3.3 nm. The terrace width at 3.7° miscut is about 3.3 nm. When the miscut angle is less than 3.7°, the dot diameter is smaller than the terrace width; however, when the miscut angle is larger than 3.7°, the dot diameter is larger than the terrace width. The switch of T_c occurs at about 3.7°.

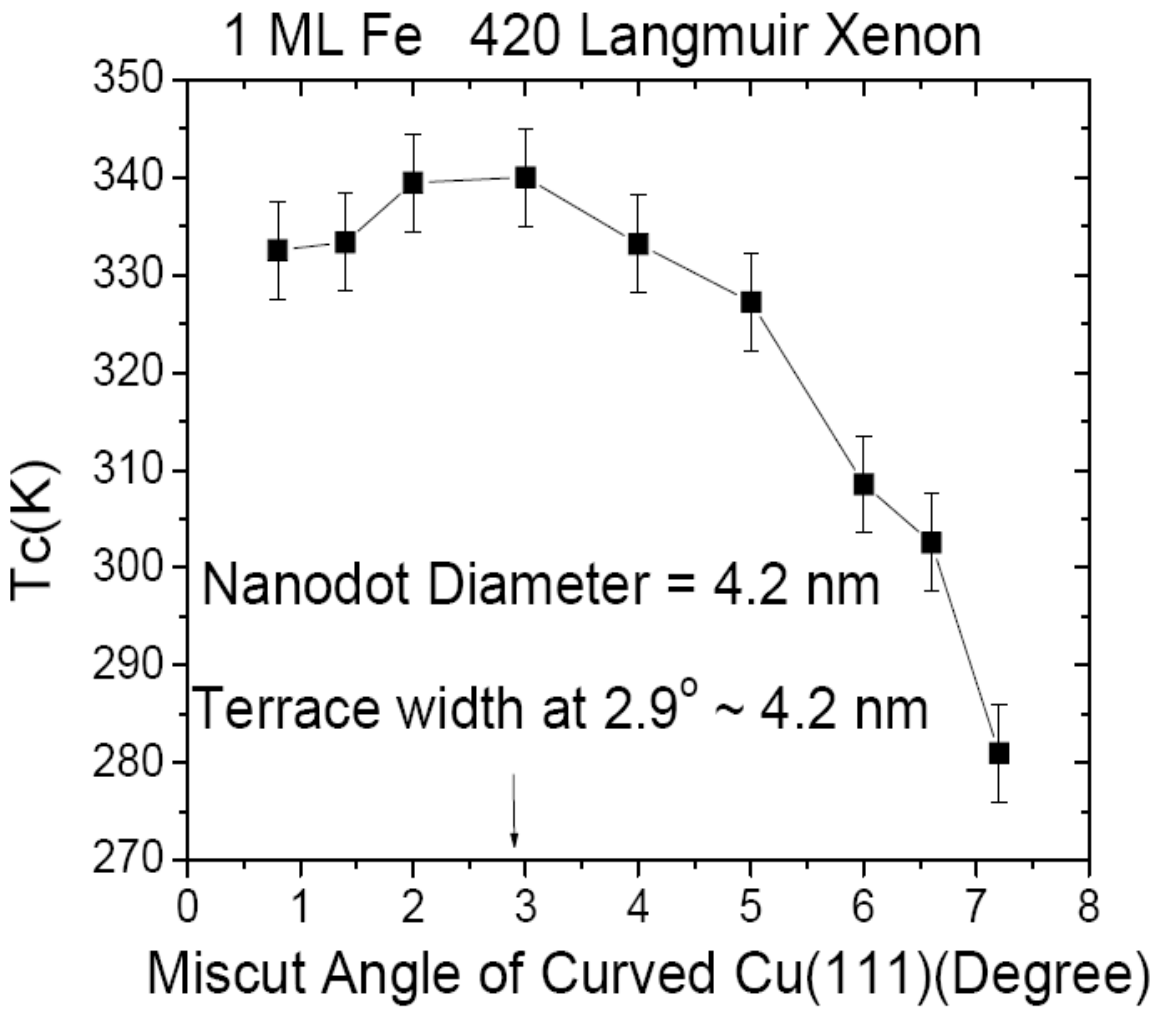

Figure 4.7: Critical temperature (T_c) of 1.0 ML Fe with 420 L Xe as a function of Cu(111) miscut angle. The nanodot diameter is about 4.2 nm. The terrace width at 2.9° miscut is about 4.2 nm. When the miscut angle is less than 2.9°, the dot diameter is smaller than the terrace width; however, when the miscut angle is larger than 2.9°, the dot diameter is larger than the terrace width. The switch of T_c occurs at about 2.9°.

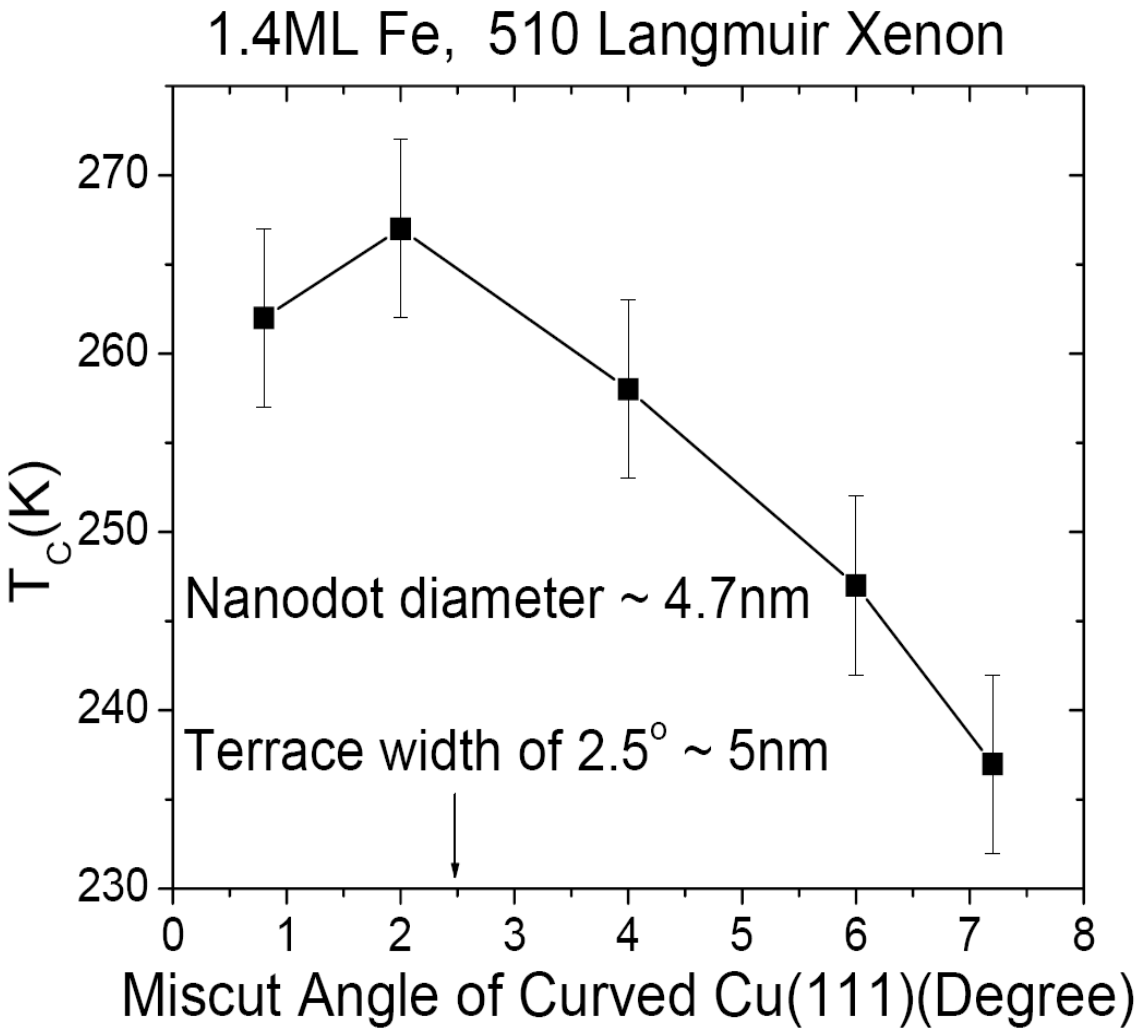

Figure 4.8: Critical temperature (T_c) of 1.0 ML Fe with 510 L Xe as a function of Cu(111) miscut angle. The nanodot diameter is about 4.7 nm. The terrace width at 2.5° miscut is about 5 nm. When the miscut angle is less than 2.5°, the dot diameter is smaller than the terrace width; however, when the miscut angle is larger than 2.5°, the dot diameter is larger than the terrace width. The switch of T_c occurs at about 2.5°.

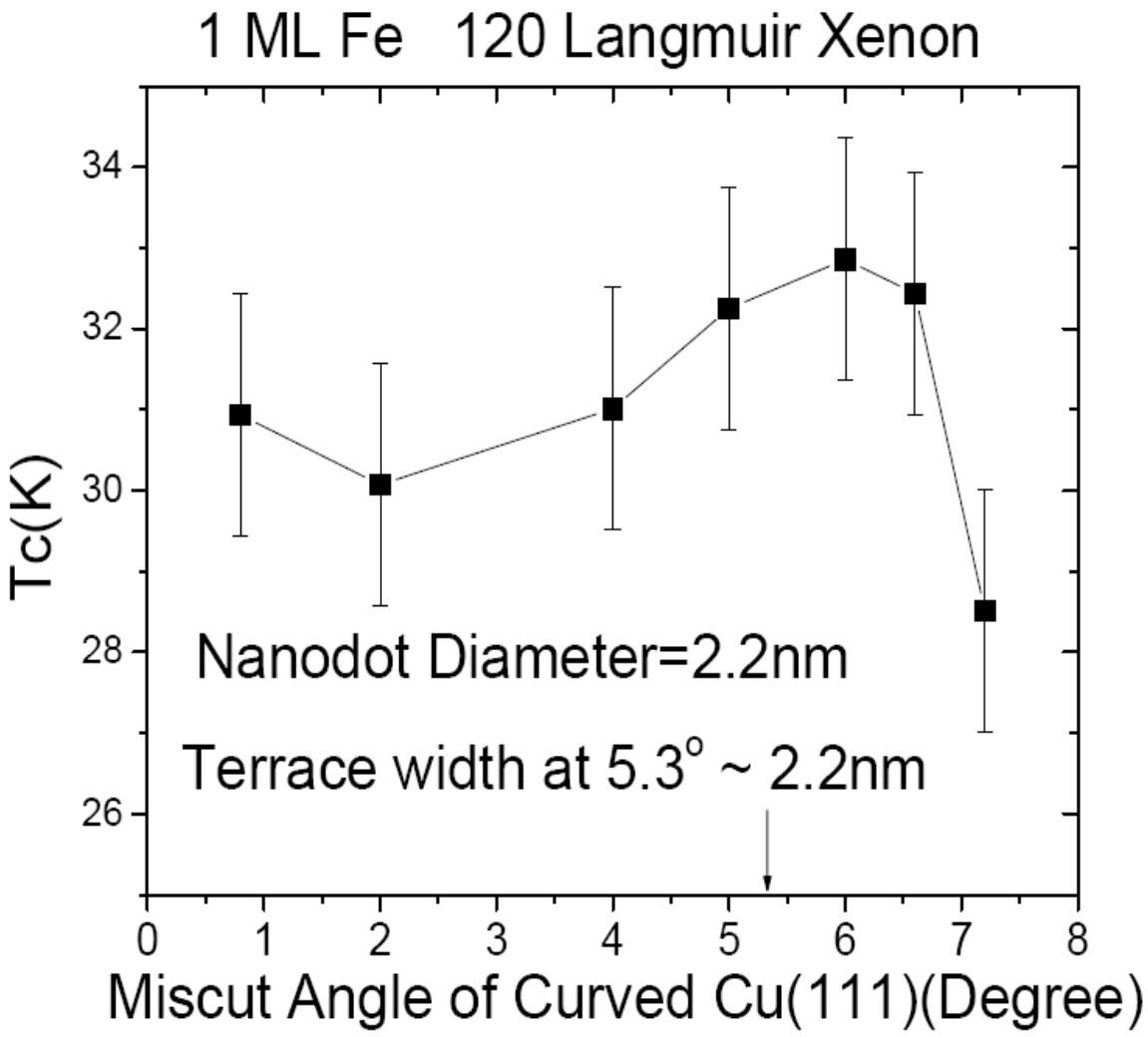

Figure 4.9: Critical temperature (T_c) of 1.0 ML Fe with 120 L Xe as a function of Cu(111) miscut angle. The nanodot diameter is about 2.2 nm. The terrace width at 5.3° miscut is about 2.2 nm. When the miscut angle is less than 5.3°, the dot diameter is smaller than the terrace width; however, when the miscut angle is larger than 5.3°, the dot diameter is larger than the terrace width. The switch of T_c occurs at about 5.3°.

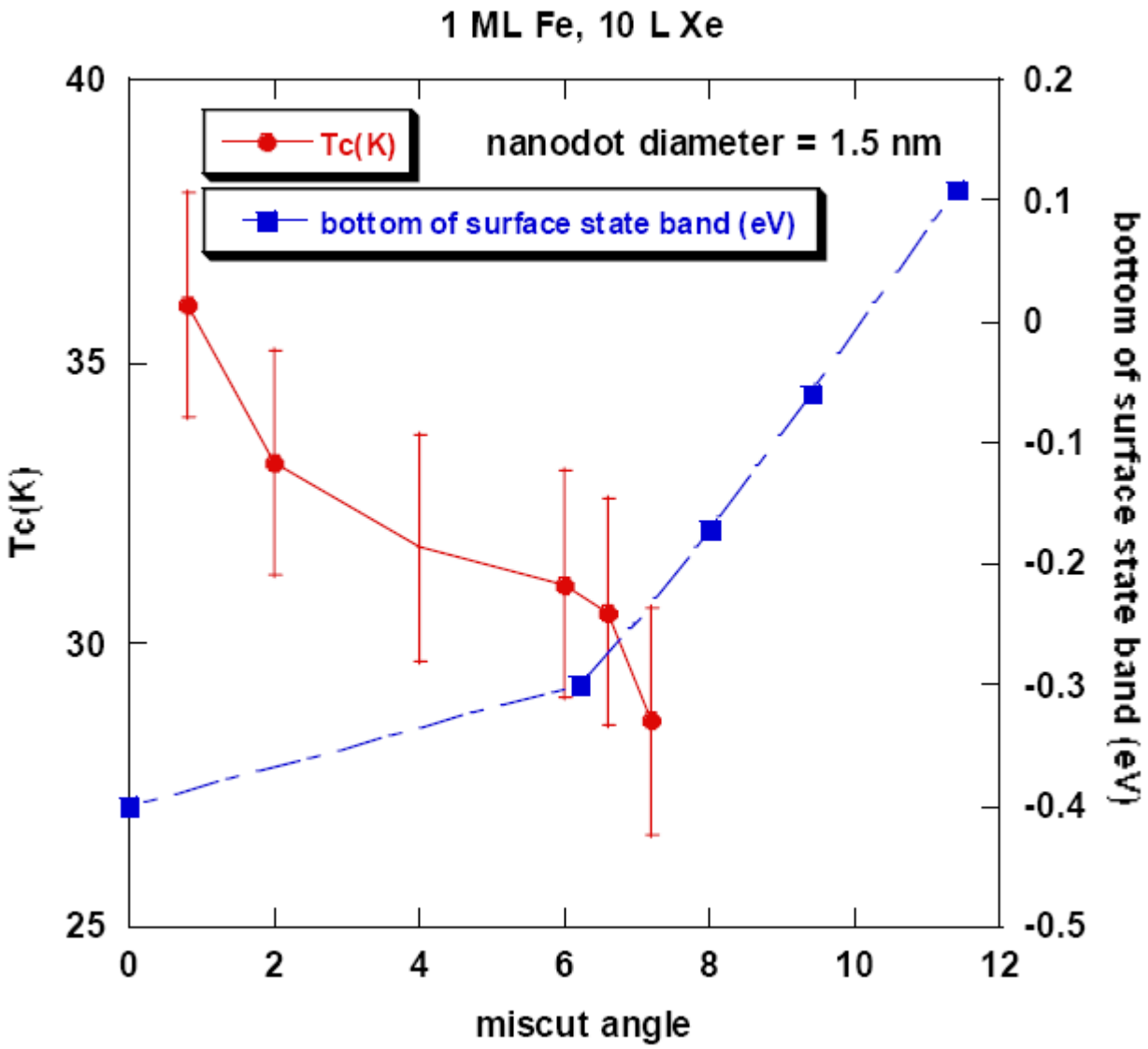

Figure 4.10: T_c of 1 ML Fe-nanodots/ 10 L Xe as a function of miscut angle Cu(111) [in red circles] and the bottom of the surface state band vs. Cu(111) miscut angle [in blue squares].

In Figure 4.10, we compare the T_c vs. miscut angle [in red circles] with the position of the bottom of the surface state band as a function of miscut [in blue squares]. For a perfect Cu(111) surface, the peak in the STS spectra is at 0.4 eV. Ignatiev *et al* [20] calculated the LDOS spectra of vicinal Cu(111). They also plot the bottom of the surface state band as a function of terrace width. There is an opposite trend between the T_c and the peak position. The T_c decreases with the increasing miscut angle away from (111) direction while the peak position increases with the increasing miscut angle. We can see clearly that the change in the Cu(111) surface state, seen by STS and/or STM [8,20], has nothing to do with our MOKE result. Instead, it was caused by the relative ratio of Cu(111) and Cu(100) mixture. Unfortunately, it is not what we have originally planned; nevertheless we have successfully achieved the tunability for lateral coupling.

4.4 Summary

We have successfully achieved the tunability for lateral coupling by introducing miscut angle. Remarkably, we have shown robust Cu(111) surface state influence in the collective ferromagnetic behavior of the Fe-dots low dimensional assemblies on vicinal Cu(111). Besides that, the competition between dot diameter and terrace width are also important. We observed two distinct regimes when the Fe dots have in-plane easy axis: (a) When the nanodot diameter is less than the terrace width, the critical temperature (T_c) slightly increases, (b) When the nanodot diameter is larger than the terrace width, the critical temperature (T_c) decreases rapidly. The switch of critical temperature (T_c) occurs when the nanodot diameter is equal to the terrace width. We explain this behavior due to very strong dot-dot interaction mediated through Cu(111) surface states. At small miscut angle, when the dot diameter is smaller than the terrace width, the

coupling originates mainly from Cu(111) surface states and the Fe dots will experience strong coupling through the Cu(111) surface states. However, when the dot diameter is larger than the terrace width, and with increasing miscut angle, the coupling starts to become more and more Cu(100)-like. Therefore, with the increasing miscut angle, the coupling of Fe dots through Cu(111) surface states decreases and T_c drops dramatically.

We have reported that Fe-dots grown on vicinal Cu(111) with the assistance of 10 L Xe have perpendicular anisotropies and a slight decreased of the critical temperature is observed with the increasing miscut angle. We explained this result due to the stronger intra-layer (within one terrace) Fe-dots interaction than the inter-layer (between terraces) Fe-dots interaction. At high miscut angle (small terrace width), there will be less Fe-dots that can be accomodated within one terrace. As a result, the intra-layer Fe-dots interaction at high miscut angle is smaller than the intra-layer Fe-dots interaction at small miscut angle. We do not see any changes in Cu(111) surface states from our MOKE data.

As a conclusion, the coupling of Fe-nanodots can be strongly modulated by vicinal surfaces. This conclusion is based on the fact that the critical temperature (T_c) depends largely on the Cu(111) miscut angle. There are three important factors in play to stabilize the collective ferromagnetic behavior in Fe-dot assemblies on vicinal Cu(111):

(1) Cu(111) surface states. Our previous and recent studies show that Cu(111) surface states play a major role in stabilizing the ferromagnetic ordering in Fe/Cu(111) assemblies ;

(2) Competition between the dot diameter and the terrace width, where two possibilities could happen. The first possibility occurs when the dot diameter is smaller than the terrace width then each dot can be accommodated within one terrace. The second possibility happens when the dot

diameter is larger than the terrace width then it will cross several terraces and no longer sensitive to individual step; and

(3) In-plane anisotropy. Fe-dots have large in-plane anisotropy due to high saturation magnetization. To further prove our hypothesis, we have to rotate our sample 90°. If our hypothesis is indeed true, we will observe further enhancement in T_c when the dots have in-plane easy axis.

The couplings between these three factors lead to the interesting behavior observed in the Fe/vicinal Cu(111) nanodot assemblies. The coupling between Fe-nanodots is strongly affected by the vicinal surface.

Chapter 5 Perpendicular Magnetic Anisotropy in Cobalt nanodots on Rutile TiO_2(110)

Abstract

We study the magnetic property of cobalt nanodots grown on rutile TiO_2(110) substrate. Significant perpendicular magnetic anisotropy is observed on SQUID magnetization data of high density and low density cobalt nanodots/ rutile TiO_2(110). No superparamagnetic-ferromagnetic transition is observed down to 2 K indicating that the system is in the superparamagnetic state in the whole temperature range taken. We do a theoretical calculation to explain the origin of the perpendicular anisotropy in this cobalt nanodots/ rutile TiO_2(110) system. The shape and the crystal anisotropy are not enough to explain the phenomena in this reduced dimensionality system. The Co/TiO_2 interface anisotropy contribution dominates the magnetic anisotropy. No strong dipolar interaction is observed.

5.1 Introduction

Isolated noninteracting magnetic nanodots are superparamagnetic resulting from the competition between thermal fluctuation and energy barrier of magnetic anisotropy. In these systems, thermal energy, which causes fluctuations in the magnetic moment of the dots, becomes significant enough to overcome the anisotropy energy barrier and randomize the orientation of the magnetic moment. This occurs at the so called blocking temperature (T_B) which typically happens far below room temperature. In real nanodot assemblies where the spacing between

magnetic nanodots is not too large, then usually the influence of magnetic interaction(s) on the superparamagnetic behavior can not be neglected [1] because the magnetic dipole-dipole interaction can affect the barrier height for flipping the spin of each individual dot as well as the collective magnetic behavior of the dot assembly. It is generally recognized that there exists two types of magnetic interactions: (1) the dipole-dipole magnetostatic interaction, and (2) the electron-mediated indirect exchange interaction [1]. The importance of the dipolar interaction is most evident in high density recording media [2]. In the strong dipolar interaction limit, Morup [3] pointed out that a transition from a superparamagnetic state to an ordered state might occur. For most nanodot systems with moderate dipolar interaction and random anisotropy, spin glass-like behavior has, however, been commonly observed in recent studies [4,5,6,7,8,9,10]. The indirect exchange interaction, due to its relatively weak strength and the oscillatory nature, should have little effect on promoting a global ferromagnetic order in a randomly distributed nanodot assembly. The situation, however, can become very different at surfaces, where pronounced surface electronic states may exist to mediate a strong interaction between the magnetic nanodots. Remarkably, Pierce *et al* [11] have reported a collective ferromagnetic behavior in two-dimensional (2D) Fe dot assemblies grown on a single crystal Cu(111) surface. Experimental evidence strongly suggests that the ferromagnetic order originates from an indirect exchange interaction via the Cu(111) surface states.

To have a better understanding in the magnetism of nanodot assemblies, we choose Co-nanodots on rutile TiO_2(110) as our playground. Co-doped anatase TiO_2 is very famous for its room temperature ferromagnetism [12]. In this study, however, we do not try to answer the question about the origin of the room temperature ferromagnetism on Co-doped TiO_2 [13]. Rather, our goal is to study the effect of spatial confinement on the magnetic anisotropy.

We first focus on the interplay between magnetic anisotropy, dipolar interaction and tunneling induced coupling in nanodot assemblies. For this purpose, magnetic dot assemblies grown on insulating or semiconducting templates can be used to rule out indirect exchange interaction. Co-nanodots grown on a semiconducting TiO_2(110) serves this purpose very well. Meanwhile, the rather short-ranged tunneling induced coupling can be conveniently ruled in or out by changing the dot-dot spacing. We will show later that this strategy can be achieved by changing the density of the nanodots.

TiO_2 is a wide band gaps dilute magnetic semiconductor and can be found in three crystal structures: anatase, rutile, and brookite. Their unit cells are best described in figure 5.1. The crystal structure of rutile TiO_2 is tetragonal with the lattice parameters are a = 4.59 Å and c = 2.96 Å. Rutile TiO_2 is thermodynamically more stable than other type of crystal structures. Besides thermodynamically more stable, there is another reason we choose Co-nanodots/ rutile TiO_2(110) as a prototype system to be investigated. In order to guarantee the growth of nanodots on a particular substrate, the surface free energy of the magnetic nanodots element has to be larger than the substrate. The surface free energy of cobalt is higher than the surface free energy of TiO_2 ($\gamma_{Co} \rangle \gamma_{TiO_2}$) which means that Co-nanodots can be formed directly on TiO_2.

5.2 Experiment

Co-nanodots were grown on top of the rutile TiO_2(110) substrate. The growth of Co-nanodots was carried out in an ultrahigh vacuum (UHV) chamber with base pressure below 1 x 10^{-10} Torr. The rutile TiO_2(110) single crystal surface was prepared by cycles of 1 keV Ar ion sputtering and annealing at 650 °C before it was cooled naturally to room temperature. We use

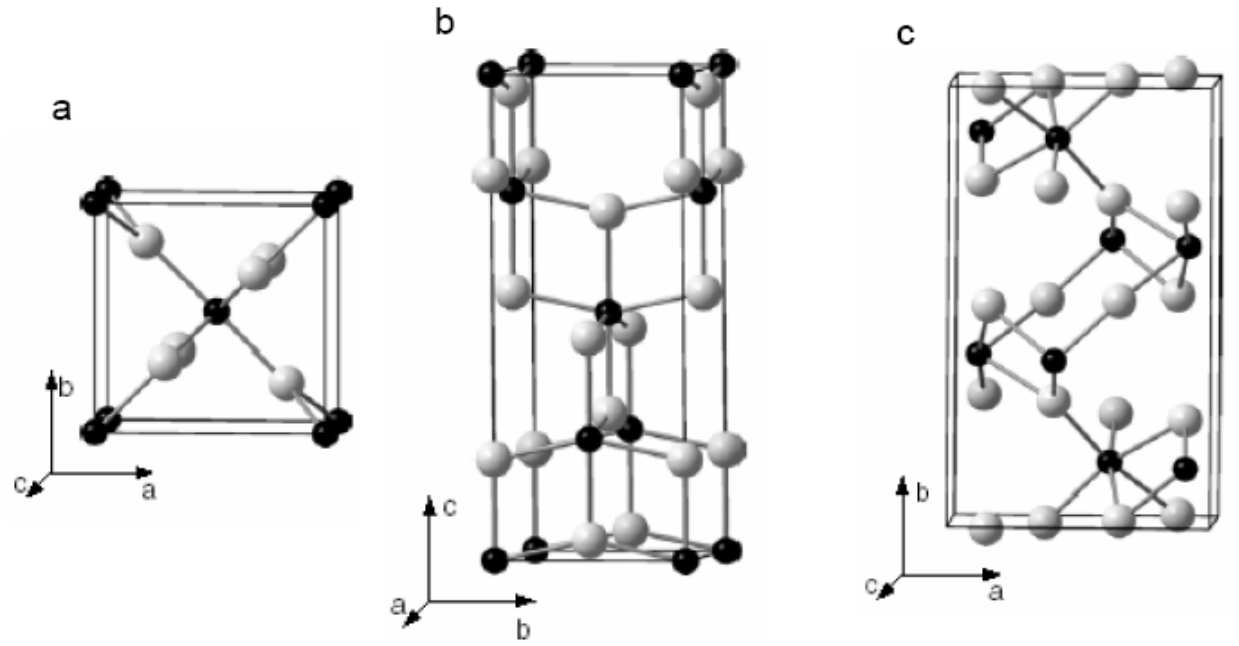

Figure 5.1: Schematic diagrams of the polymorphs of TiO_2: a) rutile, b) anatase, c) brookite. The bigger spheres denote O atoms; the smaller spheres denote Ti atoms.

Scanning Tunneling Microscope (STM) to confirm the cleanliness of the TiO_2 substrate. Cobalt was then evaporated from a wire that was heated by electron bombardment. After the thermal deposition of cobalt dots at room temperature, in situ STM was performed at room temperature to determine the typical height and the diameter of the dots. We can assure that the temperature during the growth was very stable because it took us only about 30 and 10 seconds to grow high density and low density of Co dots. The system was then capped with insulating NaCl to prevent cobalt oxidation for further ex situ magnetization study by using Quantum Design Superconducting Quantum Interference Device (SQUID).

Two TiO_2 substrates with different coverage of Co-dots were prepared. The magnetic properties were measured by a commercial SQUID magnetometer. For mounting purposes, a clear straw was used which has negligible magnetic signal. Then the straw with the sample inside was attached to a measuring probe and loaded into SQUID. Centering was performed to ensure the measured signal is from the sample. The signal from the substrate was carefully subtracted from the resulted data during the analysis. The magnetic field is applied both perpendicular and parallel to the surface during the magnetic measurement.

To check the existence of ferromagnetism, measurements of magnetization as a function of applied magnetic field at certain temperatures were performed. Zero Field Cooled-Field Cooled (ZFC-FC) measurement was also performed to determine the blocking temperature (T_B). For ZFC-FC measurement, the sample was brought to the lowest measurable temperature at zero field ($H = 0$). After centering with an applied field of H~0, a small magnetic field ($H << H_{saturation}$) was applied and the magnetization vs temperature (ZFC curve) was measured when the temperature increased. After the ZFC curve completed, the FC curve was measured in the same applied field when the temperature decreased.

5.3 Result and discussion

We prepared two TiO_2 substrates with two different densities of cobalt nanodots. Figure 5.2 shows the morphology and the typical line profile of our dots obtained by the STM imaging. Both figures (figure 5.2a and figure 5.2b) show the scanning area of 50 x 50 nm^2. From figure 5.2a (top), we can extract the information about the height and the density of our large coverage cobalt nanodots which is about 0.7 nm and 1.4 x $10^5/\mu m^2$, respectively. The height and the density of our small coverage cobalt nanodots is about 0.3 nm and 0.8 x $10^5/\mu m^2$, as can be seen in figure 5.2b (bottom) [14].

Figure 5.3 shows Zero Field Cooled and Field Cooled (ZFC-FC) measurement for 0.7 nm Cobalt nanodots/ TiO_2(110). In the figure, no split/ divergence were observed in the ZFC-FC curve down to 2 K, the lowest possible temperature accessible with SQUID. The two curves overlap with each other in the whole temperature range, an indication that the Cobalt nanodots were superparamagnetic in the whole temperature range. If there is a transition from a ferromagnetic state to a superparamagnetic state, the FC curve will diverge from the ZFC curve at temperature lower than the blocking temperature (T_B).

Figure 5.4 shows our SQUID magnetization data of Co-dots/rutile TiO_2(110) which have zero coercive field and no remanent magnetization. The sample was about 5x5 cm^2. The data indicate significant *perpendicular magnetic anisotropy* with easy axis being perpendicular to the substrate for both large and small dot density with no sign of superparamagnetic to ferromagnetic transition observed down to 2 K.

The observed superparamagnetic behavior of Co-dots/rutile TiO_2(110) is consistent with the superparamagnetic nature of nanodot assemblies [see section 2.3.1] however contrasts with the report by Pierce *et al* [11] who observe collective ferromagnetic behavior with unusual

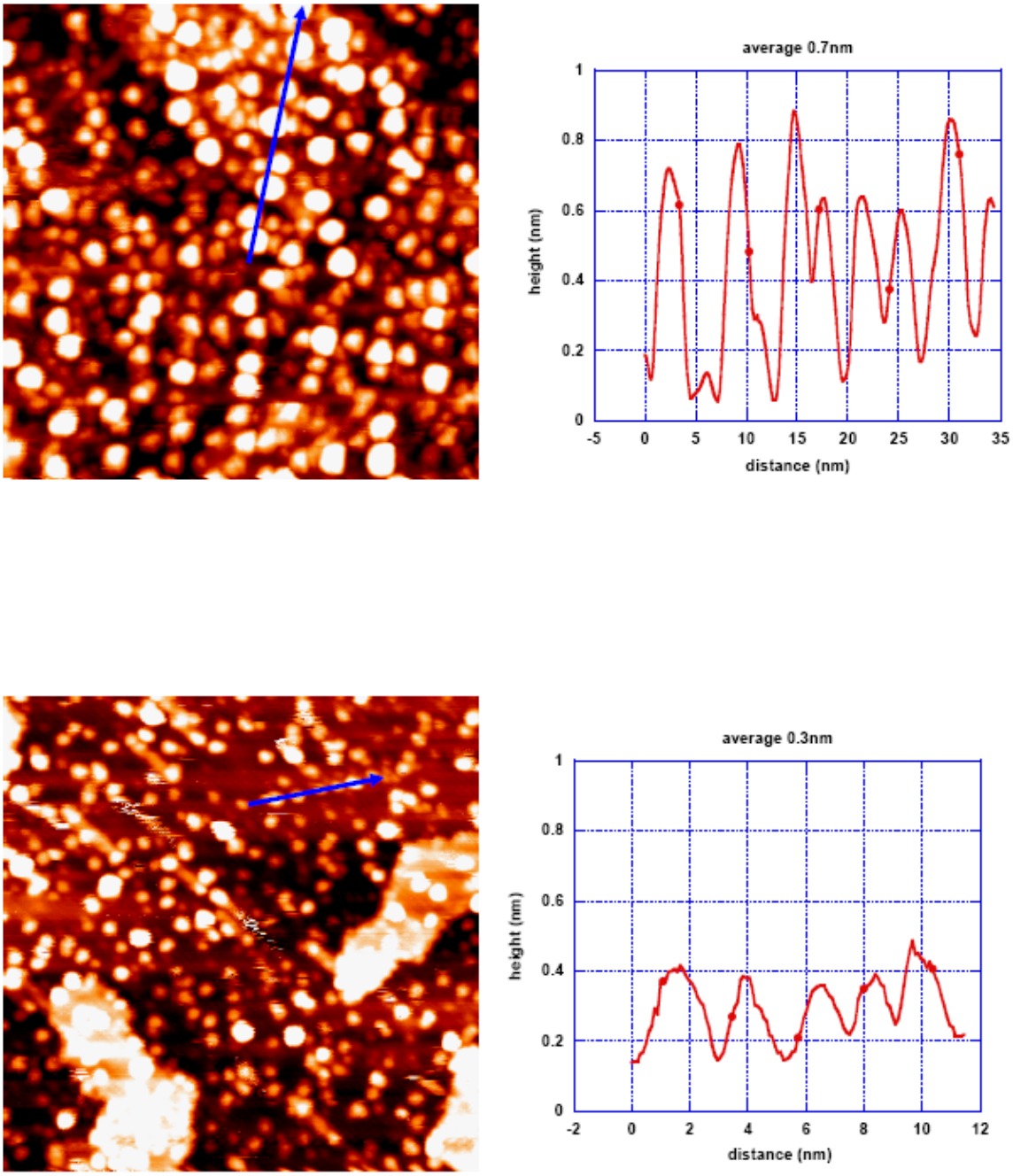

Figure 5.2: Morphology and typical line profile of Cobalt nanodots grown on rutile TiO_2(110) with (top) 0.7 nm height and $1.4x10^5/\mu m^2$ density of dots, and (bottom) 0.3 nm height and $0.8x10^5/\mu m^2$ density of dots.

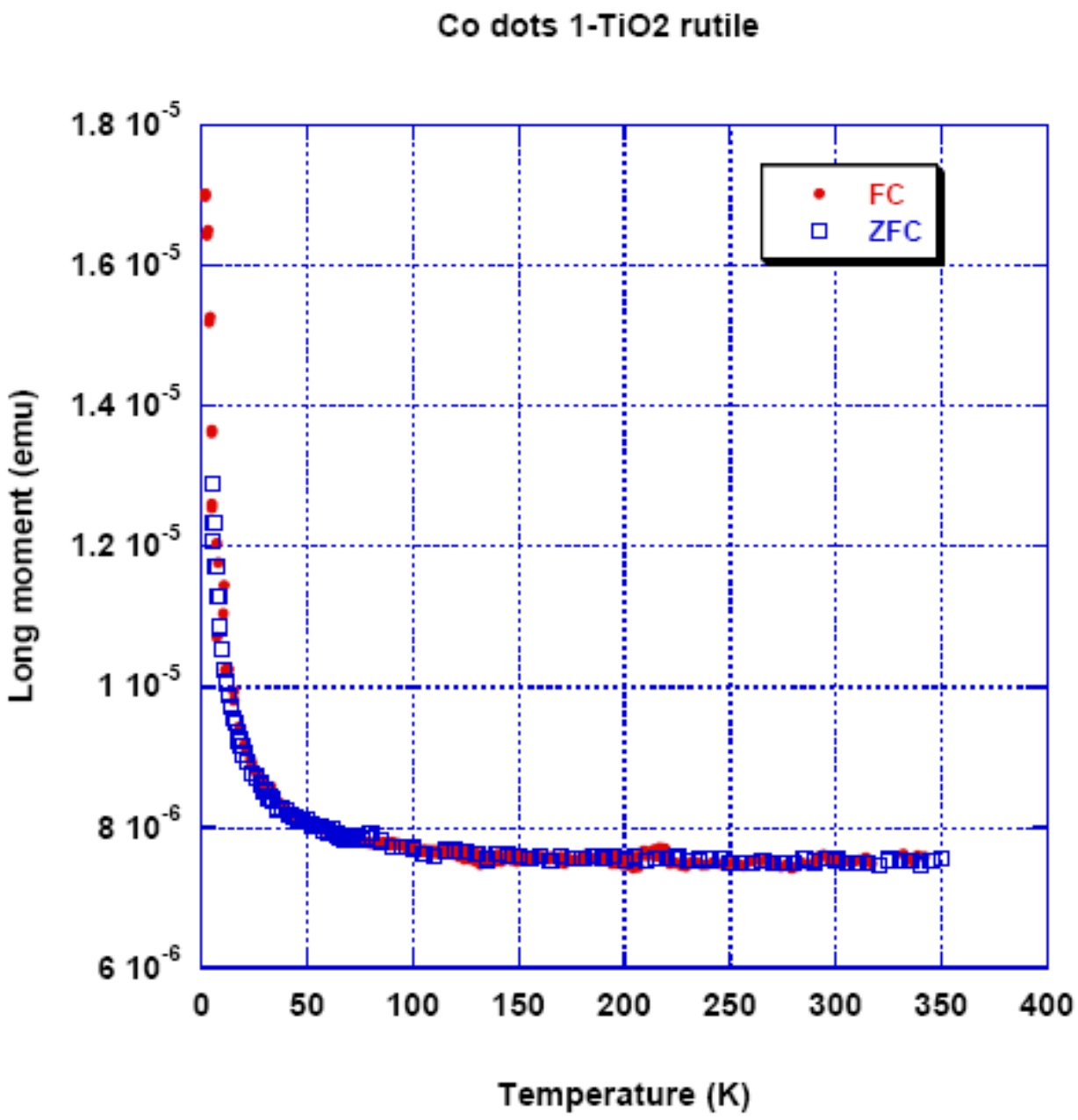

Figure 5.3: Zero Field Cooled and Field Cooled (ZFC-FC) measurement for 0.7 nm Co-dots/ TiO_2(110). No split/ divergence were observed in the ZFC-FC curve down to 2 K, the lowest possible temperature accessible with SQUID. This feature indicates that the Co-dots were superparamagnetic in the whole temperature range.

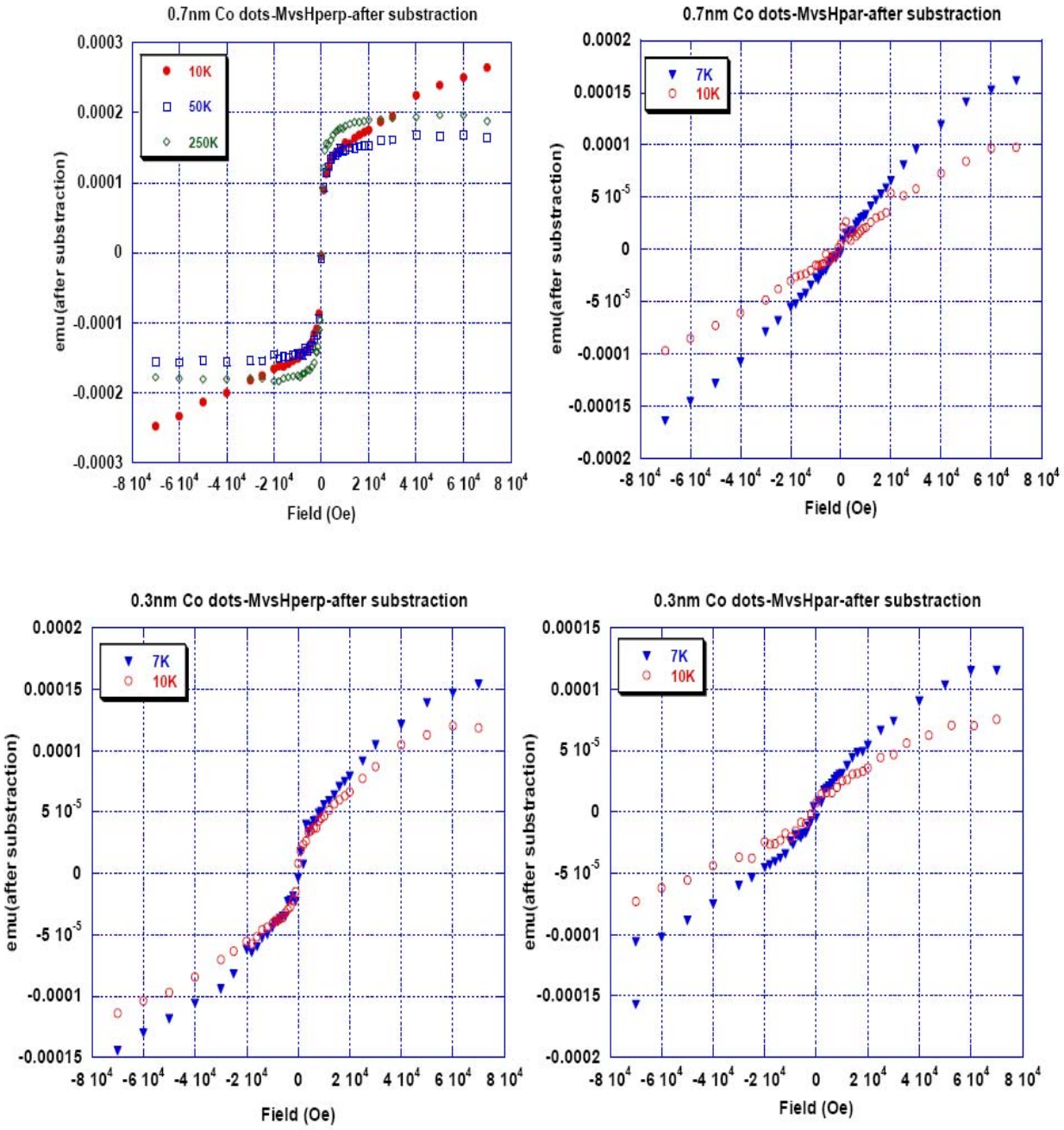

Figure 5.4: Magnetization data of Co-dots on TiO_2(110) for 0.7 nm Co-dots (top), and 0.3 nm Co-dots (bottom). Significant perpendicular magnetic anisotropy is observed for both large and small coverage. Left figures: field applied perpendicular to the plane; right figures: field applied parallel to the plane.

high Curie temperatures (T_C) in Fe-nanodots assemblies on Cu(111). In ferromagnetic nanodots, the formation of single domain is more favorable than multi domain and the whole system is in the superparamagnetic state.

The zero coercive field in our data can also be explained from figure 5.5 which shows the variation of coercive field with particle diameter crossing the transition from superparamagnetic particles to single domain (not superparamagnetic) particles. We can see that $D < D_P$ (S-P: superparamagnetic) is an unstable region and $D_P < D < D_S$ is a stable region. The variance of H_C when crossing the transition from superparamagnetic to single domain (not superparamagnetic) can be understood as follows. At a temperature which is lower than T_B but close to T_B, the thermal activation can still overcome the anisotropy energy of some particles because there is always a distribution of particle size. For an assembly of particles with smaller average volume, more particles are reversed, resulting in a state closer to superparamagnetism with a smaller coercive field. On the other hand, with bigger average size particles, H_C will be larger.

To understand the origin of this perpendicular magnetic anisotropy, we studied the competition between crystal anisotropy and shape anisotropy. The crystal anisotropy arises from the spin-orbit coupling interaction. The shape anisotropy arises from the magnetic field energy associated with each magnetic particle. We calculate these anisotropy energies assuming that the dot is enclosed by a spherical dome $z = \sqrt{R^2 \csc^2 \alpha - x^2 - y^2}$, and a plane at $z = R \tan \alpha$, where R is the radius of the bottom of the dot, and α is the polar angle of the spherical dome. The crystal anisotropy of the dots, U_{CAE}, is equal to the bulk crystal anisotropy, while the shape anisotropy requires a longer derivation which we only briefly outline here. In short, we assume the magnetization is uniform in the dot and calculate the field energies for two configurations with

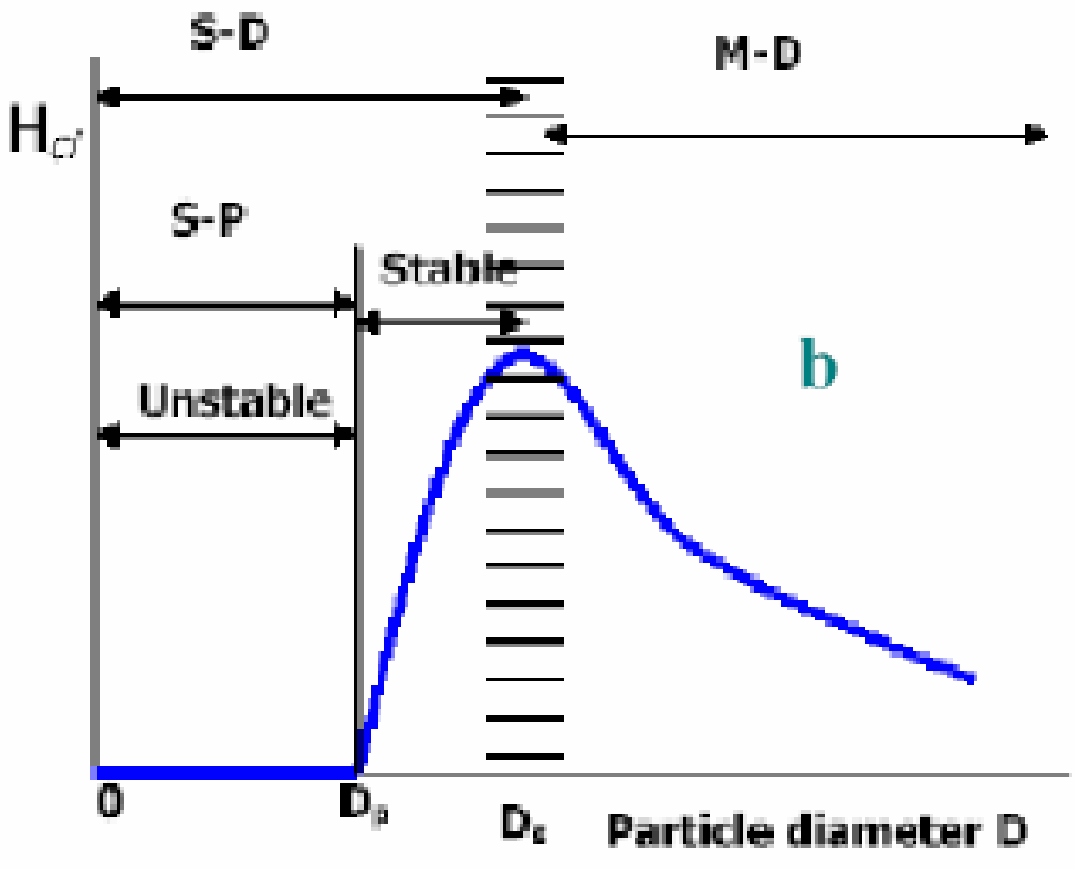

Figure 5.5: Coercive field (H_C) as a function of mean particle diameter (D). S-P: superparamagnetic, S-D: single domain, M-D: multidomain. [after reference 15]

in-plane or out-of-plane magnetizations. Their difference gives the shape anisotropy energy. A dimensional analysis predicts $U_{SAE}(\alpha) \propto M^2 R^3$, where M is the magnetization density. The proportional constant has to be calculated numerically for arbitrary α. To compare $U_{SAE}(\alpha)$ with U_{CAE}, we define a dimensionless coefficient $K_{eff}(\alpha)$:

$$\frac{U_{SAE}(\alpha)}{U_{CAE}} = K_{eff}(\alpha)\frac{M^2}{K} \quad . \tag{5.1}$$

The function $K_{eff}(\alpha)$ is plotted in figure 5.6. There is a large interval of α where $K_{eff}(\alpha)$ increases gradually as α decreases. However, as α goes to zero and the shape of the dot becomes very flat, $K_{eff}(\alpha)$ diverges. This implies that the shape anisotropy becomes more important if the dot is flattened, and eventually overcomes the crystal anisotropy, which is consistent with the well-known in-plane magnetic anisotropy of ferromagnetic thin films. In our samples, α is about 1.0 for 0.7 nm dots and 0.72 for 0.3 nm dots. We observe from figure 5.6 that $K_{eff}(\alpha)$ is still changing slowly at these values of α, so the shape anisotropy should not be excessively large for these dots.

Now we can estimate the value of the shape and the crystal anisotropy of our Co-dots by using equation (5.1) and $K_{eff}(\alpha)$ curve. The crystal anisotropy energy of Co dots is equal to the bulk crystal anisotropy energy. The direction of the magnetization then depends on which anisotropy is stronger, if only these two anisotropies occur. In calculating the magnetization, *M*, of the Co-dots, we have used the bulk value 1.7 μ_B/atom for the magnetic moment. The Co-dots are shaped like 'flattened spheres', thus their shape anisotropy will favor an in-plane magnetization. Both hcp Co and fcc Co can be stabilized at room temperature. There are two possible scenarios to explain our perpendicular magnetic anisotropy data:

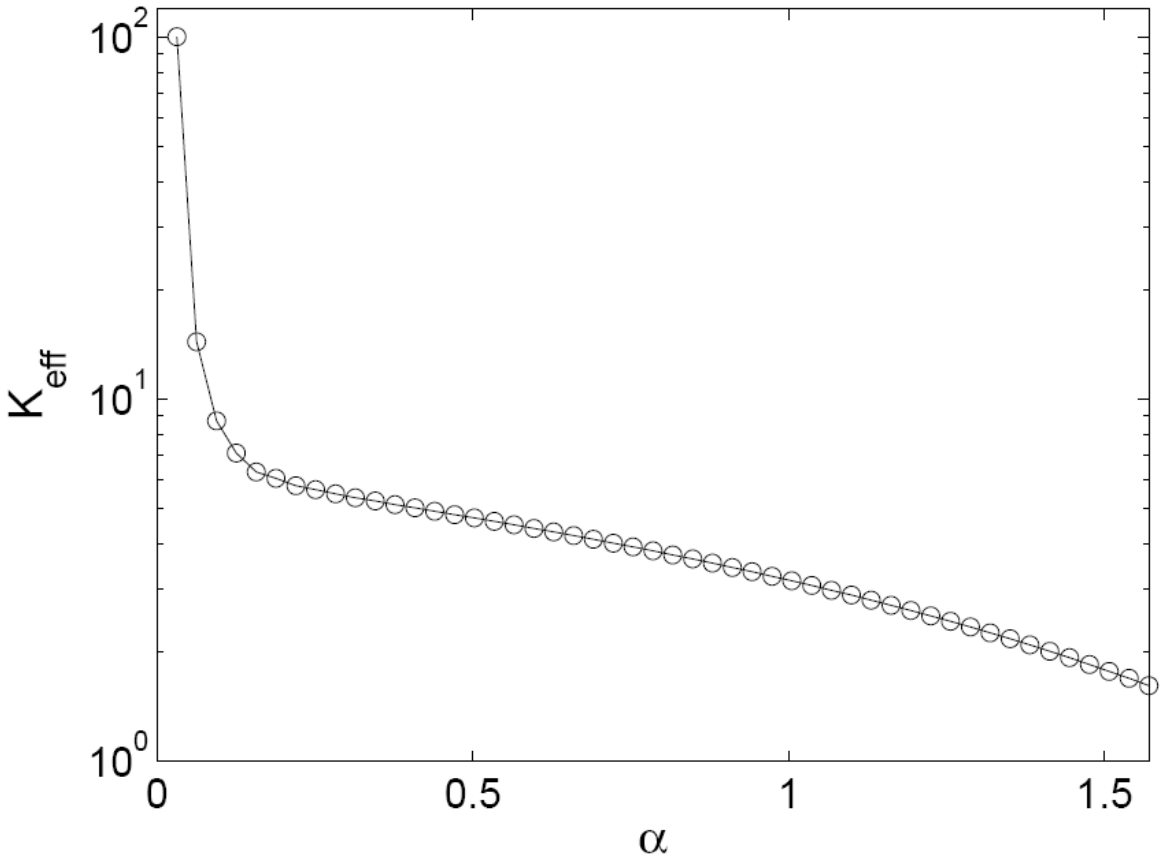

Figure 5.6: Effective anisotropy curve of flattened hemisphere.

1) If the Co dots took the fcc crystal structure, the magnetocrystalline anisotropy for bulk fcc Co would be negligible. Thus, the shape anisotropy of fcc Co dots would be significantly larger than the magnetocrystalline anisotropy. If this first scenario were true, then we would see in-plane anisotropy, contrary to our data that shows significant perpendicular anisotropy.

2) If the Co dots took the hcp crystal structure, the magnetocrystalline anisotropy for bulk hcp Co (lattice parameters: a = 2.5 Å, c = 4.07 Å) would be $5.3\times10^{6}\ erg/cm^{3}$ at room temperature [18] and favored perpendicular easy direction. The shape anisotropy for hcp Co dots can be calculated by using equation (5.1) and $K_{eff}(\alpha)$ curve. It equals to $8.2\times10^{6}\ erg/cm^{3}$ and $6\times10^{6}\ erg/cm^{3}$ for 0.7 nm and 0.3 nm dots, respectively. Our perpendicular anisotropy Co data seem supporting the hcp crystal structure.

By assuming there is no or very small external stress present, we can neglect the contribution from magneto-elastic anisotropy. Without magneto-elastic contributions, one therefore expects a larger critical thickness, $t_{\perp}$, for perpendicular to in-plane spin reorientation transition for Co with a hexagonal structure. Our calculation of the shape and crystal anisotropy roughly indicates that the shape anisotropy wins by a small amount of energy, therefore we can exclude a perpendicular magnetization at low temperatures, and leads us to infer the existence of a perpendicular surface or interface anisotropy. The observed interface anisotropies for Co are often positive, i.e. favoring a perpendicular easy direction. The surface or interface anisotropy arises from the broken symmetry at the dots/ substrate interface or dots/ vacuum surface. As the size of the magnetic nanodots is reduced and the symmetry is broken at the dots/substrate interface, the surface or interface anisotropy energy contribution to the overall magnetic anisotropy energy becomes more pronounced. However, for symmetric particles, (e.g. perfect spheres or slight

deviation from perfect spheres), symmetries reduce the surface contribution to the overall magnetic anisotropy [17].

The absent of coercive field (H_c) and remanance magnetization (M_R) is consistent with a very low blocking temperature (T_B). We can estimate the blocking temperature of our superparamagnetic nanodots by using a very well known formula:

$$KV \approx 25 k_B T_B , \tag{5.2}$$

where K is the magnetic anisotropy energy density, V is the volume of the superparamagnetic particles, and k_B is the Boltzmann constant. Unlike the case for bulk samples where K depends primarily on the bulk magnetocrystalline anisotropy and is sample independent, the K for superparamagnetic particles is sample dependent and it depends not only on the crystal anisotropy, but also on the stress, strain, shape and surface anisotropy. By using the low temperature value of the magnetic anisotropy energy density for very small superparamagnetic Co-particles [19], $K \approx 3 \times 10^8 erg/cm^3$, we estimate the blocking temperature of our Co-nanodots is around 1 K and 0.1 K for 0.7 nm and 0.3 nm dots, respectively.

5.4 Summary

In conclusion, we observed a significant perpendicular magnetic anisotropy in Co-nanodots on rutile TiO_2(110) with no sign of superparamagnetic-to-ferromagnetic transition observed down to 2 K. Our theoretical calculation rules out the contribution from the shape and the crystal anisotropy energy to explain the perpendicular magnetic anisotropy. We believe the Co/TiO_2 interface anisotropy completely dominates the magnetic anisotropy energy. The estimated very low blocking temperature of our Co-dots (< 1 K) explains very well the lack of

hysteresis loop in the *M vs. H* data. This system does not exhibit significant interaction between the dots. The dipolar interaction is also negligible in the temperature range accessible with the SQUID magnetometer.

Since there is no sign of dot-dot interaction or dipolar interaction at the temperature range accessible with the SQUID, we could not use this system to study the relative role of magnetic anisotropy and the dipolar interaction.

5.5 Future direction

We have found that significant perpendicular magnetic anisotropy was observed in the Co-dots/ TiO_2(110) systems and the dots were in the superparamagnetic state in the whole temperature range observed, however we did not really pin the origin of the perpendicular magnetic anisotropy. Tunneling Electron Microscopy (TEM) data would support our argument that the Co-dots took on hcp crystal structure. Besides that, we also need the precise lateral size of the dots for the theoretical calculation. This can be done by knowing the monolayer (ML) coverage of the dots. The STM and SQUID magnetization data of the same ML Fe-dots/ TiO_2(110) coverage could support the result of our Co-dots/ TiO_2(110). For Fe-based systems, the observed values for $t_{\perp}$ are generally smaller than the Co-based systems, notwithstanding the often larger positive interface anisotropies. This is mainly due to the large in-plane shape anisotropy owing to its large demagnetizing field (high saturation magnetization) and to the absence of significant bulk magnetocrystalline anisotropies; therefore Fe-dots will favor in-plane magnetic anisotropy and higher blocking temperature.

Chapter 6 Conclusion

It was predicted that magnetic ordering could not exist in the low dimensional system. However, nowadays scientists have widely accepted the fact that it is possible to stabilize the ferromagnetic ordering in monoatomic chain and assemblies of nanodot. In this dissertation, I report new evidence about the relative role of magnetic anisotropy, dipolar interaction, and indirect exchange interaction through surface state electrons. I present the results obtained from two major projects during my graduate study at University of Tennessee, i.e. Perpendicular Magnetic Anisotropy in Cobalt nanodots on Rutile TiO_2(110) and Artificial Nanomagnet with Lateral Confinement achieved by depositing Fe-dots on vicinal Cu(111).

In the first project, we study the role of in-plane uniaxial magnetic anisotropy, indirect exchange interaction mediated by the surface state electrons and competition between the dot diameter and the terrace width. We report that the critical temperature of Fe-dots grown on vicinal Cu(111) largely depends on the Cu(111) surface states. When the Xe buffer layer coverage is increased beyond 20 langmuir, in-plane magnetization easy axis and critical terrace width are observed. Above the critical terrace width, the critical temperature slightly increases due to the decreasing coupling of Fe-dots through the vicinal Cu(111) surface states and the increasing role of in-plane anisotropy of Fe-dots. When the dot diameter is smaller than the terrace width, the surface state behaves like Cu(111) and the Fe dots will experience strong coupling through the Cu(111) surface states. However, when the dot diameter is larger than the terrace width, the surface state will be more (100)-like and the coupling of Fe dots through surface states will decrease and T_c drops dramatically. Cu(111) has stronger surface state than

Cu(100) surface state. Perpendicular anisotropies and a slight decreased of the critical temperature are observed for low buffer layer (Xe) coverage assisted growth. This result is explained due to the stronger intra-layer (within one terrace) Fe-dots interaction than the inter-layer (between terraces) Fe-dots interaction. At high miscut angle (small terrace width), there will be less Fe-dots that can be accomodated within one terrace. Besides the Fe-dots interaction, there is another factor in play which is the barrier strength of the vicinal surface state. The barrier strength of vicinal surfaces and the coupling of Fe-dots through Cu(111) surface state decreases for larger miscut angle.

In the second project, Co-dots on rutile TiO_2(110), we focus on the interplay between magnetic anisotropy and dipolar interaction in nanodot assemblies. We observe a significant perpendicular magnetic anisotropy with no sign of superparamagnetic to ferromagnetic transition observed down to 2 K. Our theoretical calculation rules out the contribution from the shape and the crystal anisotropy energy to explain the perpendicular magnetic anisotropy. We believe the Co/TiO_2 interface anisotropy completely dominates the magnetic anisotropy energy. The very low blocking temperature of our Co-dots (< 1 K) explains very well the lack of hysteresis loop in the *M vs. H* data. This system does not exhibit significant interaction between the dots. There is no sign of dot-dot interaction of dipolar interaction at the temperature range accessible with the SQUID.

References

References for Chapter 1

[1] W. Hansen, J. P. Kotthaus, U. Merkt. Semicond. Semimetals 35, 279 (1992).

M. Kastner. Phys. Today, January 24 (1993).

[2] *Magnetic Nanostructures.* F. J. Himpsel, J. E. Ortega, G. J. Mankey, R. F. Willis. Advances in Physics 47, 511-597 (1998).

[3] *Absence of ferromagnetism or antiferromagnetism in one- or two-dimensional isotropic Heisenberg.* N. D. Mermin, H. Wagner. Phys. Rev. Lett. 17, 133 (1966).

[4] *Beitrag zur Theorie des Ferromagnetismus.* Ising, E. Z. Phys. 31, 253-258 (1925).

[5] *Ferromagnetism in one-dimensional monoatomic metal chain.* P. Gambardella, A. Dallmeyer, K. Maiti, M. C. Malagoli, W. Eberhardt, K. Kern, C. Carbone. Nature 416, 301 (2002).

[6] *Magnetism in one dimension: Fe on Cu(111).* J. Shen, R. Skomski, M. Klaua, H. Jenniches, S. Sundar Manoharan, J. Kirschner. Phys. Rev. B. 56, 5 (1997).

[7] *Submonolayer magnetism of Fe(110) on W(110): finite width scaling of stripes and percolation between islands.* H. J. Elmers, J. Hauschild, H. Hoche, and U. Gradmann, H. Bethge, D. Heuer, and U. Kohler . Phys. Rev. Lett. 73, 898 (1994).

[8] *Ferromagnetic Stability in Fe nanodot assemblies on Cu(111) induced by indirect coupling through the substrate.* J. P. Pierce, M. A. Torija, Zheng Gai, Junren Shi, T. C. Schulthess, G. A. Farnan, J. F. Wendelken, E. W. Plummer, J. Shen. Phys. Rev. Lett, 92, 237201 (2004).

[9] *Tailoring magnetism in artificially structured materials: the new frontier.* J. Shen, J. Kirschner. Surf. Sci. 500, 300-322 (2002).

[10] *The effect of spatial confinement on magnetism: films, stripes and dots of Fe on Cu(111).* J. Shen, J. P. Pierce, E. W. Plummer, J. Kirschner. Journal of Physics: Condensed Matter 15, R1-R30 (2003).

[11] *Growth and magnetism of metallic thin films and multilayers by pulsed-laser deposition.* J. Shen, Zheng Gai, J. Kirschner. Surf. Sci. Rep. 52, 163-218 (2004).

[12] J. P. Pierce. Tailored magnetic nanostructures on surfaces. Ph.D Thesis Dissertation University of Tennessee, Knoxville (2003).

[13] M. A. Torija. The role of novel magnetic interactions in surface-supported magnetic nanodot assemblies. Ph.D Thesis Dissertation University of Tennessee, Knoxville (2005).

[14] *Giant magnetoresistance of (001)Fe/(001)Cr magnetic superlattices.* M. N. Baibich, J. M. Broto, A. Fert, F. Nguyen Van Dau, F. Petroff, P. Etienne, G. Creuzet, A. Friederich, J. Chazelas. Phys. Rev. Lett. 61, 2472 (1988).

[15] *Enhanced magnetoresistance in layered magnetic structures with antiferromagnetic interlayer exchange.* G. Binasch, P. Grunberg, F. Saurenbach, W. Zinn. Phys. Rev. B. 39, 4828 (1989).

[16] *Electrons in transition metals.* N. Mott. Adv. Phys. 13, 325-422 (1964).

[17] Two-current conduction in nickel. A. Fert, I. A. Campbell. Phys. Rev. Lett. 21, 1190-1192 (1968).

[18] *Electrical resistivity of ferromagnetic nickel and iron based alloys.* A. Fert, I. A. Campbell. J. Phys. F 6, 849-871 (1976).

References for Chapter 2

[1] Stephen Blundell. Magnetism in Condensed Matter. Oxford master series in condensed matter physics: 1st edition (2001).

[2] *Superparamagnetism in Co ion-planted epitaxial anatase TiO_2 thin films.* D. H. Kim, J. S. Yang, Y. S. Kim, Y. J. Chang, T. W. Noh, S. D. Bu, Y.-W. Kim, Y. D. Park, S. J. Pearton and J.-H. Park. Annalen Der Physik 13, 70 (2004).

[3] *Magnetic anisotropy in metallic multilayers.* M. T. Johnson, P. J. H. Bloemen, F. J. A. den Broeder, J. J. de Vries. Rep. Prog. Phys. 59, 1409 (1996).

[4] *Superparamagnetism and Spin-Glass Ordering in Magnetic Nanocomposites.* S. Morup. Europhys. Lett. 28, 671 (1994).

[5] *Sudden jump of the curie temperature at the coalescence of Co islands on Cu(001).* U. Bovensiepen, P. Poulopoulos, W. Platow, M. Farle, K. Baberschke. J. Magn. Magn. Mater. 192, L386 (1999).

[6] *Metastable magnetic properties of Co/Cu(001) films below the T_c jump.* P. Poulopouls, P. J. Jensen, A. Ney, J. Linder, K. Baberschke. Phys. Rev. B. 65, 064431 (2002).

[7] *Ferromagnetic Stability in Fe nanodot assemblies on Cu(111) induced by indirect coupling through the substrate.* J. P. Pierce, M. A. Torija, Zheng Gai, Junren Shi, T. C. Schulthess, G. A. Farnan, J. F. Wendelken, E. W. Plummer, J. Shen. Phys. Rev. Lett, 92, 237201 (2004).

[8] *Long-range magnetic interaction due to the casimir effect.* P. Bruno. Phys. Rev. Lett. 88,240401 (2002).

[9] *Shell effect in exchange coupling of transition metal dots and their arrays.* V. N. Kondratyev, H. O. Lutz. Phys. Rev. Lett. 81, 4508 (1998).

[10] *Magnetic order in two-dimensional arrays of nanometer-sized superparamagnets.* M. R. Scheinfein, K. E. Schmidt, K. R. Heiim, G. G. Hembree. Phys. Rev. Lett. 76, 1541 (1996).

[11] *"Live" surface ferromagnetism in Fe dot multilayers on Cu(111).* M. A. Torija, A. P. Li, C. Guan, E. W. Plummer, J. Shen. Phys. Rev. Lett. 95, 257203 (2005).

[12] M. A. Torija. The role of novel magnetic interactions in surface-supported magnetic nanodot assemblies. Ph.D Thesis Dissertation University of Tennessee, Knoxville (2005).

[13] *Quantum well structures in thin metal films: simple model physics in reality?* M. Milun, P. Pervan, D. P. Woodruff. Rep. Prog. Phys. 65, 99-141 (2002).

[14] *Confinement of Surface State Electrons in Fabry-Perot Resonators*. L. Burgi, O. Jeandupeux. A. Hirstein, H. Brune, and K. Kern. Phys. Rev. Lett. 81, 5370 (1998).

[15] J. P. Pierce. Tailored magnetic nanostructures on surfaces. Ph.D Thesis Dissertation University of Tennessee, Knoxville (2003).

References for Chapter 3

[1] *Perpendicular magnetic anisotropy and coercivity of Co/ Ni multilayers.* F. J. A. den Broeder, E. Janssen, W. Hoving, W. B. Zeper. IEEE Trans. Magn. 28, 2760-2765 (1992).

[2] *Surface Magneto-optic Kerr Effect (SMOKE).* Z. Q. Ziu, S. D. Bader. J. Magn. Magn. Mater. 200, 644-678 (1999).

[3] *Surface Magneto-optic Kerr Effect.* Z. Q. Ziu, S. D. Bader. Review of Scientific Instruments 71, 1243-1255 (2000).

[4] *The Faraday Effect in Ferromagnetics.* H. R. Hulme. Proc. Roy. Soc. London. Ser. A. 135, 237 (1932).

[5] C. Kittel. Phys. Rev. 83, 208(A) (1951); *Surface Magneto-optic Kerr Effect (SMOKE)*. Z. Q. Ziu, S. D. Bader. J. Magn. Magn. Mater. 200, 644-678 (1999).

[6] E. R. Moog, S. D. Bader. Superlattices & Microstructures 1, 542 (1985).

References for Chapter 4

[1] *Magnetism in one dimension: Fe on Cu(111).* J. Shen, R. Skomski, M. Klaua, H. Jenniches, S. S. Manoharan, and J. Kirschner. Phys. Rev. B. 56, 2340 (1997).

[2] *Monitoring and modifying properties of metal surfaces by electronic surface states*. N. Memmel Surf. Sci. Rep. 32, 91 (1998).

[3] *Imaging standing waves in a two-dimensional electron gas.* M. F. Crommie, C. P. Lutz, and D. M. Eigler. Nature 363, 524 (1993).

[4] *Confinement of Surface State Electrons in Fabry-Perot Resonators*. L. Burgi, O. Jeandupeux. A. Hirstein, H. Brune, and K. Kern. Phys. Rev. Lett. 81, 5370 (1998).

[5] *Lateral confinement of surface states on stepped Cu(111).* O. Sanchez, J. M. Garcia, P. Segovia, J Alvarez, A. L. Vazquez de Parga, J. E. Ortega, M. Prietsch, and R. Miranda. Phys. Rev. B. 52, 7894 (1995).

[6] *Electron Wave Function at a Vicinal Surface: Switch from Terrace to Step Modulation.* J. E. Ortega, S. Speller, A. R. Bachmann, A. Mascaraque, E. G. Michel, A. Narmann, A. Mugarza, A. Rubio, and F. J. Himpsel. Phys. Rev. Lett. 84, 6110 (2000).

[7] *Localization of Surface States in Disordered Step Lattices*. F. Baumberger, M. Hengsberger, M. Muntwiler, M. Shi, J. Krempasky, L. Patthey, J. Osterwalder, and T. Greber. Phys. Rev. Lett. 92, 196805 (2004).

[8] *Scanning tunneling spectroscopy study of Cu(554): Confinement and dimensionality at a stepped surface.* M. Hansmann, J. I. Pascual, G. Ceballos, H.-P. Rust, and K. Horn. Phys. Rev. B. 67, 121409 (R) (2003).

[9] *Ferromagnetism in one-dimensional monoatomic metal chain.* P. Gambardella, A. Dallmeyer, K. Maiti, M. C. Malagoli, W. Eberhardt, K. Kern, C. Carbone. Nature 416, 301 (2002).

[10] *Confining Barriers for Surface State Electrons Tailored by Monoatomic Fe Rows on Vicinal Au(111) Surfaces.* Susumu Shiraki, Hideki Fujisawa, Masashi Nantoh, and Maki Kawai. Phys. Rev. Lett. 92, 096102 (2004).

[11] *Ferromagnetic Stability in Fe nanodot assemblies on Cu(111) induced by indirect coupling through the substrate.* J. P. Pierce, M. A. Torija, Zheng Gai, Junren Shi, T. C. Schulthess, G. A. Farnan, J. F. Wendelken, E. W. Plummer, J. Shen. Phys. Rev. Lett, 92, 237201 (2004).

[12] *"Live" surface ferromagnetism in Fe dot multilayers on Cu(111).* M. A. Torija, A. P. Li, C. Guan, E. W. Plummer, J. Shen. Phys. Rev. Lett. 95, 257203 (2005).

[13] *Magnetism of Fe clusters formed by buffer-layer assisted growth on Pt(997).* J. Zhang, D. Repetto, V. Sessi, J. Honolka, A. Enders, and K. Kern. Eur. Phys. J. D. 45, 515 (2007).

[14] *Magnetic Moment of fcc Fe(111) Ultrathin Films by Ultrafast Deposition on Cu(111)*. J. Shen, P. Ohresser, Ch. V. Mohan, M. Klaua, J. Barthel, and J. Kirschner. Phys. Rev. Lett. 80, 1980 (1998).

[15] *Structural and magnetic phase transitions of Fe on stepped Cu(111)*. J. Shen, R. Skomski, M. Klaua, H. Jenniches, S. Sundar Manoharan, and J. Kirschner. Phys. Rev. B. 56, 11134 (1997).

[16] *Buffer Layer Assisted Growth of Nanocrystals: Ag-Xe-Si(111)*. Lin Huang, S. Jay Chey, and J. H. Weaver. Phys. Rev. Lett. 80, 4095 (1994).

[17] J. P. Pierce. Tailored magnetic nanostructures on surfaces. Ph.D Thesis Dissertation University of Tennessee, Knoxville (2003).

[18] M. A. Torija. The role of novel magnetic interactions in surface-supported magnetic nanodot assemblies. Ph.D Thesis Dissertation University of Tennessee, Knoxville (2005).

[19] *Fermi surfaces of the two-dimensional surface states on vicinal Cu(111)*. F. Baumberger, T. Greber, and J. Osterwalder. Phys. Rev. B. 64, 195411 (2001).

[20] *Electronic confinement on stepped Cu(111) surfaces: Ab initio study.* P. A. Ignatiev, V. S. Stepanyuk, A. L. Klavsyuk, W. Hergert, and P. Bruno. Phys. Rev. B. 75, 155428 (2007).

[21] *One-dimensional versus two-dimensional surface states on stepped Au(111).* J. E. Ortega, A. Mugarza, V. Repain, S. Rousset, V. Perez-Dieste, and A. Mascaraque. Phys. Rev. B. 65, 165413 (2002).

[22] *Interacting quantum box superlattice by self-organized Co nanodots on Au(788).* C. Didiot, A. Tejeda, Y. Fagot-Revurat, V. Repain, B. Kierren, S. Rousset, and D. Malterre. Phys. Rev. B. 76, 081404(R) (2007).

References for Chapter 5

[1] *Models of the Dynamics of Interacting Magnetic Particles.* M. F. Hansen and S. Morup. J. Magn. Magn. Mater. 184, 262 (1998).

[2] *Nanostructured magnetic films for extremely high density recording.* D. J. Sellmyer, M. Yu, and R. D. Kirby. Nanostruct. Mater. 12, 1021 (1999).

[3] *Superparamagnetism and Spin Glass Ordering in Magnetic Nanocomposites.* S. Morup. Europhys. Lett. 28, 671 (1994).

[4] *Aging in a magnetic particle system.* T. Jonsson, J. Mattsson, C. Djurberg, F. A. Khan, P. Nordblad, and P. Svedlindh. Phys. Rev. Lett. 75, 4138 (1995).

[5] *Dynamics of an Interacting Particle System: Evidence of Critical Slowing Down.* C. Djurberg, P. Svedlindh, and P. Nordblad, M. F. Hansen, F. Bodker, and S. Morup. Phys. Rev. Lett. 79, 5154 (1997).

[6] *Static Scaling on an Interacting Magnetic Nanoparticle System.* T. Jonsson, P. Svedlindh, and M. F. Hansen. Phys. Rev. Lett. 81, 3976 (1998).

[7] *Blocking and Freezing of Magnetic Moments for Iron Nitride Fine Particle Systems.* H. Mamiya, I. Nakatani, and T. Furubayashi. Phys. Rev. Lett. 80, 177 (1998).

[8] *Slow Dynamics for Spin-Glass-Like Phase of a Ferromagnetic Fine Particle System.* H. Mamiya, I. Nakatani, and T. Furubayashi. Phys. Rev. Lett. 82, 4332 (1999).

[9] *Nonequilibrium dynamics in an interacting Fe-C nanoparticle system.* P. Jonsson, M. F. Hansen, and P. Nordblad. Phys. Rev. B 61, 1261 (2000).

[10] *Memory Effect in an Interacting Magnetic Nanoparticle System.* Y. Sun, M. B. Salamon, K. Garnier, and R. S. Averback. Phys. Rev. Lett. 91, 167206 (2003).

[11] *Ferromagnetic Stability in Fe nanodot assemblies on Cu(111) induced by indirect coupling through the substrate.* J. P. Pierce, M. A. Torija, Z. Gai, Junren Shi, T. C. Schulthess, G. A. Farnan, J. F. Wendelken, E. W. Plummer, and J. Shen. Phys. Rev. Lett. 92, 237201 (2004).

[12] *Room-Temperature Ferromagnetism in Transparent Transition Metal-Doped Titanium Dioxide.* Y. Matsumoto, M. Murakami, T. Shono, T. Hasegawa, T. Fukumura, M. Kawasaki, P. Ahmet, T. Chikyow, Shin-ya Koshihara, H. Koinuma. Science 291, 854 (2001).

[13] *Ferromagnetism Induced by Clustered Co in Co-doped Anatase TiO_2 Thin Films.* J.-Y. Kim, J.-H. Park, B.-G. Park, H.-J. Noh, S.-J. Oh, J. S. Yang, D.-H. Kim, S. D. Bu, T.-W. Noh, H.-J.

Lin, H.-H. Hsieh, and C. T. Chen. Phys. Rev. Lett. 90, 017401 (2003); *Intrinsic Ferromagnetism in Insulating Cobalt Doped Anatase TiO_2.* K. A. Griffin, A. B. Pakhomov, C. M. Wang, S. M. Heald, and K. M. Krishnan. Phys. Rev. Lett. 94, 157204 (2005).

[14] STM line profiles often exaggerate the lateral size of the dots due to tip effect. The lateral size of the dots was thus calculated based on the dot density and dot height.

[15] B. D. Cullity. Introduction to magnetic materials (1972).

[16] *Spin-other-orbit interaction and magnetocrystalline anisotropy.* M. D. Stiles, S. V. Halilov, R. A. Hyman, and A. Zangwill. Phys. Rev. B 64, 104430 (2001).

[17] *Surface Contribution to the Anisotropy of Magnetic Nanoparticles.* D. A. Garanin and H. Kachkachi. Phys. Rev. Lett. 90, 065504 (2003); *Magnetic Anisotropy of a Single Cobalt Nanocluster.* M. Jamet, W. Wernsdorfer, C. Thirion, D. Mailly, V. Dupuis, P. Melinon, and A. Perez. Phys. Rev. Lett. 86, 4676 (2001).

[18] *Magnetic anisotropy in metallic multilayers.* M. T. Johnson, P. J. H. Bloemen, F. J. A. den Broeder, J. J. de Vries. Rep. Prog. Phys. 59, 1409 (1996).

[19] *Enhanced magnetic anisotropy energy density for superparamagnetic particles of cobalt.* B. J. Hickey, M. A. Howson, D. Greig, and N. Wiser. Phys. Rev. B 53, 32 (1996).

Vita

Noppi Widjaja was born in Jakarta, Indonesia on November 10, 1978. She attended private schools in Indonesia in the city of Jakarta, and graduated from Karunia High School in 1997. For the next three and half years, she studied physics at Bandung Institute of Technology, a public university in Bandung, West Java, Indonesia. She earned a Bachelor of Arts degree in Physics in May 2001 with cum laude predicate. Upon completing her bachelor degree, she pursued her career as a teacher for two years. In August 2003, her desire for higher education made her go to Florida State University, Tallahassee, and graduated with the master degree in Physics in December 2004. She did a little bit summer research in 2004 at National High Magnetic Field Laboratory (NHMFL), Tallahassee. In August 2005, she attended University of Tennessee, Knoxville and joined the Low Dimensional Group by Design at Oak Ridge National Laboratory (ORNL) to study the surface physics and nanomagnetism. She was granted the Ph.D. in Physics from University of Tennessee in December 2008.